LIN, BEARTRON SHIUN CHIAN

STUDY OF THE LITHIUM-7(HELIUM-3, ALPHA)LITHIUM-6* REACTION

City University of New York PH.D. 1980

PLEASE NOTE:

In all cases this material has been filmed in the best possible way from the available copy. Problems encountered with this document have been identified here with a check mark ✓.

1. Glossy photographs _____
2. Colored illustrations _____
3. Photographs with dark background _____
4. Illustrations are poor copy _____
5. Print shows through as there is text on both sides of page _____
6. Indistinct, broken or small print on several pages ✓
7. Tightly bound copy with print lost in spine _____
8. Computer printout pages with indistinct print _____
9. Page(s) _____ lacking when material received, and not available from school or author
10. Page(s) _____ seem to be missing in numbering only as text follows
11. Poor carbon copy _____
12. Not original copy, several pages with blurred type _____
13. Appendix pages are poor copy _____
14. Original copy with light type _____
15. Curling and wrinkled pages _____
16. Other _____

University Microfilms International

300 N. ZEEB RD., ANN ARBOR, MI 48106 (313) 761-4700

STUDY OF THE $^{7}Li(^{3}He,\alpha)^{6}Li^{*}$ REACTION

by

BEARTRON SHIUN-CHIAN LIN

A dissertation submitted to the Graduate Faculty in Physics in partial fulfillment of the requirements for the degree of Doctor of Philosophy, The City University of New York.

1980

This manuscript has been read and accepted for the Graduate Faculty in Physics in satisfaction of the dissertation requirement for the degree of Doctor of Philosophy.

Aug. 25, 1980
date

Peter M. A. Fenves
Chairman of Examining Committee

Aug. 27, 1980
date

Frank M. Astone RC
Executive Officer

Supervisory Committee

The City University of New York

Abstract

STUDY OF THE $^{7}Li(^{3}He,\alpha)^{6}Li^{*}$ REACTION

by

Beartron S. Lin

Advisor: Professor Peter M.S. Lesser

Differential cross sections for formation of the 5.37 MeV ($J^{\pi}=2^{+},T=1$) level in ^{6}Li have been measured via the reaction $^{7}Li(^{3}He,\alpha)^{6}Li$ at incident ^{3}He energies in the range 0.7-2.5 MeV and for angles in the range $20^{o}\leq\theta(Lab)\leq160^{o}$. Data for the g.s., 2.18 and 3.56 MeV excited states of ^{6}Li were also obtained. The results for the g.s. and the first two excited states are in good agreement with previous measurements and show no clear resonance structure. The excitation function for the 5.37 MeV state, however, exhibits resonance structure at incident ^{3}He energies of 1.45 and 2.15 MeV, corresponding to formation of states in the compound nucleus, ^{10}B, at 18.8 and 19.3 MeV excitation respectively. The experimental data were compared with the results of DWBA calculations using the computer code DWUCK4.

Coincident events between the first emitted alpha particle and the decay alpha's or proton's were detected using a counter telescope in the reaction plane at several appropriately chosen angle pairs at an incident ^{3}He energy of 2.15 MeV. Branching ratios for the allowed decay modes $^{5}He+p$ and $\alpha+p+n$, as well as the isospin forbidden decay into $\alpha+d$, were deduced from the data.

ACKNOWLEDGEMENTS

I am deeply indebted to Prof. Peter M.S. Lesser for his guidance and encouragement to make this task easier, and for his continuous assistance in the course of collecting and analyzing data. I am also grateful to all members of the committee for their valuable advice which enabled me to complete this work. The assistance of the Dynamitron Laboratory Staff is greatly acknowledged.

TABLE OF CONTENTS

LIST OF TABLES

LIST OF ILLUSTRATIONS

I. INTRODUCTION

As a result of the large mass excess(14.93 MeV) of ^{3}He(Ref.1), ^{3}He induced reactions are characterized by high Q values and by highly excited compound systems. Hence, it is possible to study energetic states of light nuclei using a low incident ^{3}He energy. The large Q values available in ^{3}He induced reactions frequently lead to multibody final state systems. Experimental evidence(Ref.2) indicates that most of the multibody final state nuclear reactions induced by low energy projectiles proceed to the final state by various "sequential" processes. The simultaneous process plays a significant role only in unusual circumstances at low bombarding energies. The investigation of such reactions that lead to multibody final states has been especially useful in obtaining spectroscopic information about intermediate systems, because they frequently allow one to study simultaneously the formation process of a particular system as well as all of its possible decay modes(Ref.3). In addition, angular correlation measurements for various decay modes can often provide information about the spin and parity of the intermediate state as well as the mechanism of the primary interaction leading to the intermediate system.

The ^{7}Li(^{3}He,α)^{6}Li(g.s.) reaction has a Q-value of 13.328 MeV(Ref.4). A reaction between ^{7}Li and ^{3}He can lead to a multibody final state in a variety of ways. In this

thesis, attention will be focused on the $^{7}Li(^{3}He,\alpha_1 d)\alpha_2$, the $^{7}Li(^{3}He,\alpha p)^{5}He$ and the $^{7}Li(^{3}He,\alpha_1)pn\alpha_2$ reactions which may proceed by sequential processes through intermediate states of either ^{6}Li and ^{8}Be or ^{6}Li and ^{9}Be respectively. The sequential processes proceeding through ^{6}Li are :

$$^{7}Li + {}^{3}He \longrightarrow \alpha_1 + {}^{6}Li^{*}$$
$$^{6}Li^{*} \longrightarrow d + \alpha_2$$
$$^{6}Li^{*} \longrightarrow \alpha_2 + p + n$$
$$^{6}Li^{*} \longrightarrow {}^{5}He + p$$
$$^{5}He \longrightarrow \alpha_2 + n$$

The sequential processes leading to the same multi-body final state, but proceeding through intermediate states of ^{8}Be or ^{9}Be are the following :

$$^{7}Li + {}^{3}He \longrightarrow d + {}^{8}Be$$
$$^{8}Be \longrightarrow \alpha_1 + \alpha_2$$

$$^{7}Li + {}^{3}He \longrightarrow p + {}^{9}Be$$
$$^{9}Be \longrightarrow \alpha_1 + {}^{5}He$$
$$^{5}He \longrightarrow \alpha_2 + n$$
$$^{9}Be \longrightarrow n + {}^{8}Be$$
$$^{8}Be \longrightarrow \alpha_1 + \alpha_2$$

The energetically allowed intermediate states of ^{8}Be, ^{9}Be, which are known to break up predominantly by α-decay are (with $J^{\pi};T$ given in parentheses): g.s.($0^{+};0$), 2.94 MeV($2^{+};0$), 11.4 MeV($4^{+};0$), 16.62 MeV(2^{+}), and 16.92

MeV(2^+) states for ^{8}Be, 1.68 MeV($\frac{1}{2}^+;\frac{1}{2}$), 2.43 MeV($\frac{5}{2}^-;\frac{1}{2}$), 2.78 MeV($\frac{1}{2}^-;\frac{1}{2}$), 3.06 MeV($\frac{5}{2}^+;\frac{1}{2}$), 4.70 MeV($\frac{3}{2}^+;\frac{1}{2}$), 6.76 MeV($\frac{7}{2}^-;\frac{1}{2}$), 11.28 MeV($\pi$ = -), and 11.81 MeV($\frac{1}{2}$) states for ^{9}Be. The first few excited states in ^{6}Li are : g.s.($1^+;0$), 2.18 MeV($3^+;0$), 3.56 MeV($0^+;1$), 4.57 MeV($2^+;0$) and 5.37 MeV($2^+;1$).

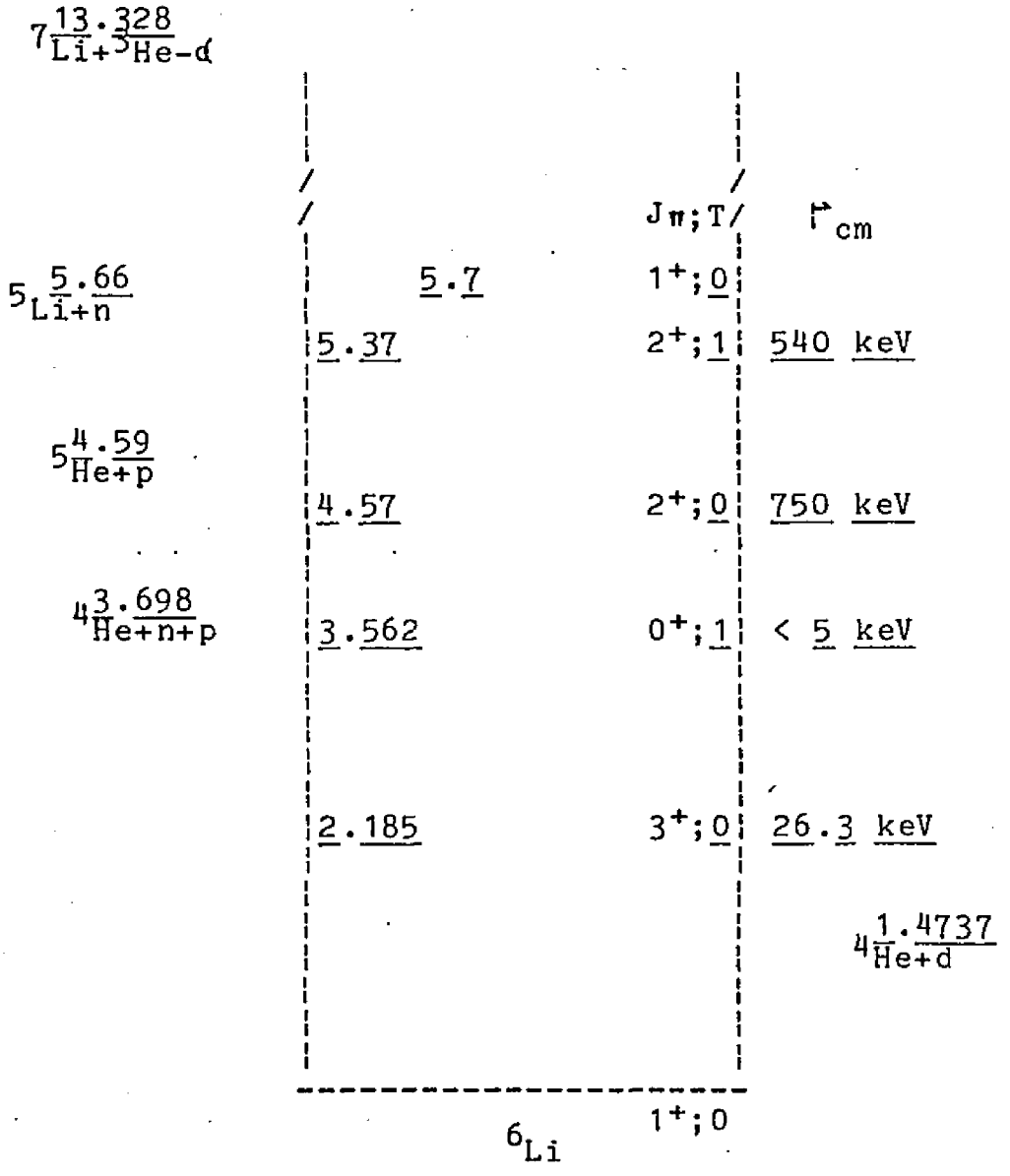

Fig.1 Energy Levels of ^{6}Li

It is easily determined from isospin considerations that only a T=0 level can decay to α + d, since both alpha and deuteron have isospin T=0. As can be seen from the energy level diagram(Fig.1), the ground state is stable, while the first excited state, which is above the 1.4737 MeV threshold, can decay into α + d. The 3.56 MeV level is a T=1 level and is a member of the isospin triplet which includes the ground states of ^{6}He and ^{6}Be. This level cannot decay into α + d (violation of both parity and isospin conservation) and because no other particle decays are energetically allowed it can only decay by γ emission. The T=0 level at 4.57 MeV, first suggested by Galonsky et al.(Ref.5) from the phase-shift analysis of d-α scattering, has a very broad width(~1 MeV). ^{4}He + d decay from this state has been observed(Ref.6) as peaks on the appropriate kinematic loci in agreement with its T=0 assignment. The 5.37 MeV level has a T=1 assignment making it a member of the isospin triplet including the 1.80 MeV level of ^{6}He and the 1.67 MeV level of ^{6}Be.

Several experiments studying the reaction mechanism for the first few states of ^{6}Li have been done. Experimental evidence indicates that ^{7}Li(^{3}He,α)^{6}Li(g.s.,2.18) reaction proceeds largely via a DI(direct interaction) processes for incident energy in the range 1.5-5.0 MeV although there is evidence for some contribution from a CN(compound nucleus) mechanism at around 2.2 MeV incident energy(Ref.11). Reso-

nance at this energy has been observed by Wolicki et al.(Ref.12) in this reaction, by Duggan et al. and Din et al. in the $^{7}Li(^{3}He,n_{o})^{9}B$ reaction(Ref.13-14), and by Paul et al. in the $^{7}Li(^{3}He,\gamma)^{10}B$ reaction(Ref.15). In the $(^{3}He,\alpha)$ reaction, angular distributions for α_{o}, α_{1}, α_{2} at 1.2 and 1.8 MeV are in most cases not symmetric about 90° and do not show pronounced forward or backward peaking(Ref.11), suggesting that the reaction is not dominated by either DI or CN processes. The experimental results of Ref.11 are in disagreement with those of Bromley(Ref.16) which indicated angular distributions were isotropic at 2.1 MeV.

A number of experiments(Ref.6,8,10,17,18) on the reaction $^{7}Li+^{3}He\text{-->}\alpha_{1}+^{6}Li^{*}\text{-->}d+\alpha_{2}$ have been carried out, primarily to investigate the isospin purity of the T=1, 5.37 MeV excited state of ^{6}Li. Valkovic et al.(Ref.7) and Bray et al.(Ref.8) have found no evidence for contribution of sequential decay $^{6}Li(5.37)$ --> α + d through the 5.37 MeV excited state in ^{6}Li. Kane et al.(Ref.6) have suggested a T=1 assignment with a small T=0 impurity caused by mixing of the 5.37 and 4.57 MeV levels, both having approximately 500 KeV width. Debevec et al.(Ref.9) have obtained the isospin mixing ratio $\alpha^{2}=0.008$. Artemov et al.(Ref.10) have obtained branching ratios of <0.1, 0.35 ± 0.10, 0.65 ± 0.10 for decay of the $^{6}Li(5.37$ MeV) state via α + d, p + ^{5}He, α + p + n channels respectively. The reaction mechanism involved in the subsequent step of this process appears to be predominantly

a direct breakup into α + p + n. In similar studies of the reaction $^{6}Li + ^{3}He$, it has been shown to be predominantly a direct reaction in the first step, at some bombarding energies(Ref.19-22), for both ^{5}Li and ^{8}Be outgoing channels. However , in the ^{8}Be channel, Vignon et al.(Ref.19) have shown that the compound nucleus ^{9}B at 17.64 MeV excitation is formed in the first step, at a ^{3}He bombarding energy of 1.6 MeV. As to the characteristics of the break up of ^{5}Li(g.s.) in the second step of the reaction, several experimental studies(Ref.20-22) have interpreted the observation of an asymmetric breakup on the basis of the RMV model(Ref.20). Heggie and Martin(Ref.23) have also seen an asymmetry in the neutron breakup of ^{5}He in the reaction of $^{7}Li(d,\alpha)^{5}He(g.s) \rightarrow n + \alpha$ at a deuteron bombarding energy of 1 MeV. They explained their data in terms of the formation of the ^{9}Be 17.48 MeV state($\frac{3}{2}^{+}$) with an admixture arising from the tail of the 17.28 MeV($\frac{5}{2}^{-}$) state, in the first step of the reaction. More recently, Gupta(Ref.24) has observed the formation of the ^{9}B 16.74 MeV state in the first step of the reaction $^{6}Li(^{3}He,\alpha_{1})^{5}Li(g.s) \rightarrow p + \alpha_{2}$ at 1.58 MeV resonance bombarding energy. At off-resonance bombarding energies of 1.47 and 1.69 MeV Gupta has shown the mechanism to be qualitatively consistent with a direct reaction involving both neutron and deuteron transfer in the first step.

Review of the literature cited above provided the

motivation for the present study of the $^{7}Li(^{3}He,\alpha)^{6}Li$ reaction. Measurements were concentrated on the 5.37 MeV $(2^{+},1)$ level for a number of reasons.

(1) Differential cross sections for the 5.37 MeV state have never been measured before, presumably because the underlying background coming from the α + d, ^{5}He + p and α + p +n continua makes analysis of the experimental data more difficult for this state. Also the ^{6}Li recoils in the g.s. and first excited state partly overlap the 5.37 MeV state in the spectrum at most of the angular ranges.

(2) The relevant energy levels of ^{10}B corresponding to the incident ^{3}He energy region studied are all T=1 states. Should resonances occur in the $^{7}Li(^{3}He,\alpha)^{6}Li$ reaction, they should populate T=1 states in ^{6}Li.

(3) The applicability of the optical model and DWBA to a reaction in which a target, containing only a few nucleons, interacts with a particle of comparable mass, is somewhat uncertain, and it is therefore of interest to see how well the DWBA calculations fit the observed angular distributions and what sort of optical model potentials best describe the interaction.

(4) The decay of this level into α + d is isospin forbidden since both alpha and deuteron have T=0, However, the broad widths and close proximities of the 4.57(T=0) and 5.37(T=1) states allows the possibility of isospin mixing. Thus, the 5.37 MeV state might contain a small admixture of T=0, permitting a weak decay branch into α + d.

(5) Previously reported branching ratios for the decay modes of this level at a bombarding energy of 32.5 MeV has assumed isotropic decay which is undoubtedly incorrect since the decay through the intermediate state involves L=1 & 3 couplings. The interpretation of these earlier measurements seems questionable.

For the present thesis work, the main purpose is to study several features of the reaction $^{7}Li(^{3}He,\alpha)^{6}Li^{*}$, going through the intermediate state at 5.37 MeV($2^{+};1$) and subsequently decaying to α + d, p + ^{5}He or α + p + n. Both the angular distribution and excitation function measurements of the first emitted alpha-particle have been measured in this work and are useful in deducing the mechanisms involved in the first step of the reaction. The study of the behavior of the angular correlation can also yield information about the nature of the initial interaction and is needed for the determination of decay branching ratios. The branching ratios for the various decay modes of the ^{6}Li(5.37) state have been measured by taking coincidence spectra at as many appropriately chosen angle pairs as possible.

II. THEORETICAL BACKGROUND

A. Transformations Between Reference Systems

The descriptions of many nuclear phenomena are expressed most simply in a moving reference system located at the center of mass of the interacting particles. It is necessary to calculate and express quantities in the CM-system for comparison of theoretical with experimental results. Transformations between reference systems using appropriate formulae are described as follows: Primed symbols denote quantities expressed in the CM-system, while unprimed symbols denote quantities expressed in the Lab-system.

If the center of mass of the system travels with velocity V_c in the Lab-system, then the velocities of the incident particle and target relative to the center of mass are

$$V_I' = V_I - V_c, \qquad V_T' = V_c$$

By conservation of momentum

$$V_c = \frac{m_I}{m_I+m_T}V_I = \frac{M_I}{M_I+M_T}V_I, \text{ where } M_i = m_i c^2$$

hence $$V_I' = \frac{M_T}{M_I+M_T}V_I$$

$$V_T' = \frac{M_I}{M_I+M_T}V_I = V_c$$

The total kinetic energy in the CM-system is thus

$$T_{tot}' = \frac{M_T}{M_I+M_T} T_I$$

Transformation of Angles

The position of M_I at time t in the Lab-system is

$$x = V_I'\cos\theta' t + V_c t \qquad (1)$$

$$y = V_I'\sin\theta' t \qquad (2)$$

$$\text{hence} \quad \tan\theta = \frac{y}{x} = \frac{V_I'\sin\theta'}{V_I'\cos\theta' + V_c} = \frac{\sin\theta'}{\cos\theta' + K'} \qquad (3)$$

$$\text{where} \quad K' = \frac{V_c}{V_I'}$$

It is also possible to perform the inverse transformation, the result is

$$\tan\theta' = \frac{\sin\theta}{\cos\theta - K}, \quad \text{where} \quad K = \frac{V_c}{V_I} \qquad (4)$$

Transformation of Momentum and Kinetic Energy

Multiplying the two velocity transformations (1)-(2) by $\frac{M_I}{c}$, and using P = pc

$$M_I V_I \cos\theta/c = M_I V_I'\cos\theta'/c + M_I V_c/c$$

$$M_I V_I \sin\theta/c = M_I V_I'\sin\theta'/c$$

or $P_I \cos\theta = P_I'(\cos\theta' + K')$ (5)

$P_I \sin\theta = P_I' \sin\theta'$ (6)

From these equations

$$P_I^2 = P_I'^2(1 + 2K'\cos\theta' + K'^2) \quad (7)$$

and the inverse transformations are

$$P_I' \cos\theta' = P_I(\cos\theta - K) \qquad P_I'^2 = P_I^2(1 - 2K\cos\theta + K^2)$$

Similarly, the transformation formulae for the kinetic energy are

$$T = T'(1 + 2K'\cos\theta' + K'^2) \qquad T' = T(1 - 2K\cos\theta + K^2)$$

Transformation of Differential Cross-Section

Consider the differential cross-section at the angle θ(Lab), defined by

$$\left(\frac{d\sigma}{d\Omega}\right)_\theta = \frac{n}{n_o N \Delta\Omega}$$

where n is the number of particles scattered through an angle θ into a detector of solid angle $\Delta\Omega$, when n_o particles are incident on a target containing N particles per cm^2. Similarly, in the CM-system we define the differential cross-section at the corresponding angle θ' as

$$\left(\frac{d\sigma}{d\Omega'}\right)_{\theta'} = \frac{n}{n_o N \Delta\Omega'}$$

The total number of detected particles is independent of the reference system, thus

$$n = n_o N\left(\frac{d\sigma}{d\Omega}\right)_\theta \Delta\Omega = n_o N\left(\frac{d\sigma}{d\Omega'}\right)_{\theta'}\Delta\Omega'$$

from which

$$\left(\frac{d\sigma}{d\Omega}\right)_\theta / \left(\frac{d\sigma}{d\Omega'}\right)_{\theta'} = \frac{\Delta\Omega'}{\Delta\Omega} = \frac{\sin\theta' d\theta'}{\sin\theta d\theta} \qquad (8)$$

From formulae (6) and (7)

$$\frac{\sin\theta'}{\sin\theta} = \frac{P_I}{P_I'} = (1 + 2K'\cos\theta' + K'^2)^{1/2}$$

From equation (3)

$$\frac{d\theta'}{d\theta} = \frac{d(\tan\theta)}{d\theta}\Big/\frac{d(\tan\theta)}{d\theta'} = \frac{(1 + \tan^2\theta)(\cos\theta' + K')^2}{(1 + K'\cos\theta')}$$

$$= [1 + \sin^2\theta'/(\cos\theta' + K')^2](\cos\theta' + K')^2$$

$$= \frac{1 + K'^2 + 2K'\cos\theta'}{1 + K'\cos\theta'}$$

Therefore, from equation (8)

$$\left(\frac{d\sigma}{d\Omega}\right)_\theta / \left(\frac{d\sigma}{d\Omega'}\right)_{\theta'} = \frac{(1 + 2K'\cos\theta' + K'^2)^{3/2}}{1 + K'\cos\theta'}$$

$$= \frac{\sin^3\theta'}{\sin^3\theta(1 + K'\cos\theta')} = \frac{[(1 - K'^2\sin^2\theta)^{1/2} + K'\cos\theta]^2}{(1 - K'^2\sin^2\theta)^{1/2}}$$

$$= \frac{1}{(1 - 2K\cos\theta + K^2)^{1/2}(1 - K\cos\theta)}$$

B. Kinematics of A Three Body Breakup Reaction

When a nuclear system decays into three particles it may be represented by the following reactions(Ref.2) :

$$I + T \xrightarrow[t_1=t_2=0]{} 1 + 2 + 3 \quad \text{(a)}$$

$$I + T \xrightarrow[t_1>0]{} C^* \xrightarrow[t_2=0]{} 1 + 2 + 3 \quad \text{(b)}$$

$$I + T \xrightarrow[t_1>0]{} C^* \xrightarrow{} 1 + (2+3)^* \xrightarrow[t_2>0]{} 2 + 3 \quad \text{(c)}$$

$$I + T \xrightarrow[t_1=0]{} 1 + (2+3)^* \xrightarrow[t_2>0]{} 2 + 3 \quad \text{(d)}$$

Here t_1 and t_2 represent the time delays(if any) of the two steps of the reaction. Reaction (a) is called a direct-direct or simultaneous reaction. Reaction (b) may be called a delayed-direct reaction since a compound nucleus C* is formed in the first step then simultaneously breaks up into three particles. Reaction (c) and (d) may be, respectively , termed delayed-delayed or direct-delayed reactions. These latter two types of reactions are expected to show a peaked energy structure in their spectra since there will be preferential emission of particle 1 to produce the semi-stable state of (2+3)*.

Let us write a three body breakup reaction proceeding through a sequential process as I + T --> 1 + (2+3) --> 2 + 3, where (2+3) represents a bound state of 2 and 3. Furthermore, assuming that all the particles are confined in a

plane, the conservation of energy is written as

$$M_I + M_T + T_I = M_1 + M_2 + M_3 + T_1 + T_2 + T_3 \qquad (9)$$

where $M_i = m_i c^2$, $T_i = p_i^{2}/2m_i$ and initially the particle M_T is taken to be at rest. Since reaction energy or Q value is defined as

$$Q = (M_I + M_T) - (M_1 + M_2 + M_3)$$

equation (9) can be rewritten as

$$T_I + Q = \sum_{i=1}^{3} T_i \qquad (10)$$

The conservation of momentum for a coplanar reaction gives

$$P_I = \sum_{i=1}^{3} P_i \cos\theta_i \qquad (11)$$

$$0 = \sum_{i=1}^{3} P_i \sin\theta_i \qquad (12)$$

where θ_i are the angles with respect to the direction of the incoming projectile for the ith particles. T_3 and θ_3 can be eliminated from equations (10)-(12) in a straighforward manner. The resultant equation may be expressed in a form of

$$AT_2 + 2BT_2^{1/2} + C = 0$$

that is, T_2 as a function of T_1 if θ_1, θ_2 are fixed, where

$$A = M_2 + M_3$$

$$B = (M_1M_2T_1)^{1/2}(\cos\theta_1\cos\theta_2 + \sin\theta_1\sin\theta_2) - (M_IM_2T_I)^{1/2}\cos\theta_2$$

$$C = T_1(M_1 + M_3) + T_I(M_I - M_3) - 2(M_IM_1T_IT_1)^{1/2}\cos\theta_1 - M_3Q$$

The solutions of the above equation

$$T_2^{1/2}(T_1) = \frac{-B \pm (B^2 - AC)^{1/2}}{A}$$

define a curve in the $T_1 - T_2$ kinematic plane, which will hereafter be referred to as the kinematic curve.

For the first step of a sequential process in a three-body final state reaction I + T --> 1 + (2+3), the conservation of energy gives

$$T_I + Q = T_1 + T_{23} + E_{23} \qquad (13)$$

where $Q = M_I + M_T - M_1 - M_{23}$, T_{23} is the kinetic energy of the bound state (2+3) and E_{23} is the excitation energy of the state in (2+3). Since the first step of a sequential process reaction results in a two-body final state, the momentum conservation equations for the reaction occurs in a plane are given by

$$P_I = P_1\cos\theta_1 + P_{23}\cos\theta_{23} \qquad (14)$$

$$0 = P_1\sin\theta_1 + P_{23}\sin\theta_{23} \qquad (15)$$

By eliminating P_{23} and θ_{23} from equations (13)-(15) and using $T_I = \frac{P_I^2}{2M_I}$ $T_1 = \frac{P_1^2}{2M_1}$, the resulting equation is

$$M_I T_I - 2(M_I M_1 T_I T_1)^{1/2}\cos\theta_1 + M_1 T_1 = M_{23}(T_I + Q - T_1 - E_{23})$$

from which the possible excitation energies of the intermediate state (2+3) are given by

$$E_{23} = T_I(1 - \frac{M_I}{M_{23}}) - T_1(1 + \frac{M_1}{M_{23}}) + \frac{2(M_I M_1 T_I T_1)^{1/2}}{M_{23}}\cos\theta_1 + Q$$

Similarly, for the reaction of I + T --> 2 + (1+3)

$$E_{13} = T_I(1 - \frac{M_I}{M_{13}}) - T_2(1 + \frac{M_2}{M_{13}}) + \frac{2(M_I M_2 T_I T_2)^{1/2}}{M_{13}}\cos\theta_1 + Q$$

For a sequential process E_1 is related to E_2 in such a way that it corresponds to a segment on the kinematic curve, whose length is determined by the width of the intermediate state and whose location is determined by the energy of the state. As examples, the kinematic curves corresponding to sequential processes in the $^7Li(^3He,\alpha_1 d)\alpha_2$ reaction occurring via the formation of either ^6Li or ^8Be, in the $^7Li(^3He,\alpha p)^5He$ reaction via the formation of either ^6Li or ^9Be, at a ^3He bombarding energy of 2.15 MeV and $^6Li(5.37)$ recoil angle of -129.6^o are shown in Fig.2. These serve as one means of testing the consistency of the data which will be taken from the experiment. If the reaction proceeds sequentially, it is expected that intensity peaks will appear along the kinematically allowed line in the (E_1, E_2) plane at positions which correspond to levels populated in the intermediate nuclei. However, the kinematic curve for a simultaneous process, in which the bound state of (2+3) is

α–α Kinematic Curve for the Reaction $^{7}Li(^{3}He,\alpha d)\alpha$

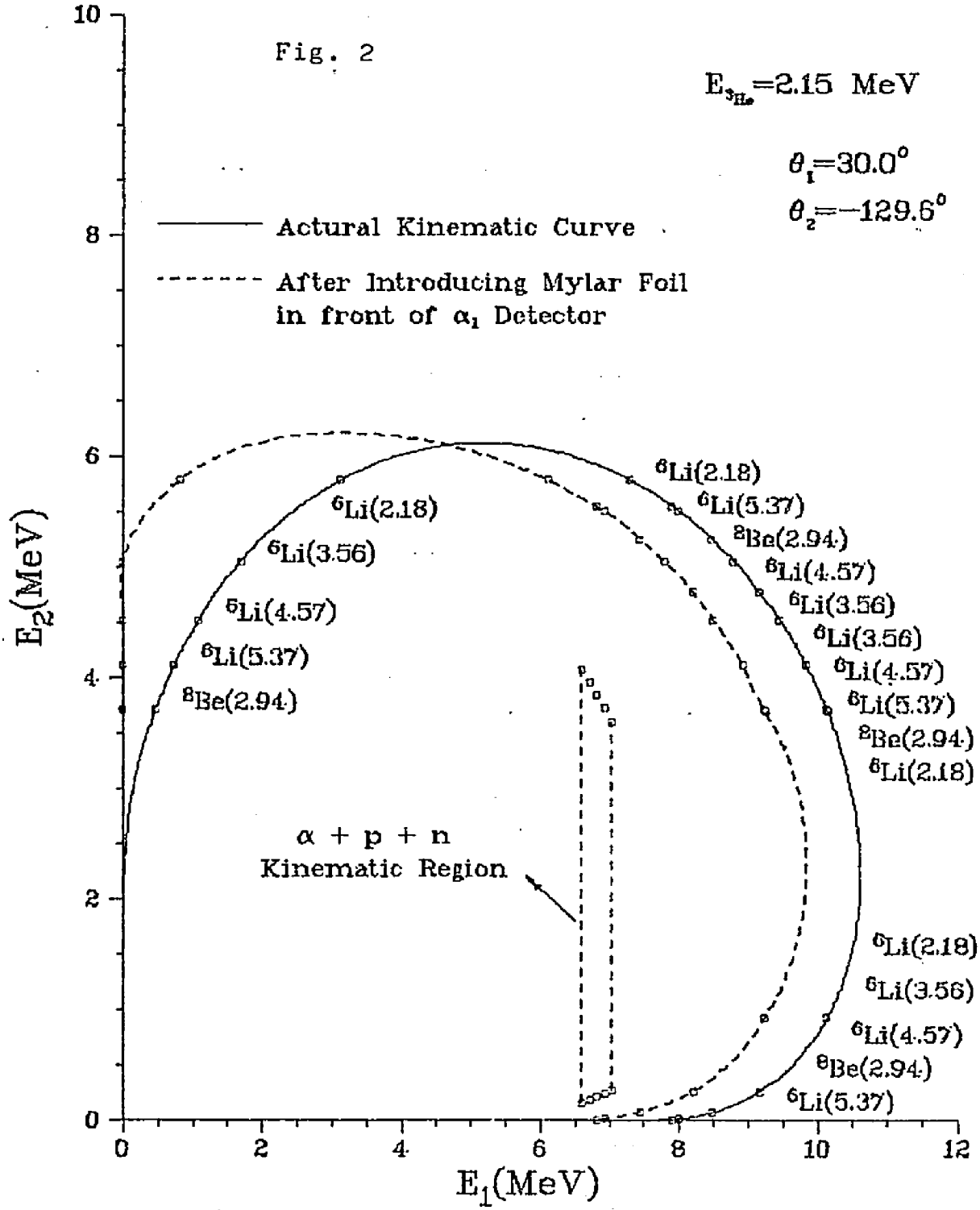

not formed, is a continuous curve, i.e, E_1 lies all over the kinematic curve as a function of E_2.

For the four-body final state reactions, there is a kinematic region instead of a kinematic curve. A vertical band with its two ends corresponding to the maximum and minimum of E_2 defines this region, which represents the process of direct breakup into α + p + n.

C. Velocity Vector Diagram

While the cross section for a two particle reaction depends only on two independent kinematical variables, there are five such variables in the case of a three body final state reaction. Therefore, the kinematics of the final state of a three body breakup reaction can not be completely specified by using a single detector. However, it can be specified thoroughly by detecting two of the particles in the final state in coincidence and measuring the energy of at least one of them.

The most convienent way of looking at the kinematics of a three body breakup reaction is by drawing a velocity vector diagram. A velocity vector diagram has been drawn for both the $^{7}Li(^{3}He,\alpha_1 d)\alpha_2$ and the $^{7}Li(^{3}He,p\alpha_1)^{5}He \rightarrow n + \alpha_2$ reaction and is shown in Fig.3. All the vector lengths and relevant angles needed to draw a velocity vector diagram can

Velocity Vector Diagram for the Reaction $^{7}Li(^{3}He,\alpha)^{6}Li$

Fig. 3

$E_{^{3}He}$=2.15 MeV

θ_{α_1}=30.0°

θ_{R}=−129.6°

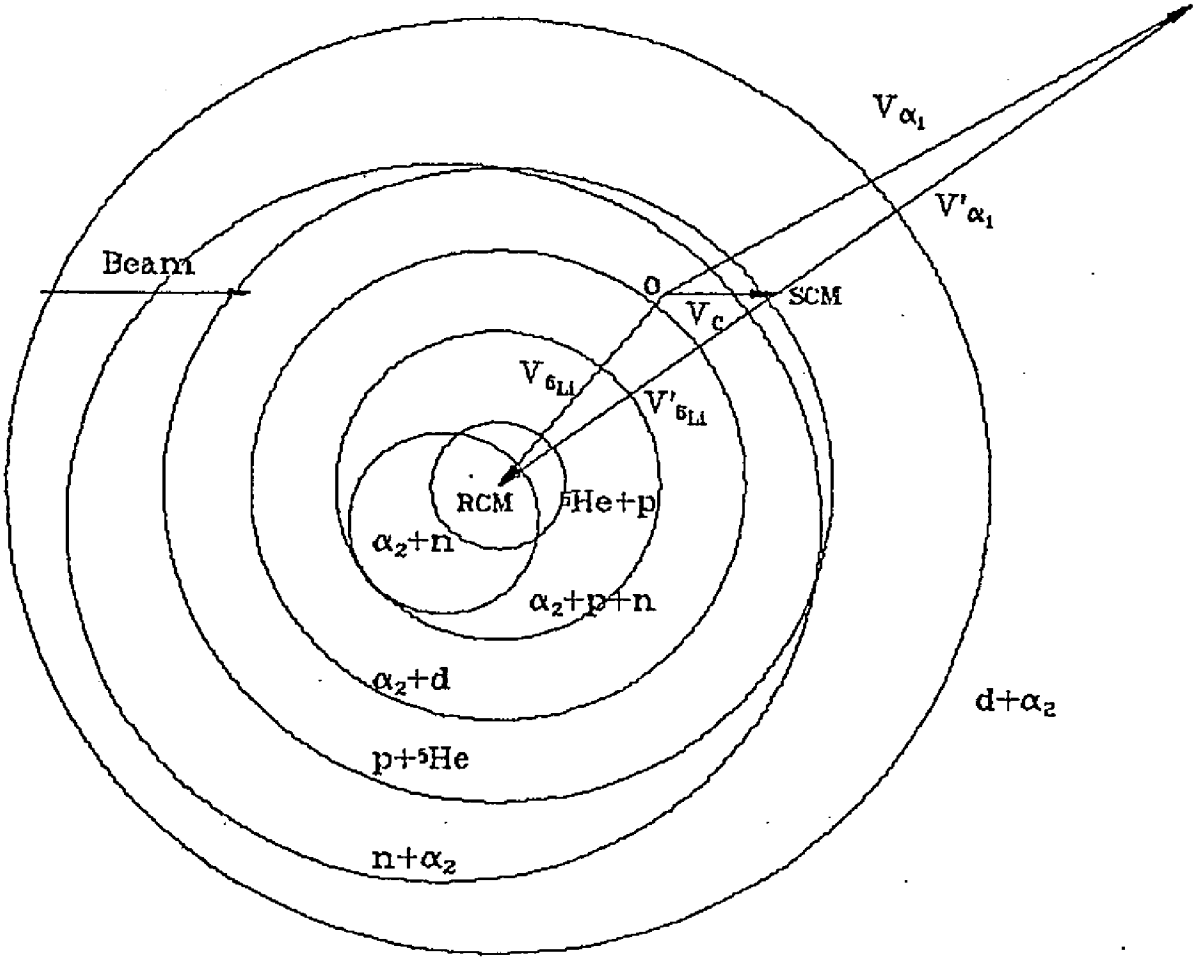

be calculated by using the conservation of energy and momentum equations.

The various velocities required in the velocity vector diagrams can be calculated by using the following expressions:

$$V_c = \frac{M_1}{M_1+M_2}\left(\frac{2E_1}{M_1}\right)^{1/2}$$

$$V_3' = \left[\frac{2M}{M_3(M_3+M)}\left(\frac{M_2E_1}{M_1+M_2}+Q^n\right)\right]^{1/2}$$

$$V' = \left[\frac{2M_3}{M(M_3+M)}\left(\frac{M_2E_1}{M_1+M_2}+Q^n\right)\right]^{1/2} = \frac{M_3}{M}V_3'$$

$$V_4'' = \left[\frac{2M_5}{M_4M}(Q^m-Q^n)\right]^{1/2}$$

$$V_5'' = \left[\frac{2M_4}{M_5M}(Q^m-Q^n)\right]^{1/2} = \frac{M_4}{M_5}V_4''$$

$$V_6''' = \left[\frac{2M_7}{M_5M_6}E^m\right]^{1/2}$$

$$V_7''' = \frac{M_6}{M_7}V_6'''$$

where particle 1 is the incident projectile; 2, the target; 3, the first particle emitted in the sequence; 4 and 5 are the breakup particles from the recoiling nucleus; and 6 and 7 are the breakup particles resulting from the decay of particle 5. The variables without subscripts refer to the recoiling system, (4+5).

$$Q^m = [M_1+M_2-M_3-M_4-M_5]c^2$$

where the superscript m refers to a specific combination of internal states of particles 3, 4 and 5.

$$Q^n = [M_1+M_2-M_3-M^n]c^2$$

where n refers to a particular combination of internal states of the recoiling system.

$$E^m = (M_5{}^m-M_6-M_7)c^2$$

when particle 5 undergoes break up into 6 and 7.

D. Analysis of Reaction Mechanism

The occurrence of resonance structure in the excitation curves for ^{3}He induced reactions indicates that these reactions proceed at least partially through both compound nucleus(CN) and direct interaction(DI) mechanisms and interference between the corresponding amplitudes makes detailed analysis of the angular distribution data complicated(Ref.16).

The angular distributions of CN-dominated reaction cross sections have qualitative properties that depend on the extent of averaging over resonances(Ref.26). Thus an isolated resonance incorporates basis states of only one parity, therefore in each exit channel it couples only to

partial waves that are all odd or all even. Therefore the ensuing differential cross sections are symmetric about 90^{o} scattering angle in the CM system. Any overlap of resonances of opposite parity allows simultaneous coupling to both odd and even partial waves and therefore allows fore-aft asymmetry to appear. The angular distribution may peak in either the forward or backward hemisphere. However, this interference of resonances of opposite parity may be eliminated by averaging over many resonances, either by averaging over E or by going to circumstances in which many resonances overlap. Such averaging again yields a cross section that is symmetric about 90^{o}. Under special conditions(Ref.27,28), this cross section may be isotropic.

Rapidly oscillatory angular distributions involve states of high angular momentum(Ref.29), and they probably indicate a DI mechanism(Ref.26). Angular distributions that show a fore-aft asymmetry that persists over a large energy range also must involve a DI reaction mechanism. Persistent asymmetries indicate persistent phase relations among overlapping CN levels of opposite parity and these indicate the presence of an underlying simple reaction mechanism. Although a pure CN mechanism also allows asymmetric angular distribution, it causes backward peaking as often as forward(Ref.26).

The persistent DI angular distributions often show strong forward peaking. However, strong distortion effects

can spoil the forward peaking of DI angular distributions and can even cause peaking in the backward hemisphere(Ref.26). Such failures of forward peaking are especially likely at low bombarding energy.

The partial waves that are most strongly distorted by the field of the target core tend not to initiate DI processes. This may be the reason why forward peaking survives as a major aspect of DI reactions(Ref.26).

The relatively rapid change of angular distributions with bombarding energy suggests a compound nucleus mechanism while the persistence of structural features such as the forward peaking or backward peaking, which becomes more pronounced with increasing energy, suggests a direct reaction(Ref.16). For example, angular distributions in the $^{16}O(^{3}He,\alpha)^{15}O$ reaction measured at on-resonance energy show characteristic symmetry about 90^{o} in the center of mass system(Ref.30,31). At slightly higher energy, at the minimum in the alpha excitation curve, the angular distribution shows a lack of symmetry and an increase in the cross section at backward angles, suggesting that the reaction has a small direct interaction amplitude, which is almost completely masked at strong compound nucleus resonances. In the case of the $^{14}N(^{3}He,p)^{16}O^{*}$ reaction(Ref.31), the isotropy of all the proton and γ radiation angular distributions as well as of the p-γ angular correlations, together with the observed lack of structure in the excitation curves, suggest a

compound system reaction mechanism.

An asymmetry about RCM(recoiling center of mass) system for the secondary decay in the sequential reaction $^{6}Li(^{3}He,\alpha)^{5}Li-->\alpha+p$ was accounted for as a proton localization by Reimann, Martin, and Vogt using the RMV model(Ref.20). According to this model, which is essentially geometrical, there are two possible types of direct interactions that can occur in the first step of the $^{6}Li(^{3}He,\alpha)^{5}Li$ reaction; either a neutron transfer or a deuteron transfer from the ^{6}Li target nucleus to the incoming ^{3}He. A forward peaking in the angular distribution curve will indicate a neutron-transfer while a backward peaking in the angular distribution curve probably indicates a deuteron-transfer.

Heggie et al. have indicated that a shift in the minimun of the angular correlation pattern away from the recoil direction can also be produced by a CN formation in the first step of a sequential process reaction provided two CN states of opposite parities participate in the reaction(Ref.23). Such a possibility might exist in the $^{7}Li(^{3}He,\alpha p)^{5}He$ reaction at 1.44 MeV ^{3}He bombarding energy where the 18.8 MeV ^{10}B state (<600 KeV, 2^{+}) will be formed. At this bombarding energy, either the 18.43 MeV level in ^{10}B (340 KeV, 2^{-}) and/or the 19.3 MeV level (190 ± 20 KeV, 2^{-}) may be excited(Fig.4). Therefore, an observation of an asymmetry about the recoil axis could be due to interference between the two CN states of opposite parities. Further

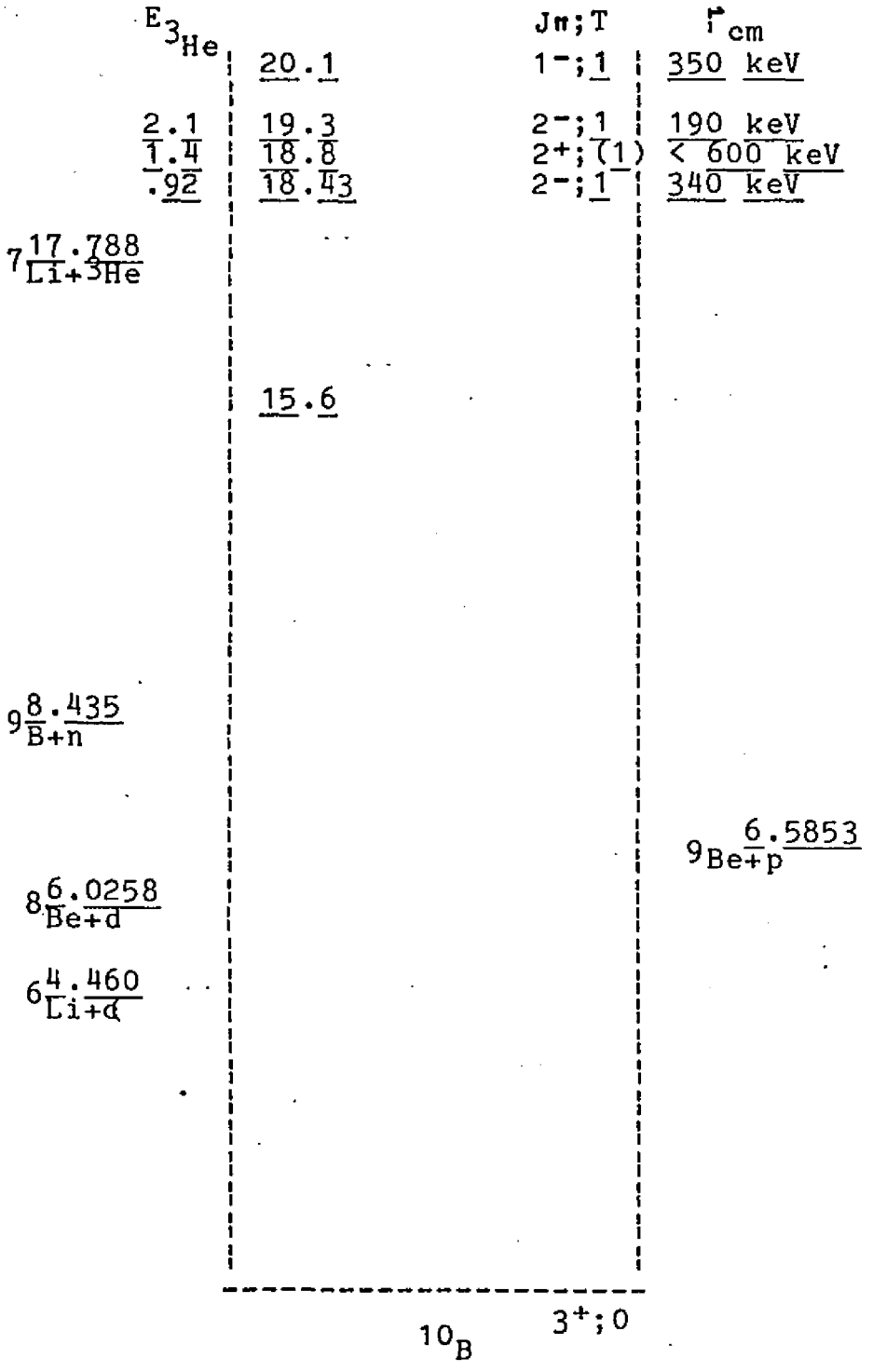

Fig.4 Relevant Part of Energy Levels of ^{10}B

information can be obtained by examing the periodicity in the secondary decay with respect to the recoiling rest frame. By application of Bohr's symmetry principle(Ref.32), a 180^{o} periodicity in the angular correlation data measured in the frame of reference of the recoiling system will indicate that the reaction proceeds through intermediate states of well defined parity.

E. DWBA Theories

The transition amplitude for the reaction A(a,b)B using DWBA is of the form

$$T_{if}^{DW} = J\int dr_f \int dr_i X_f^{(-)*}(k_f,r_f)\langle bB|V|aA\rangle X_i^{(+)}(k_i,r_i) \qquad (16)$$

where $X_f^{(-)}$ and $X_i^{(+)}$ are the distorted waves, $r_i = r_a - r_A$ and $r_f = r_b - r_B$ are the relative coordinates, and J is the Jacobian of the transformation to these coordinates. The quantity $\langle bB|V|aA\rangle$ is the form factor for the reaction and must contain a delta function for the coordinates r_a and r_b. It contains all the information on nuclear structure, on angular momentum selection rules, and even on the type of reaction being considered. If we define the transfer angular momentum to be

$$j = J_B - J_A \qquad s = s_a - s_b \qquad l = j - s$$

then the nuclear matrix element becomes

$$J\langle bB|V|aA\rangle = J\langle J_B M_B, s_b m_b|V|J_A M_A, s_a m_a\rangle$$

$$= \sum_{lsj} i^{-l} G_{lsj,m}(r_f,r_i;bB,aA)(-)^{s_b-m_b}\langle J_A j; M_A, M_B-M_A|J_B M_B\rangle \quad X$$

$$\langle s_a s_b; m_a,-m_b|s,m_a-m_b\rangle\langle ls;m,m_a-m_b|j,M_B-M_A\rangle \qquad (17)$$

where $m = M_B + m_b - M_A - m_a$. The symbols bB, aA as arguments of $G_{lsj,m}$ denote its dependence on the various nuclear quantum numbers(other than z-components of spin). It is often helpful to write $G_{lsj,m}$ as a product of two factors

$$G_{lsj,m}(r_f,r_i) \equiv A_{lsj}\, f_{lsj,m}(r_f,r_i)$$

so that standard types of form factors with simple normalization may be used in computation. With the introduction of (17) into (16) the DW transition amplitude reduces to a sum over multipole contributions in a standard form of

$$T_{if}^{DW} = \sum_{lsj} (2l+1)^{1/2} A_{lsj} (-)^{s_b-m_b}\langle J_A j; M_A, M_B-M_A|J_B M_B\rangle \quad X$$

$$\langle ls;m,m_a-m_b|j,m-m_b+m_a\rangle\langle s_a s_b; m_a,-m_b|s,m_a-m_b\rangle \beta_{sj}^{lm}$$

Here the reduced amplitude β_{sj}^{lm} is defined so that

$$(2l+1)^{1/2} i^l \beta_{sj}^{lm} = \int dr_f \int dr_i X_f^{(-)*}(k_f,r_f) f_{lsj,m}(r_f,r_i) \quad X$$

$$X_i^{(+)}(k_i,r_i) \qquad (18)$$

In most current distorted waves calculations the difficulty in evaluating the six-dimensional integral is removed by the assumption that the form factor is of very

small range. This zero-range approximation has the physical meaning that the light particle b in channel f is assumed to be emitted at the same point at which the light particle a in channel i is absorbed. For example, if the reaction involves x-particle transfer: B-A=x=a-b, the ZRA implies $r_a = r_b = r_x$ and therefore

$$r_f = r_b - r_B = r_a - \frac{M_A r_A + M_x r_x}{M_A + M_x} = \frac{M_A}{M_B} r_i$$

where $M_B = M_A + M_x$. The form factor can thus be expressed as

$$f^{(zero)}_{lsj,m}(r_f,r_i) = \delta(r_f - \frac{M_A}{M_B} r_i)\int f_{lsj,m}(s + \frac{M_A}{M_B} r_i, r_i)d^3s$$

$$\simeq F_{lsj}(r_i)Y_l^{m*}(\hat{r}_i)\delta(r_f - \frac{M_A}{M_B} r_i)$$

Consequently, equation (18) reduces to the form of

$$(2l+1)^{1/2} i^l \beta^{lm}_{sj} = \int d^3r X_f^{(-)*}(k_f, \frac{M_A}{M_B} r) F_{lsj}(r) Y_l^{m*}(\hat{r}) \quad X$$

$$X_i^{(+)}(k_i,r) \qquad (19)$$

The distorted waves in the form of the partial wave expansions are

$$X_i^{(+)}(k_i,r_i) = \frac{4\pi}{k_i r_i} \sum_{l,m} i^l e^{i\sigma_{il}} f_{il}(k_i,r_i) Y_l^m(\hat{r}_i) Y_l^{m*}(\hat{R}_i)$$

$$X_f^{(-)*}(k_f,r_f) = \frac{4\pi}{k_f r_f} \sum_{l,m} i^{-l} e^{i\sigma_{fl}} f_{fl}(k_f,r_f) Y_l^m(\hat{R}_f) Y_l^{m*}(\hat{r}_f)$$

inserting into (19) and integrate the angular part yields

$$\beta_{sj}^{lm} = \sum_{\substack{L_i L_f \\ M_i M_f}} i^{L_i - L_f - l} e^{i\sigma_i L_i + i\sigma_f L_f} \left[\frac{4\pi(2L_f + 1)}{(2L_i + 1)}\right]^{1/2} I_{L_f L_i}^{lsj} \; X$$

$$\langle L_f l; 00 | L_i 0\rangle \langle L_f l; M_f m | L_i M_i\rangle Y_{L_f}^{M_f}(\hat{R}_f) Y_{L_i}^{M_i *}(\hat{R}_i) \qquad (20)$$

where

$$I_{L_f L_i}^{lsj} = \frac{M_B}{M_A} \frac{4\pi}{k_i k_f} \int_0^\infty F_{lsj}(r) f_{fL_f}(k_f, \frac{M_A}{M_B} r) f_{iL_i}(k_i, r) dr$$

It is often of interest to choose the coordinate axes so that the z-axis lies along k_i and the y-axis lies along $k_i \times k_f$. In such a case equation (20) reduces to the more compact form

$$\beta_{sj}^{lm} = \sum_{L_i L_f} i^{L_i - L_f - l} e^{i\sigma_i L_i + i\sigma_f L_f} (2L_f + 1)^{1/2} I_{L_f L_i}^{lsj} \; X$$

$$\langle L_f l; 00 | L_i 0\rangle \langle L_f l; -m, m | L_i 0\rangle Y_{L_f}^{-m}(\theta, 0)$$

where θ is the scattering angle, the angle between k_i and k_f.

Insert the amplitude into

$$\frac{d\sigma_{if}}{d\Omega_f} = \frac{\mu_i \mu_f}{(2\pi\hbar^2)^2} \left(\frac{k_f}{k_i}\right) |T_{if}|^2$$

sum over final spin projections and average over initial spin projections. Therefore

$$\frac{d\sigma}{d\Omega} = \frac{\mu_i\mu_f}{(2\pi\hbar^2)^2}\left(\frac{k_f}{k_i}\right)\left(\frac{N_f}{N_i}\right)(2J_A+1)^{-1}(2s_a+1)^{-1}\sum_{\substack{M_A,M_B\\ m_a,m_b}}|T_{if}|^2 \qquad (21)$$

$$= \frac{\mu_i\mu_f}{(2\pi\hbar^2)^2}\left(\frac{k_f}{k_i}\right)\left(\frac{n_a!n_A!}{n_b!n_B!}\right)\frac{2J_B+1}{(2J_A+1)(2s_a+1)}\sum_{lsj}|A_{lsj}|^2\sum_m|B^{lm}_{sj}|^2 \qquad (22)$$

The factor $N_f/N_i = \frac{n_a!n_A!}{n_b!n_B!}$ is inserted into (21) to account for the numbers of equivalent arrangements of nucleons in channels i and f. The sum over l,s,j is incoherent as if equation (22) were a description of a total cross section for the "capture" of the l,s,j multipole. Thus different multipoles make noninterfering contributions to the differential cross section. This property is a very basic result of the distorted-waves approximation.

The computer code DWUCK4 calculates the scattering differential cross section for a general form of the distorted wave Born approximation. The calculations are performed in a zero range approximation between the coordinates of the incoming and the outgoing waves. The program computes the cross sections:

$$\sigma^{lsj}_{DW} = \frac{1}{4\pi E_a E_b}\frac{k_b}{k_a}\left(\frac{C^2}{AB}\right)^2\frac{1.0X10^4}{2s_a+1}(2l+1)\sum_{mm_am_b}|S^{mm_am_b}_{lsj}|^2$$

in units of fm^2/ster ($1fm^2$ = 10 mb), where C is the mass of the core nucleus to which the transferred particle is bound. Therefore the cross section is

$$\frac{d\sigma^{lsj}}{d\Omega} = \frac{2J_B + 1}{2J_A + 1} \frac{|B_{lsj}|^2}{1.0X10^4} \frac{\sigma^{lsj}_{DW}}{2j + 1}$$

where the relation between $S^{mm_am_b}_{lsj}$ and the reduced amplitude B^{lm}_{sj} of equation (22) is

$$S^{mm_am_b}_{lsj} = \sum_{L_b} B^{mm_am_b}_{lsj;L_b} P^{m_a-m-m_b}_{L_b}(\theta)$$

The quantity B_{lsj} is a measure of the strength of the interaction and is equal to $[(2s+1)/(2s_a+1)]^{1/2}A_{lsj}$, where A_{lsj} is the spectroscopic coefficient in equation (22).

F. Phase Space Distributions

The energy-angular distribution $d^2\sigma/dEd\Omega$ for one of the final state particles is proportional to the corresponding transition probability which has the form(Ref.43)

$$w = \frac{2\pi}{h}|\langle b|H|a\rangle|^2 \frac{dN}{dE}$$

where $\langle b|H|a\rangle$ is the matrix element for the transition from initial state a to finai state b, and dN/dE is the density of final states. For direct break-up, $\langle b|H|a\rangle$ is commonly assumed to be a constant, so that the decay probability is uniform over the available phase space.

The density of states factor dN/dE for ^{6}Li --> d+p+n decay is proportional to $[E_d(Q/3 - E_d)]^{1/2}$ (Ref.44), where E_d is the alpha-particle energy and Q=1.67 MeV is the three

body decay energy.

For comparison between the theoretical phase space distributions and the experimentally observed energy spectrum, a coordinate transformation directly from the CM-system to the LAB-system using the appropriate Jacobian has been calculated. The expression derived is as follows:

$$d^2\sigma/dEd\Omega = J^L d^2\sigma/dE'd\Omega'$$

$$\text{where} \quad J^L = \frac{\partial(E',\cos\theta')}{\partial(E,\cos\theta)} = \frac{\sin\theta'}{\sin\theta} = \frac{\cos\theta' + K}{\cos\theta}$$

$$\text{with } K = \frac{V_c}{v'}$$

primed and unprimed symbols denote quantities expressed in the CM-system and LAB-system respectively.

The partial derivatives of the coordinates are

$$\frac{\partial E}{\partial E'} = 1 + K\cos\theta', \quad \frac{\partial\theta}{\partial\theta'} = \frac{1 + K\cos\theta'}{1 + 2K\cos\theta' + K^2}$$

$$\frac{\partial E}{\partial\theta'} = -2KE'\sin\theta', \quad \frac{\partial\theta}{\partial E'} = \frac{(K/2E')\sin\theta'}{1 + 2K\cos\theta' + K^2}$$

Transformations between E and E'; θ and θ' have been derived earlier in section II with the results

$$E = E'(1 + 2K\cos\theta' + K^2)$$

$$\tan\theta = \sin\theta'/(\cos\theta' + K)$$

The expression for the energy spectrum of outgoing particle coming from the secondary break-up of a sequential

two-stage nuclear reaction of the form

$$\begin{array}{l} A + B \text{ ---> } C + D, \\ \qquad\qquad\quad \vdots \\ \qquad\qquad\quad \text{----> } F + G \end{array}$$

has been developed by Morinigo(Ref.45) for the case of intermediate states that have the shape of simple resonances. Assuming isotropic decay, the result is

$$d^2\sigma/d\Omega dE = \frac{g}{m}(g^2+u^2-2ugz)^{-1/2}\int_{v'}^{v''} W'(v)W''(w)vdv \qquad (23)$$

where u is the velocity of the center of mass of the entire system, relative to the Lab, v the velocity of C relative to the center of mass, w the velocity of G relative to the center of mass of F and G, and g the velocity of G relative to the Lab., $z=\cos\theta$, θ is the angle between u and g. The geometric relations between these velocity vectors are illustrated in Fig. 5. W'(v) and W"(v) are the probability distribution functions of v and w respectively. v' and v" are the two physically meaningful roots of

$$v = \frac{\pm\, t \pm [\mu v_o^2(1+\mu)-\mu t^2]^{1/2}}{1+\mu}$$

where $t = (g^2+u^2-2ugz)^{1/2}$

$$\mu = \frac{m_C m_F (m_D+m_C)}{m_D m_G (m_G+m_F)}$$

Assuming that W'(v) and W"(w) both have the analytic form of simple resonances,

$$W'(v) = \frac{1}{(v^2-v_R^2)^2+\lambda^2}, \qquad W''(v) = \frac{1}{(w^2-w_R^2)^2+\rho^2}$$

where $w = [\mu(v_o^2-v^2)]^{1/2}$, $v_o^2 = 2m_D\frac{Q+Em_B/(m_A+m_D)}{m_C(m_C+m_D)}$

By changing the variables $E=v^2$, $dE=2vdv$, $E'=E(v')$, $E''=E(v'')$, Equation (23) becomes

$$\frac{d^2\sigma}{d\Omega dE} = \frac{g}{m}(g^2+u^2-2ugz)^{-1/2}\mu^{-2} \times$$

$$\int_{E'}^{E''} \frac{dE}{[(E-v_R^2)^2+\lambda^2][(\mu E-\mu v_o^2-w_R^2)^2+\rho^2]}$$

Let a series of set of complex parameters

$a = v_R^2+i\lambda$, $b = a^*$, $c = v_o^2+w_R^2/\mu+i\rho$, $d = c^*$

After expanding the integrand in partial fraction and integrating it, the result is

$$\frac{d^2\sigma}{d\Omega dE} = \frac{g}{m}(g^2+u^2-2ugz)^{-1/2}\mu^{-2}\ln\left[\left|\left(\frac{E''-a}{E'-a}\right)^A\right|^2 \left|\left(\frac{E''-c}{E'-c}\right)^C\right|^2\right]$$

where $A = [(a-b)(a-c)(a-d)]^{-1}$, $C = [(c-a)(c-b)(c-d)]^{-1}$

Fig. 5

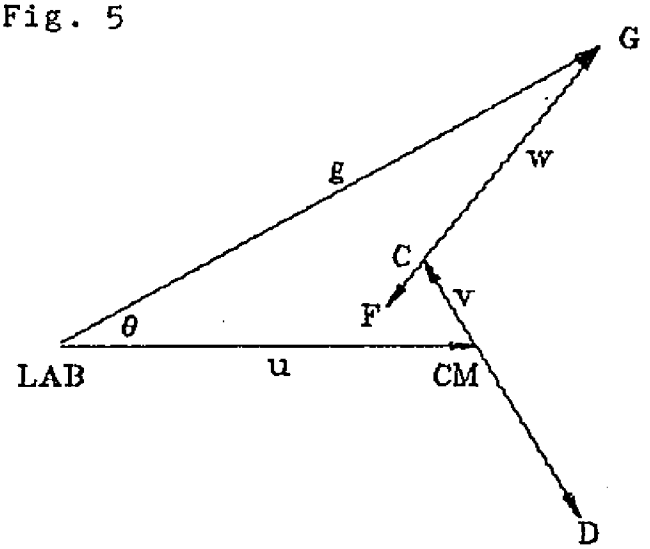

For the simplest case of sharp resonance state, which is of greatest pratical interest. The expression is

$$\frac{d^2\sigma}{d\Omega dE} = \frac{g}{m} \frac{C}{(g^2+u^2-2ugz)^{1/2}}$$

where C is an arbitrary normalization constant.

G. Angular Correlation

A sequential process in a three body breakup reaction is often examined by measuring the angular correlation between 1 and 2. Angular correlation refers to a measurement of the coincidence between 1 and 2 as a function of the angles between their directions of emission.

The angular correlation involving mixed radiations with the angular momentum sequence: $j_1(L_1L_1')J(L_2L_2')j_2$ is given by(Ref.33-38)

$$W(\theta) = \sum_k [a_k(1)A_k(1)][a_k(2)A_k(2)]P_k(\cos\theta)$$

where the coefficients $A_k(i),(i=1,2)$ have the definition:

$$A_k(i) = F_k(L_i j_i J)+2\delta_i F_k(L_i L_i' j_i J)+\delta_i^2 F_k(L_i' j_i J)$$

The F_k are defined by:

$$F_k(LL' j_i J)$$

$$= (-)^{j_i-J-1}[(2L+1)(2L'+1)(2J+1)]^{1/2}(LL'1-1|k0)W(JJLL';kj_i)$$

The mixing parameter δ_i is defined as a relative intensity, that is

$$\delta^2 = \frac{\text{Intensity of radiation } L'}{\text{Intensity of radiation } L} = [\frac{(j|L'|J)}{(j|L|J)}]^2$$

In the angular momentum sequence, J always denotes the angular momentum of the intermediate state, j_i denotes the angular momentum of the initial or final state, L_i, L_i' are the orbital angular momentum of the particle radiation, and k is restricted by $k \leq \min(2J, 2L_i, 2L_f)$.

For pure transitions, the spinless particle parameter is given by

$$a_k(LL) = \frac{2L(L+1)}{2L(L+1)-k(k+1)}$$

The charged particle parameters for mixed angular momentum L & L' are

$$a_k(LL') = a_k(L'L) = \cos(\xi_L - \xi_{L'}) \times \frac{2[L(L+1)L'(L'+1)]^{1/2}}{[L(L+1)+L'(L'+1)-k(k+1)]}$$

where

$$\exp(2i\xi_L) = \exp(2i\sigma_L) \times \frac{[G_L(\eta,kR)-iF_L(\eta,kR)]}{[G_L(\eta,kR)+iF_L(\eta,kR)]}$$

$$\sigma_L = \arg\Gamma(L+1+i\eta)$$

$$\eta = \frac{Z_1 Z_2 e^2}{\hbar v} = \frac{M Z_1 Z_2 e^2}{\hbar^2 k}$$

$$k = (2ME/\hbar^2)^{1/2}$$

F_L, G_L are the regular and irregular coulomb function respectively.

For uncharged particles, $\cos(\xi_L - \xi_{L'}) = 1$ is a useful approximation.

If the particle with spin is observed, either as a bombarding or final outgoing particle, one replaces the factor $F_k(LL'jJ)$ by the factor $F_k(LL'j_sJ)$, that is, the channel spin j_s replaces j, and the spinless particle parameter is used. $j_s = |I+s|$ where I is the initial(final) nuclear angular momentum and s is the angular momentum of the particle absorbed(or emitted) in the transition. For several channel spins, the correlation is the weighted sum of the separate correlations.

If the particle with spin is observed, but is neither a bombarding nor a final outgoing particle, one replaces j by the "fictious" channel spin $j_s' = s + j_{initial}$ and proceeds as last paragraph.

If the particle with spin is not observed, the angular correlation function with the angular momentum sequence: $j_1(L_1L_1')J(L)\mathcal{J}(L_2L_2')j_2$ is given by

$$W(\theta) = \sum_k [a_k A_k(1)][a_k A_k(2)][C_k] P_k(\cos\theta)$$

The first link, $[a_k A_k(1)]$, is given by the sequence $j_1(L_1 L_1')J$; the second link, $[a_k A_k(2)]$, is given by the sequence $J(L_2 L_2')j_2$. The term C_k is given by

$$C_k = [(2J+1)(2J+1)]^{1/2} W(jkj_p J; jJ)$$

where j_p denotes the particle's total angular momentum.

Numerical values of the F_k coefficients are tabulated in Ref.36,37. The Wigner coefficients and Racah coefficients involved in F_k are also tabulated in Ref.40,41. $P_k(\cos\theta)$ are the ordinary Legendre polynomials.

Application of the above derived formulas to the $^7Li(^3He,d)^6Li(5.37,2^+)\text{-->}^5He(\frac{3}{2}^-) + p(\frac{1}{2}^+)$ reaction gives the angular momentum sequence $2(13)2(13)\frac{1}{2}$. The particle with spin is observed, so that we use the channel spins for this stage of correlations; There are two channel spins possible; $j_s = 1, 2$. The correlation is therefore the weighted sum of two disintegration schemes $2(13)2(13)1$ for $j_s=1$, and $2(13)2(13)2$ for $j_s=2$. Thus

$$W(\theta) = W_{j_s=1} + \beta^2 W_{j_s=2}$$

with β^2 the ratio of the probabilities of forming the intermediate state via channel spin 2 relative to channel spin 1(from an experimental point of view β^2 is a parameter to be fitted to the data). For $j_s=1$

$$W_{j_s=1} = 1 + [a_2(11)F_2(122) + 2\delta a_2(13)F_2(1322) + \delta^2 a_2(33)F_2(322)][a_2(11)F_2(112) + 2\delta a_2(13)F_2(1312) + \delta^2 a_2(33)F_2(312)]P_2(\cos\theta)$$

and similarly for $j_s=2$

$$W_{j_s=2} = 1 + [a_2(11)F_2(122) + 2\delta a_2(13)F_2(1322) + \delta^2 a_2(33)F_2(322)]^2 P_2(\cos\theta)$$

As to the $^7Li(^3He,\alpha)^6Li(5.37,2^+)\text{-->}\alpha(0^+)+p+n$ reaction, the angular momentum sequence is 2(1,3)2(0,2)0, the restriction on k gives k=4. Therefore, the angular correlation function is

$$W(\theta) = \sum_{k=0}^{4} [a_k(1)A_k(1)][a_k(2)A_k(2)]P_k(\cos\theta)$$

III. EXPERIMENTAL APPARATUS AND PROCEDURES

A. Beam Production and Handling

A singly charged ^3He beam of energy ranging from 0.9 to 3.5 MeV was provided by the Brooklyn College 3.75 MV Dynamitron Accelerator. The system employs a duoplasmatron ion source, located in the high voltage terminal, to produce a beam of charged particles. High purity(99.99%) ^3He, supplied by the Monsanto Mound Laboratories, was mixed with high purity ^4He as the source gas. The mass-analysis system in the ion source permitted selection of only ^3He ions for acceleration.

The beam was accelerated to ground through an evacuated acceleration tube which was energized by a constant power supply, a multi-stage rectifier system, powered by a high frequency oscillator. Then, it was electrostatically focused and steered into a pair of 60^o bending magnets which deflected the beam through a switching magnet into the appropriate beam leg, and was focused by a quadrupole lens before it entered the scattering chamber.

The beam energy was determined and regulated by a standard slit-feedback system following the 120^o bend through the analyzing magnet. The analyzing magnetic field was measured by means of an NMR probe and was calibrated us-

ing the known threshold energy of 1880.60±0.7 KeV for the $^{7}Li(p,n)^{8}Be$ reaction, the resonance energy at 872.11±0.20 KeV for the $^{19}F(p,d\gamma)^{18}O$ reaction, and the resonance energy at 991.90 ±0.04 KeV for the $^{27}Al(p,\gamma)^{28}Si$ reaction. Energy stability was typically ~1 keV with the slit-feedback system in operation. The slits were closed down to ~0.1 inch separation, both to maintain energy stability and to limit the beam current on target. Reproducibility of beam energy was found to be within ~10 keV.

B. Scattering Chamber

A 17" diameter scattering chamber consisting of two turn-tables, one on the top and the other on the bottom, which can rotate about an axis through the center of the chamber, was used throughout the experiments. Detector systems could be mounted on either the turntables or the inside side-wall of the chamber in such a way that all the detectors were in the same plane. Short cables lead from the detectors to the BNC connectors in the chamber wall where the preamplifiers are attached.

The targets were mounted on a target ladder coupled through an O-ring seal in the top of the chamber. It can be raised, lowered and rotated. A gate-valve , located between the target ladder and the scattering chamber provides the possibility of transferring the targets without breaking va-

cuum.

A collimator system(Fig.6) made up of three circular aperture discs with spacing 1" and aperture diameter 1/4", 1/8" and 5/32" in sequence was used to obtain the required accuracy of beam direction. All aperture discs and the main collimator-locating tube were insulated from each other so that beam current on the individual apertures could be measured using a precision laboratory Keithley picoammeter. This made it possible to tune the beam precisely on the target. Typical beam spot size was ~2 mm diameter with a target to collimator current ratio of ~100:1. A Faraday cup 15" deep, located on the exit side of the chamber, was used to collect the total charge which was integrated by an ORTEC current digitizer.

High vacuum required inside the chamber was obtained by using a model LH-TURBOVAC 350 turbomolecular pump backed up by a mechanical pump. The chamber vacuum was kept better than 5×10^{-6} Torr throughout the experiments.

C. Detectors

Detector Thicknesses were chosen based upon the energies of the various outgoing particles from the reaction of $^{7}Li + {}^{3}He$, which have been plotted as a function of detection angles in Fig.7.

EXPERIMENTAL SET–UP

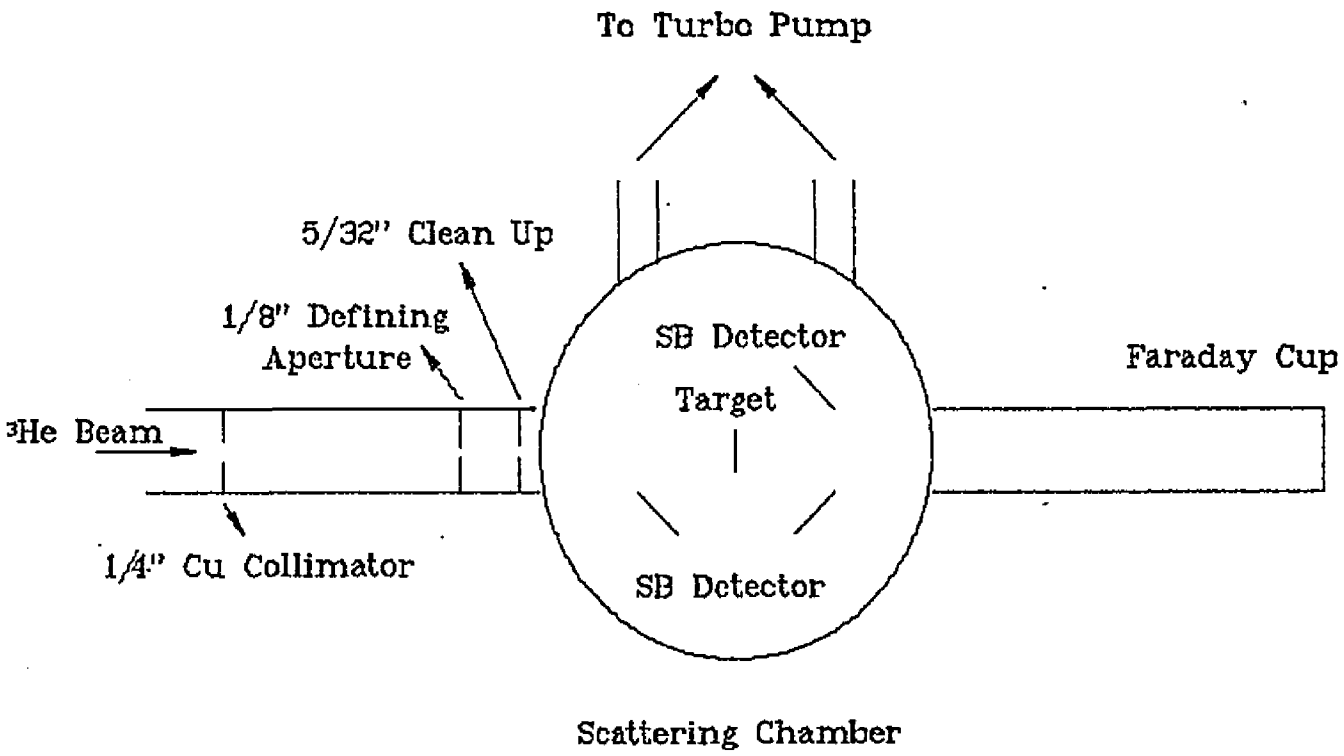

Fig. 6

Kinematics for the Reaction

$^{7}Li(^{3}He,\alpha)^{6}Li$

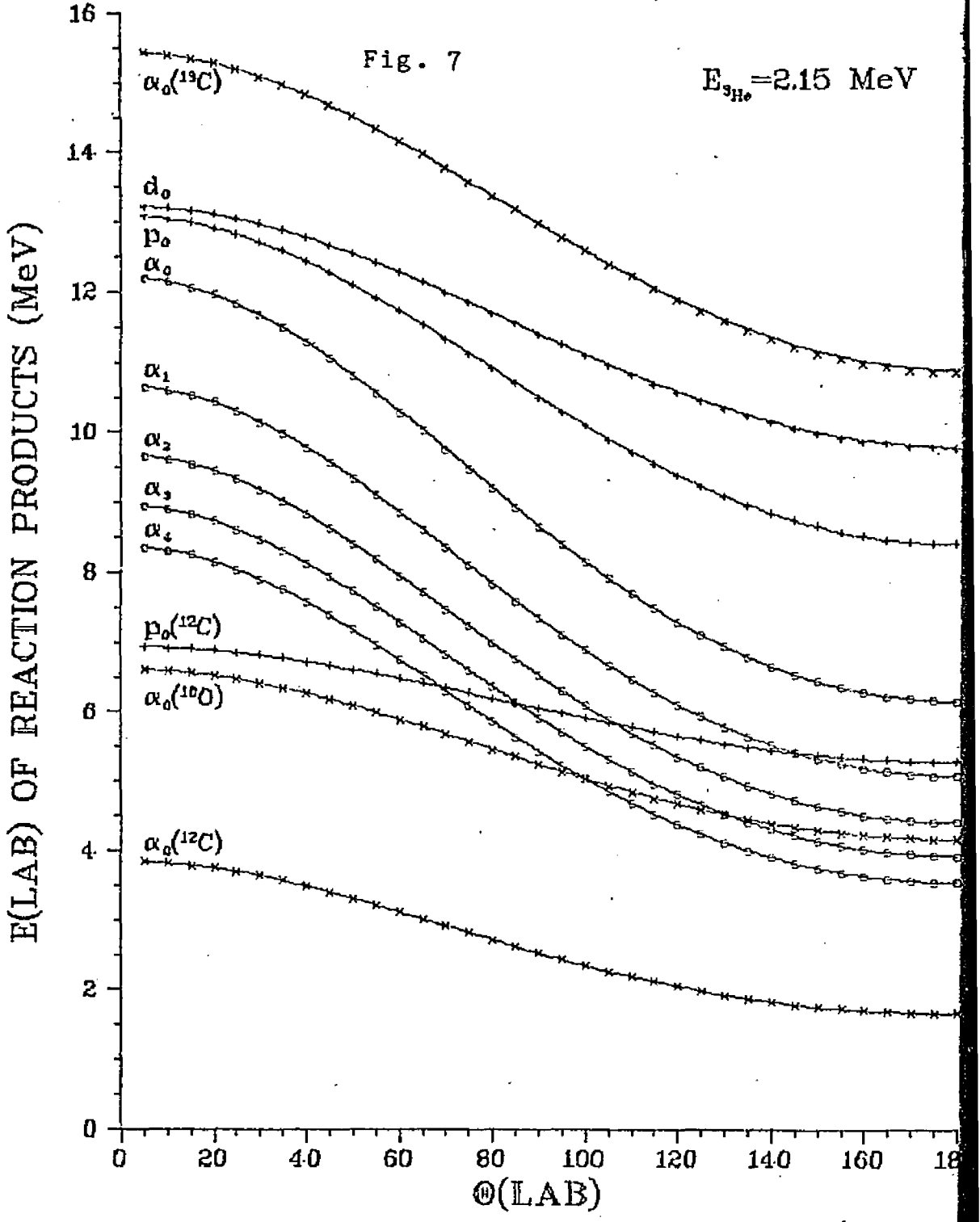

Kinematics for the Reaction

$^{7}Li(^{3}He,\alpha)^{6}Li$

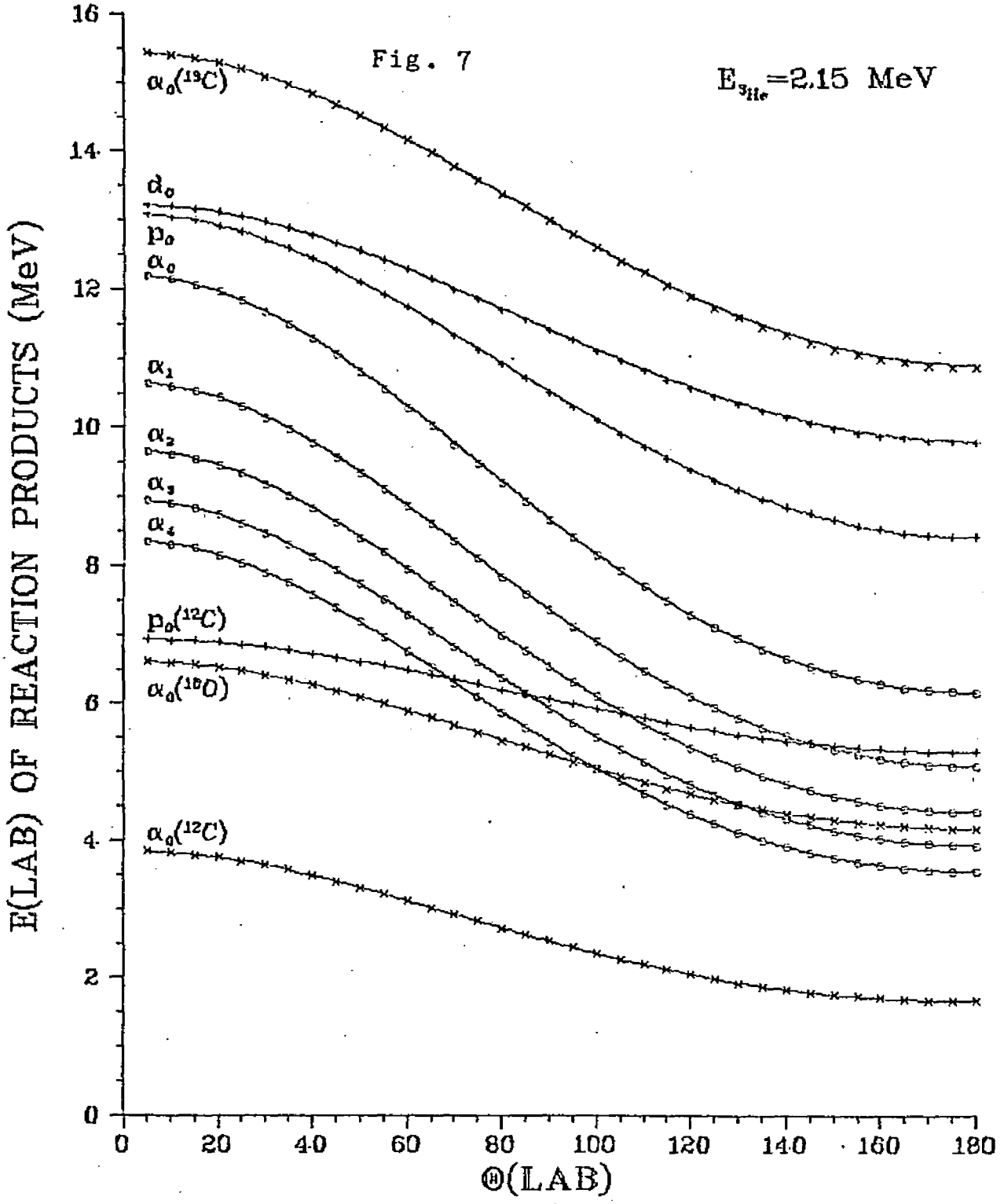

Totally depleted surface-barrier silicon detectors having a sensitive area of 50 mm^2 were used for the detection of charged particles. For detecting the first emitted α_1 particle, a detector of thickness121 μm was placed at a distance of 4.5" from the target with an oval defining aperture 5/16" X 5/32". This detector subtended a half-angle of 0.99° and a solid angle of 2.41 msr. As a 121 μm detector can stop α-particles of energies up to 14 MeV, protons of energies up to 3.6 MeV, deuterons of energies up to 4.6 MeV, discrimination between protons and α-particles was thus established since the minimum energy of interest of α_1 was 5.5 MeV. A mylar foil, 1.75 mg/cm^2 thick placed in front of the detector as to eliminate the enormous counting rate from elastically scattered ^3He ions, which was especially important at forward angles. The mylar foil also served to degrade the energy of ^6Li recoils sufficiently to move them out of the region of interest in the spectrum.

For the detection of α-α coincidences, the α_1 detector was fixed at 30°, at a distance of 3.5" form the target. This detector has a half-angle of 1.02° and a solid angle of 2.55 msr. A second α-detector, 22.7 μm thick, was placed at angles, θ_{α_2}, between -95° and -170°(Lab) corresponding to α_2 angles between -85° and -163° in the recoil ^6Li(5.37 MeV) system. This detector was placed at a distance 3.5" from the target, it has a half-angle of 1.28° and a solid angle of 3.98msr. A 22.7 μm detector can stop α-particles of energies

up to 4.8 MeV, protons of energies up to 1.22 MeV and deuterons of energies up to 1.48 MeV, thus the spectrum above 1.5 MeV consisted only of α-particles.

For the detection of α-d and α-p coincidences, a ΔE-E counter-telescope system consisting of two SB detectors, one measuring ΔE and the other measuring E-ΔE, was used to permit particle identification of the deuterons or protons. The thicknesses were chosen to be 22.7 μm and 300 μm respectively.

A 300 μm detector was used at a fixed position(30° Lab) for detecting the elastically scattered ^{3}He particles in some of the runs. A fixed detector was used for normalization purposes in all measurements of angular distributions for the first emitted α-particle.

For all runs, the detector geometry was chosen as a suitable compromise solution to the demands of optimizing the counting rate and of minimizing the kinematic broadening.

D. Targets

Metallic ^{7}Li and ^{7}LiF targets were used. Targets of ^{7}Li metal were prepared by evaporating enriched metallic ^{7}Li(99.99% purity) onto thin carbon foils(20 μg/cm^2). As the ^{7}Li metal is highly reactive with oxygen,

these targets were transferred under vacuum from target evaporation system to scattering chamber. This was done by mounting the target ladder system to the target evaporation system by means of a vacuum collar.

^{7}LiF targets ranging in thickness from 20 to 50 $\mu g/cm^2$ were also prepared by evaporating ^{7}LiF onto thin carbon foils. Target thicknesses were determined by using a quartz crystal thickness monitor.

Frequent checks on the monitor spectra were made to ensure that the target was not being evaporated by heating from the beam. No target deterioration was noticed at beam currents below 200 nA for both types of targets.

E. Electronics

A block diagram of the conventional slow-fast coincidence system is illustrated in Fig.8. The signals from two detectors were fed into ORTEC model 142A preamplifiers which provided both energy signals and time signals. The time signal in each branch was passed through a timing filter amplifier and a constant-fraction discriminator. The discriminator level was set to just barely eliminate the pulses due to detector noise. Outputs of the two fast discriminators constituted the start and stop inputs to a time to amplitude converter(TAC) with suitable delay of the stop pulse. The

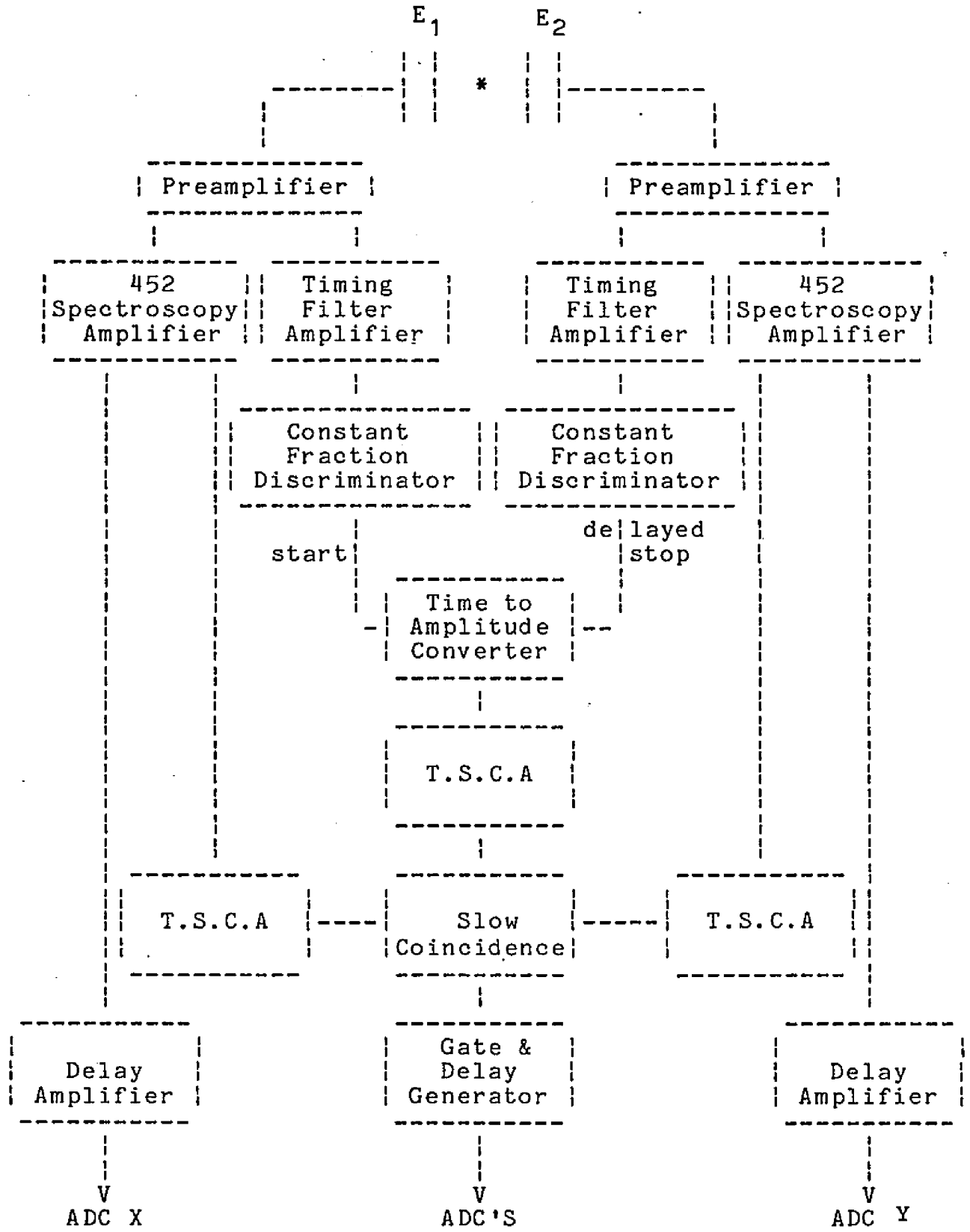

Fig.8 Block Diagram for Slow-Fast Coincidence Timing

time spectrum from TAC showed a peak of FWHM less than 10 nsec.

Energy outputs of the preamplifiers were fed into spectroscopy amplifiers in each branch. Outputs of the spectroscopy amplifiers passed into timing single channel analyzers(TSCA). Slow timing was derived by establishing a slow coincidence between the logic outputs from the TSCA's.

Outputs of the spectroscopy amplifiers were appropriately delayed and then sent into The Northern Scientific Analog to Digital Converters(ADC). The inputs to the ADC's were gated by a pulse derived from the slow-fast coincidence timing. The 8192 channel Northern Scientific Analyzer(NS636) was used in 128x64 X-Y coincidence mode to obtain the dual parameter coincidence spectra. The data were printed out on a high speed Versatec printer interfaced to a PDP 11/20 computer which was also interfaced with the NS636. Monitor spectra were stored in a 4096-channel Northern Scientific Analyzer, which were dumped onto a magnetic tape.

Test pulses generated by an ORTEC 448 Research Pulser were fed into the preamplifiers and passed through all the electronics. The slow fast coincidence timing was set and periodically checked using these test pulses. A singles spectrum was taken in each detector before and after each coincidence run to check for gain shifts in the electronics.

The kinematic curve may be seen directly by using the

two-dimensional mode of the Multichannel Analyzer(MCA), accepting the amplified E_1 and E_2 pulses directly to its X and Y ADC's respectively.

The particle identifier used in the α-d and α-p coincidence measurements generates two energy outputs. One is the sum of two energy inputs ΔE and $E-\Delta E$ which gives full energy E, the other selects the particle of interest through a build-in function $\Delta E(k\,\Delta E + E_o + E - \Delta E)$ with two adjustable parameters k and E_o.

IV. EXPERIMENTAL DATA

A. Excitation Function

Typical alpha-particle singles spectra with and without a mylar foil in front of the detector are shown in Fig.9. The alpha-particle spectra show states in ^{6}Li at excitations of 0.0, 2.18, 3.56 and 5.37 MeV consistent with several previously reported studies(Ref.11,39) of this reaction. As can be seen from the spectrum without mylar foil, the peak corresponding to the 5.37 MeV state sometimes overlaps peaks due to ^{6}Li recoil nuclei for the ground state and first excited state. By placing a mylar or gold foil of appropriate thickness in front of the detector, the recoil peaks can be shifted down so that they appear well below, and completely separated from, the 5.37 MeV peak. This is because Li nuclei lose far more energy in the foil than do alpha particles(about 2 to 1 ratio). Of course, the alpha particle resolution is degraded somewhat by the foil due to straggling effects, which are typically 10-20% of the total energy loss, about 200 keV in this case.

The underlying background coming from the breakup continuum necessitates longer run time to collect adequate statistics, after background subtraction, for the 5.37 MeV

Typical α–Particle Energy Spectrum

Fig. 9

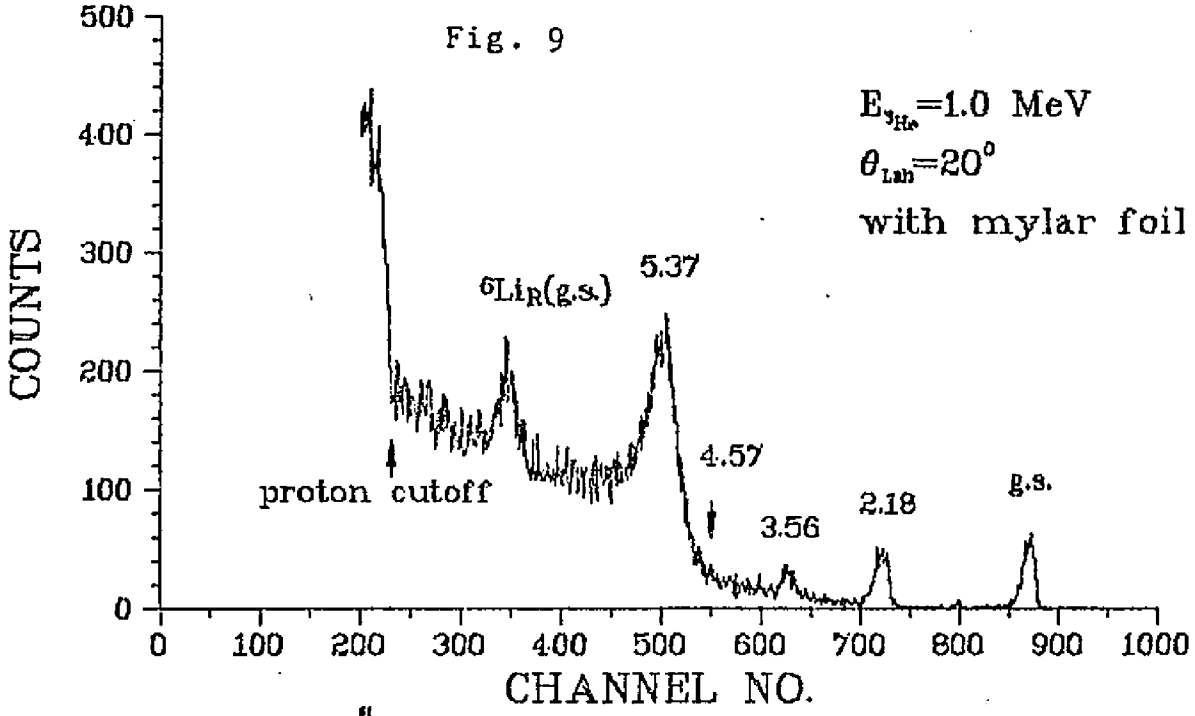

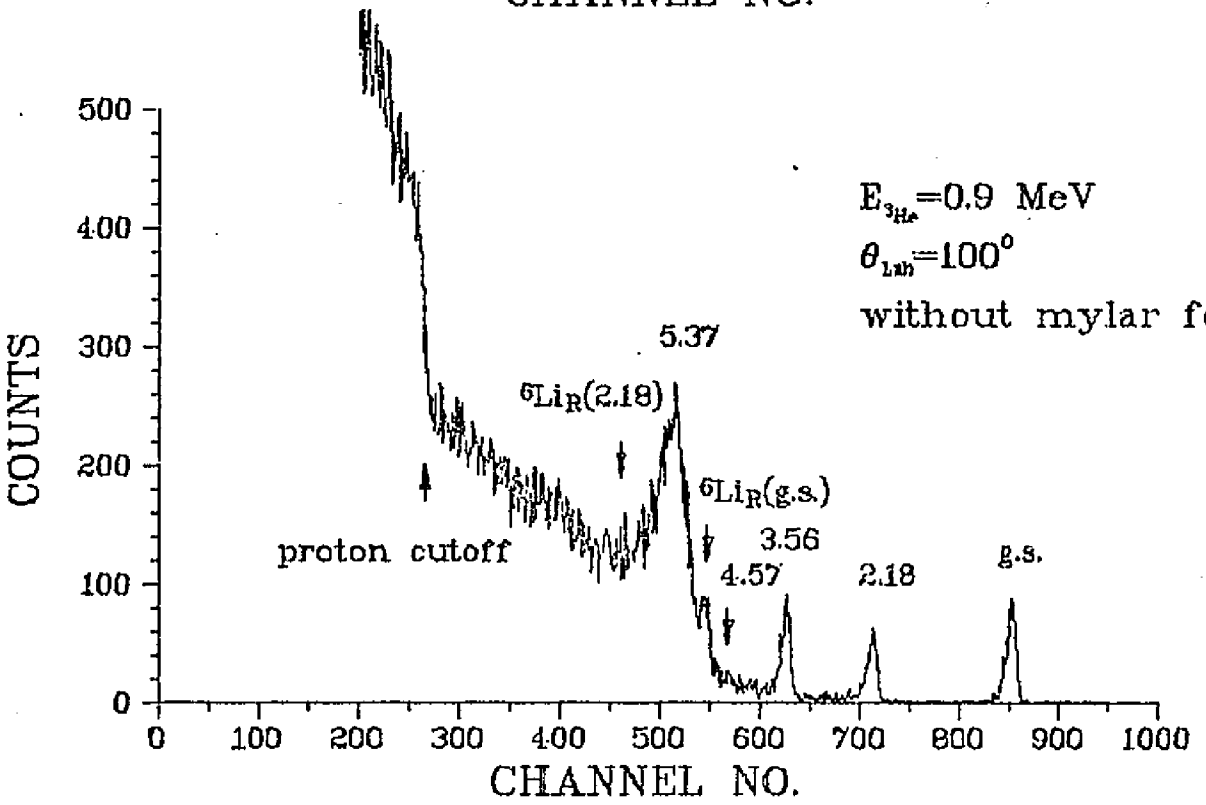

state. This provides one important reason for using Li metal targets rather than compound targets, due to the higher Li concentration for a given target thickness. Average run times per data point obtained here were about one hour at the higher energies and about two hours at energies below 1.1 MeV.

^{7}Li metal targets of thickness 16 $\mu g/cm^2$ evaporated onto a 16 $\mu g/cm^2$ carbon backing were used for these measurements. The alpha-particles were detected in a silicon surface barrier detector collimated by a 5/32" x 5/16" oval shape aperture 4.5" from the target. Thus the detector half angle was 0.99° and the solid angle 2.41 msr. The majority of the data were accumulated using thin SB detectors. The thicknesses of the detectors were chosen such that protons and deuterons from other competing reactions would pass through with energy losses small in comparison to the energies of the alpha particles. Detector depletion depths were 68 μm for the backward angle detector, 121 μm for the forward angle detector and 300 μm for the monitor detector.

The backgrounds were obtained by summing 10 channels on each side of the peak, taking averages and then multiplying the total channels spanned by the peak. For determining the yield at 5.37 MeV excited state. A Gaussian shape peak plus a quadrature form of background with adjustable parameters were fitted to the spectra, then integrating the area under the Gaussian peak. The results of this procedure com-

pared with that of using the linear background subtraction were within 2 % statistical error.

The absolute cross sections were obtained by normalizing the yields of all α groups to that of the α_0 groups which were previously measured by Paul et al(Ref.11). For those incident energies which were not given in Ref.11 the interpolated values have been used. The absolute cross sections for the first and second excited states so deduced were then compared with those measured by Paul et al. and they were consistent with each other. The results were listed in Table 6-17.

The yields of each peak were also normalized to the total charge collected in a Faraday cup and calculate the differential cross sections directly using measured target thickness and detector solid angle. cross sections obtained in this procedure are overall 30% experimental error compared with those obtained in the way described earlier. The uncertainties of this procedure include charge state correction, target thickness and solid angle determinaton.

Error bars were obtained by combining statistical with background subtraction errors in quadrature. The uncertainties in extracting cross sections of Paul et al's data were not included.

Excitation curves were obtained at laboratory angles of 30°, 90° and 150° with respect to the incident beam

direction and for ^{3}He bombarding energies ranging from 0.75 MeV to 2.5 MeV in an attempt to search for resonance structure in the $^{7}Li(^{3}He,\alpha)^{6}Li$ reaction.

The results have been plotted as a function of ^{3}He bombarding energies and are shown in Fig.10-13. The error bars include the statistical errors and the uncertainties due to the background subtraction. Where error bars are not shown, the estimated errors are within the plotted circles.

The excitation curves for the α_0 group are in general increasing monotonically at all three angles studied. The enhancement in the 30° yield at 2.2 MeV has been observed by Wolicki et al(Ref.12) at 24°, by Forsyth et al(Ref.39) at 8° and by Paul et al(Ref.11). However, the total cross section is increasing steeply in this energy region and does not show this resonance. This resonance corresponds to a level in the compound nucleus ^{10}B at 19.3 MeV excitation energy with a width of at least 300 KeV.

The α_1 group does not show any pronounced structure at any of the three angles, but its shape varies considerably in that it does not exhibit the rapid rise with increasing bombarding energy in the backward angle yield such as is observed at forward angles. This phenomenum agrees very well with Forsyth's data(Ref.39) except that the enhancement in the 8° yield at 2.4 MeV is not seen in our 30° yield data.

EXCITATION FUNCTION FOR ^{6}LI(g.s.)

Fig. 10

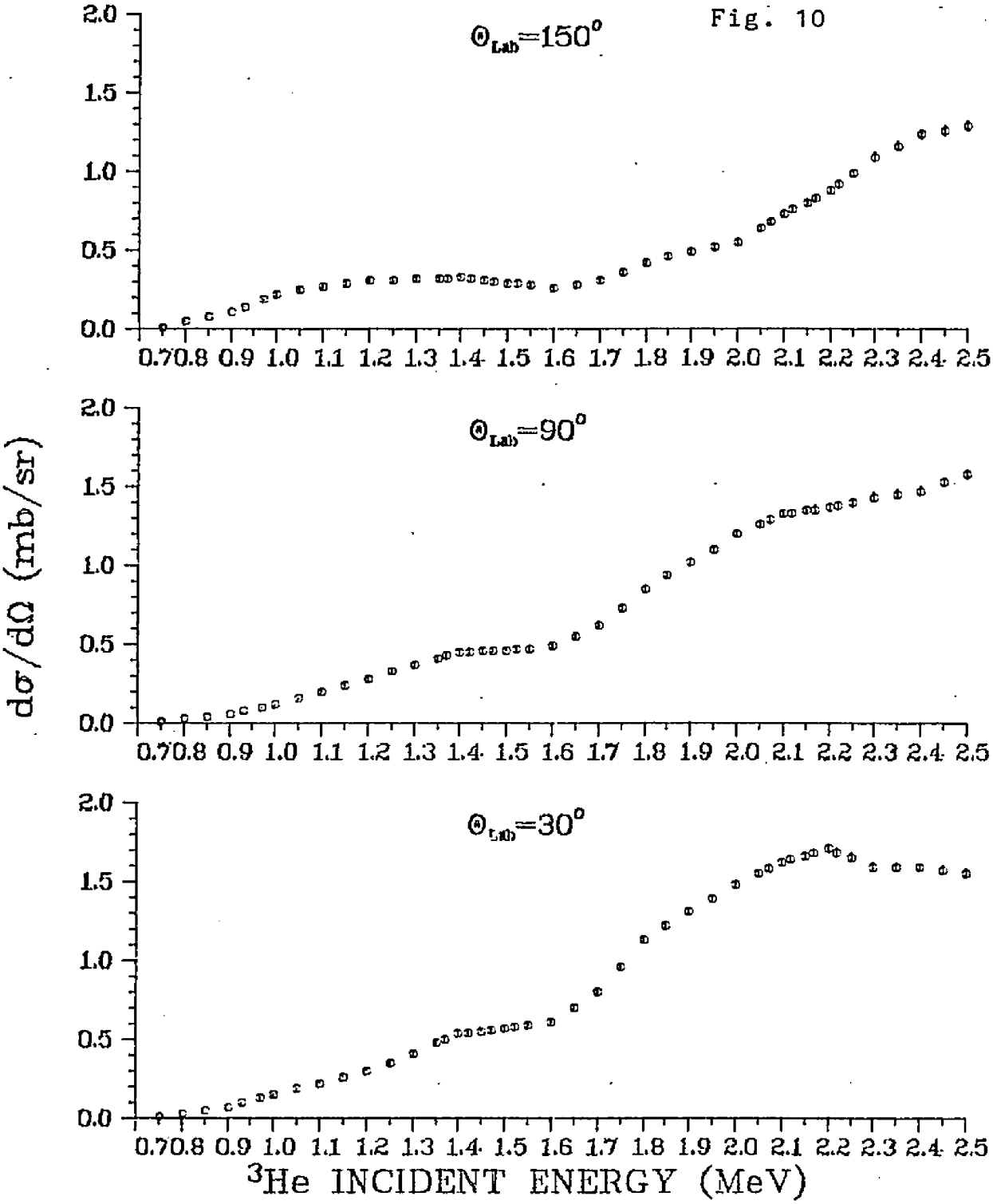

EXCITATION FUNCTION FOR ^{6}LI(2.18)

Fig. 11

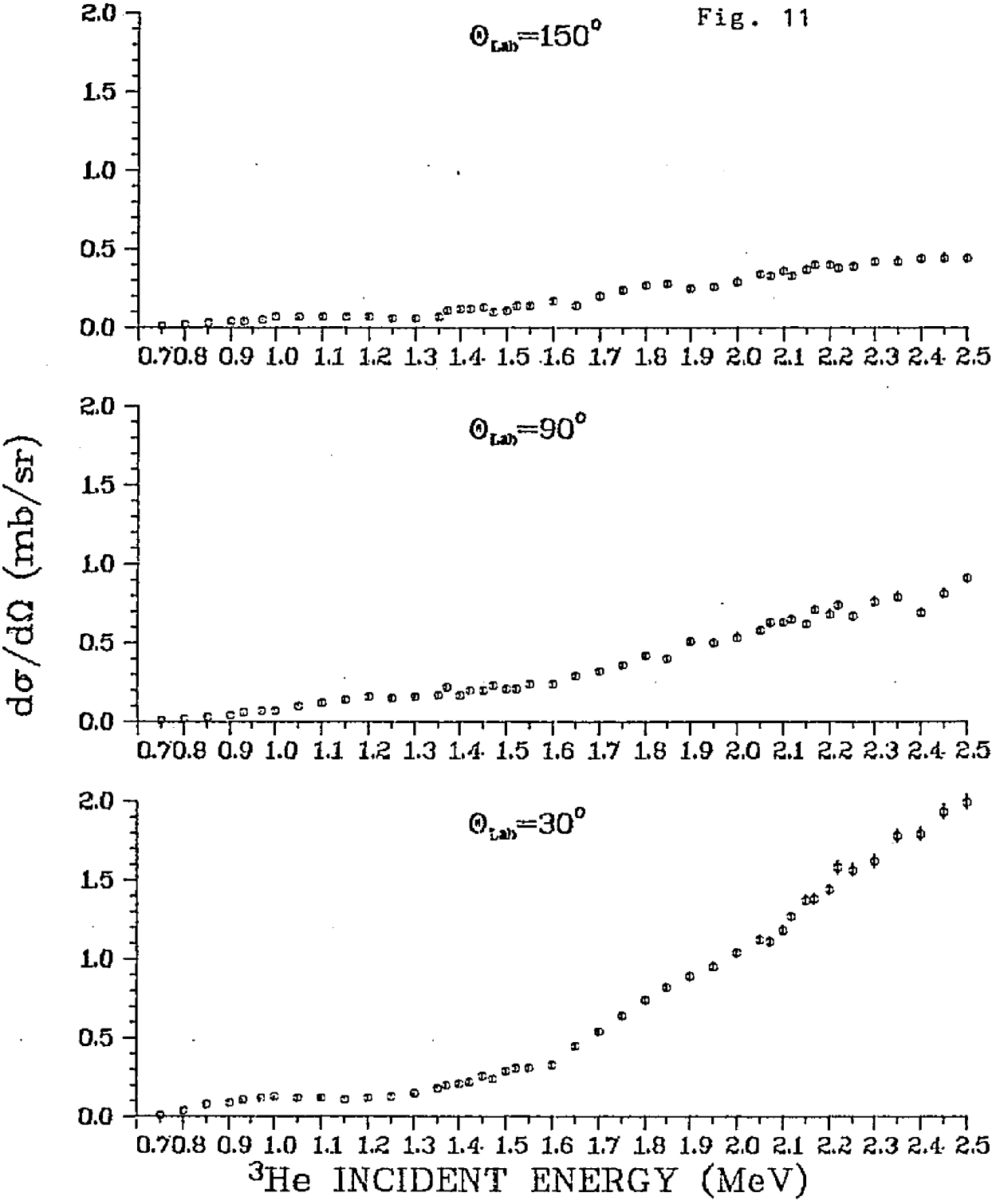

EXCITATION FUNCTION FOR ^{6}LI(3.56)

Fig. 12

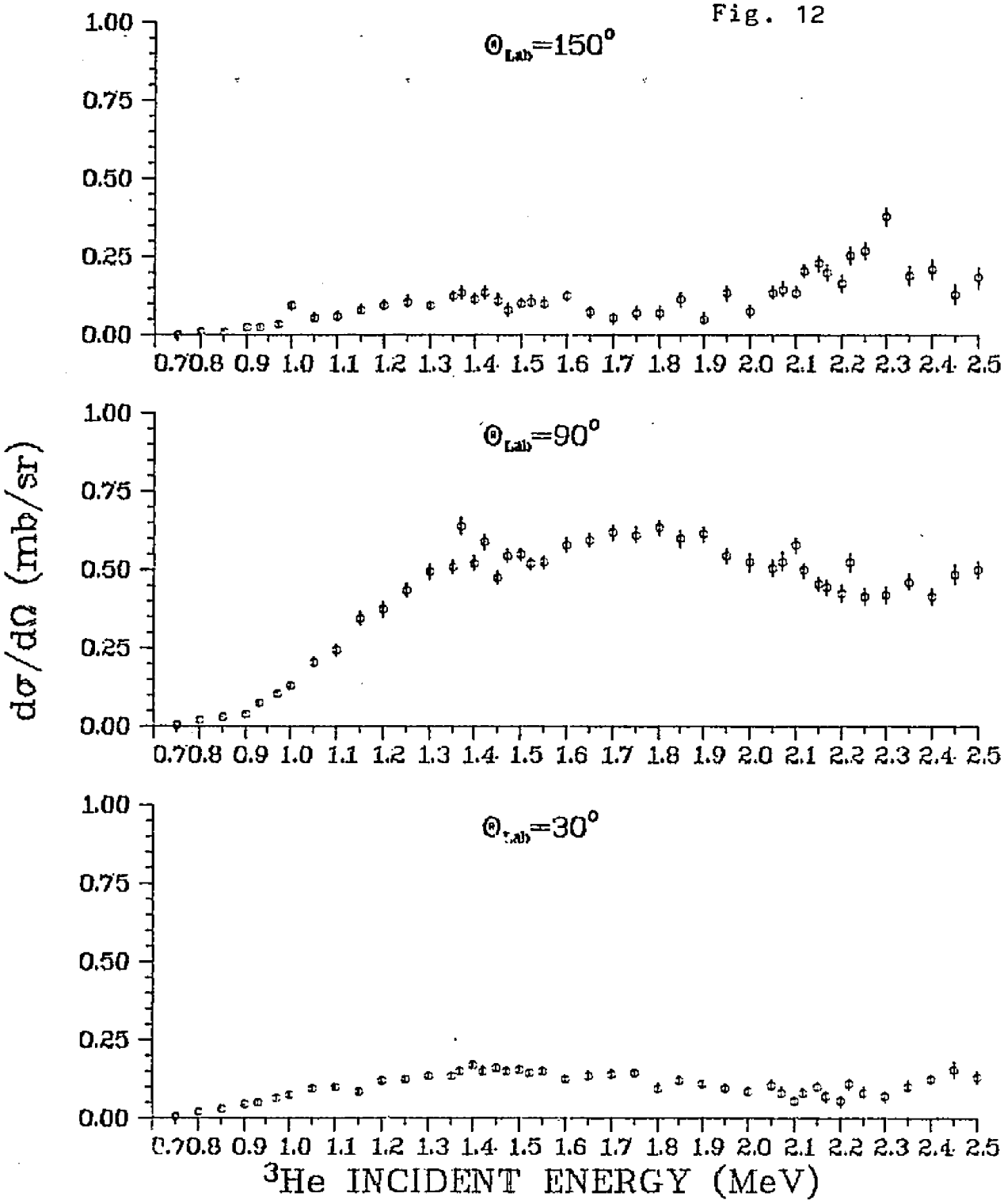

EXCITATION FUNCTION FOR ^{6}LI(5.37)

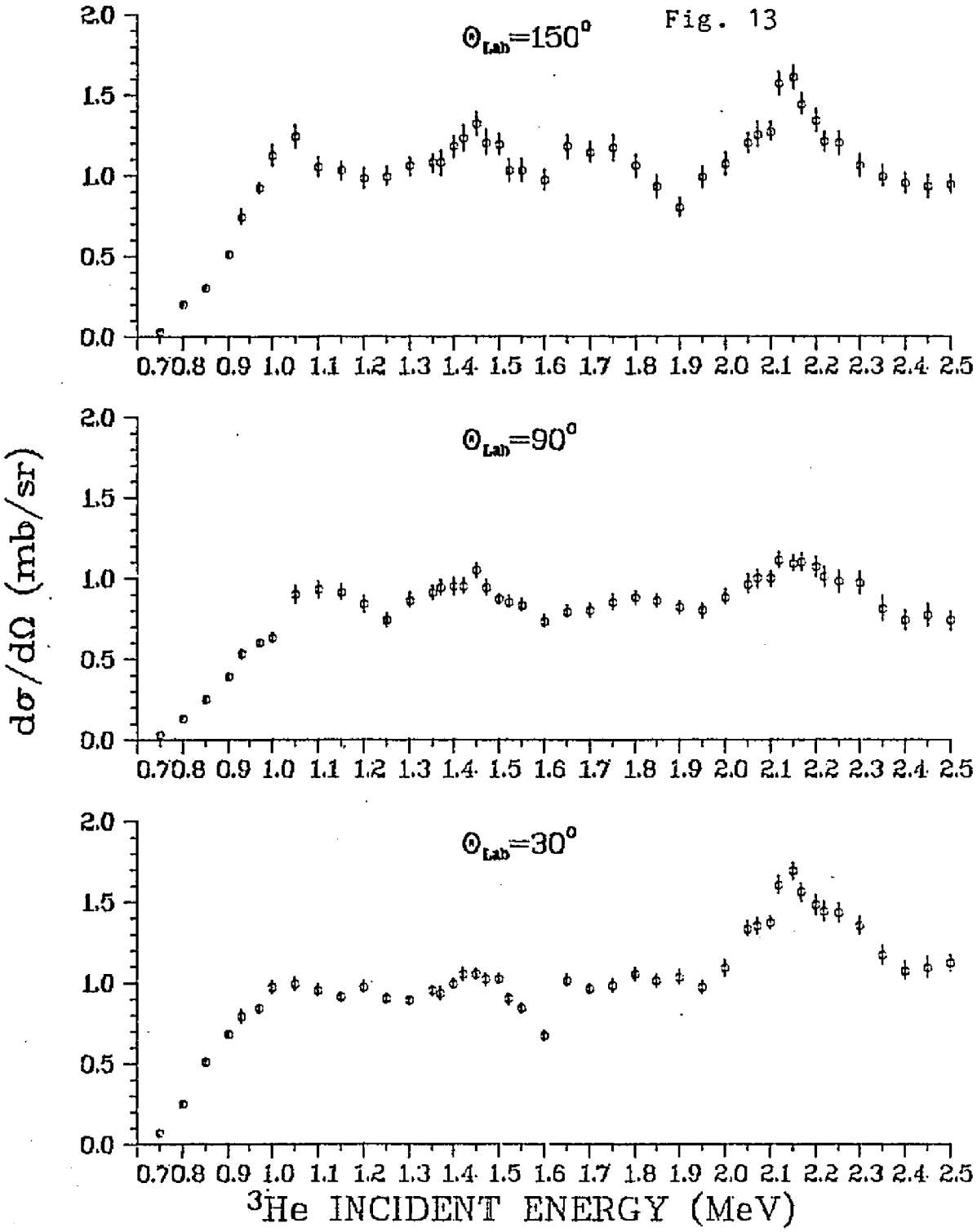

The α_2 group excitation curves show indication of resonances at 1.4 and around 2.2 MeV. Unfortunately, the peaks are not so prominent as to allow a definite conclusion. The excitation curve at 90° also agrees very well with Forsyth's data which is the only angle they have measured. It is worth noting that the yields at 90° are relatively large compared to both forward and backward yields.

The excitation curves for the 5.37 MeV excited state do show pronounced structure which persists over all three angles measured in contrast to the other α groups. These resonances are at 1.05, 1.45 and 2.15 MeV incident ^{3}He energies which correspond to the formation of the compound nucleus ^{10}B at 18.43, 18.8 and 19.3 MeV excitation energies respectively. Known levels exist in ^{10}B at just these excitation energies, and all have been previously assigned T=1. The present measurements therefore support both the location and isospin assignments of these levels in ^{10}B. The widths of these ^{10}B resonances from the present measurement are 300 ± 60, 400 ± 80 and 300 ± 60 KeV respectively.

B. Angular Distributions

The angular distribution measurements were performed for a fixed beam current of 200 nA with laboratory angles ranging from 20° to 160° in 10° steps and bombarding ener-

gies from 0.9 to 2.5 MeV. A fixed monitor detector at 20° was used to check target deterioration and also served as a normalization counter. Target orientation was kept perpendicular to the bisector of the beam direction and the detector direction, so as to optimize resolution.

The absolute cross sections were established by normalizing the yields at 20° in the same manner as described for the excitation function measurement. Analysis of spectra is in the same way as described before.

Angular distribution curves were drawn by fitting the data points with a Legendre polynomial up to fourth order. All fits gave a normalized chi-square better than 0.05. The error bars if not specified are within the size of the circle and are overall less than 8%.

The absolute differential cross sections in the CM system have been plotted(Fig.14-25) as a function of center of mass angles ranging from about 20° to 170° for the various excited states in ^{6}Li. The numerical values of the absolute differential cross sections are listed in Table 18-21.

The angular distribution for the α_0 group is much more energy dependent than that for the α_1 and α_2 group. It exhibits isotropy at 1.1 MeV and is nearly isotropic at 1.4 MeV. The α_1 angular distribution has a characteristic of tending to peak at 60° and this feature becomes more dominatant as energy increases while the general shpe does not

ANGULAR DISTRIBUTION FOR ^{6}LI(g.s.)

Fig. 14

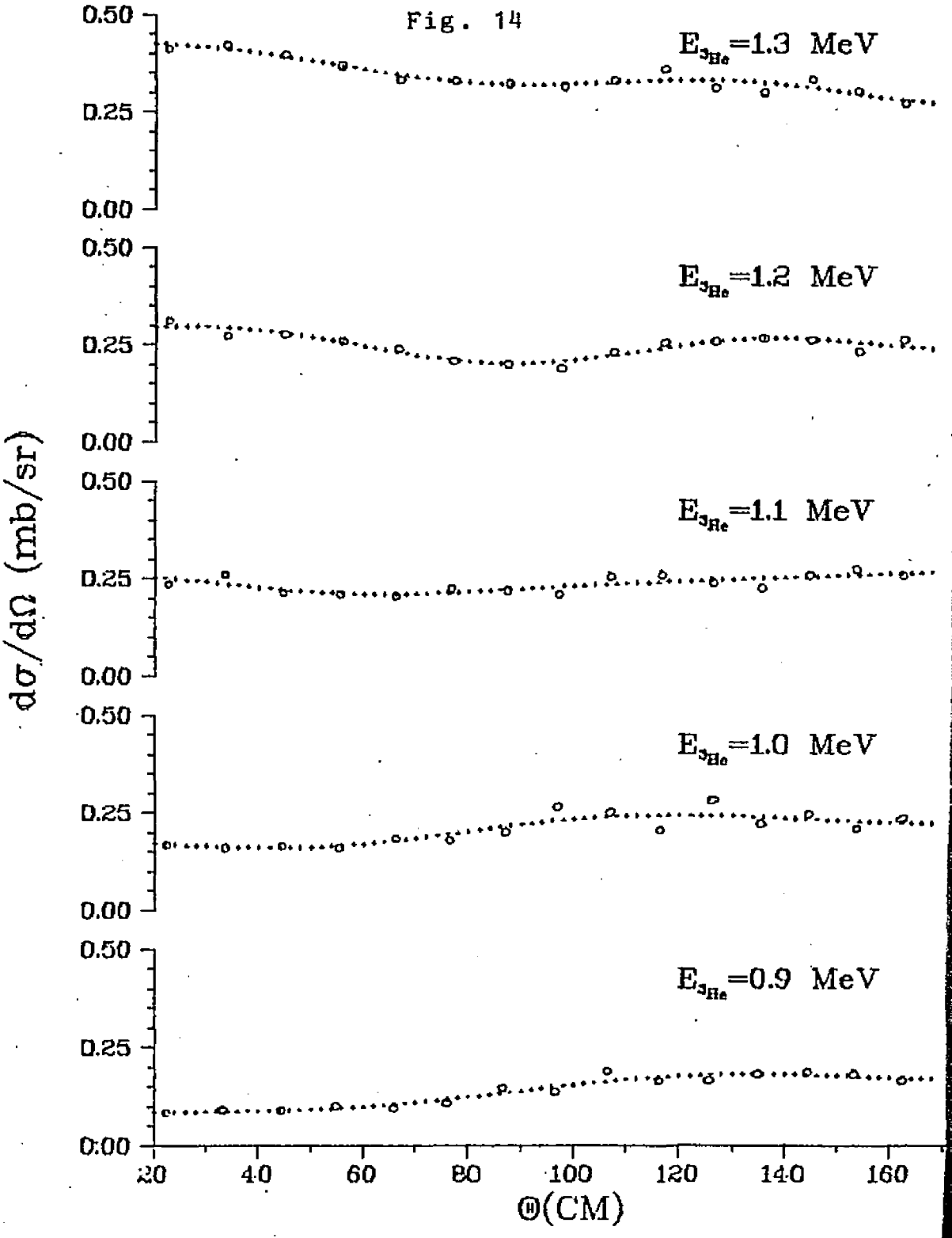

ANGULAR DISTRIBUTION FOR ^{6}LI(g.s.)

Fig. 14

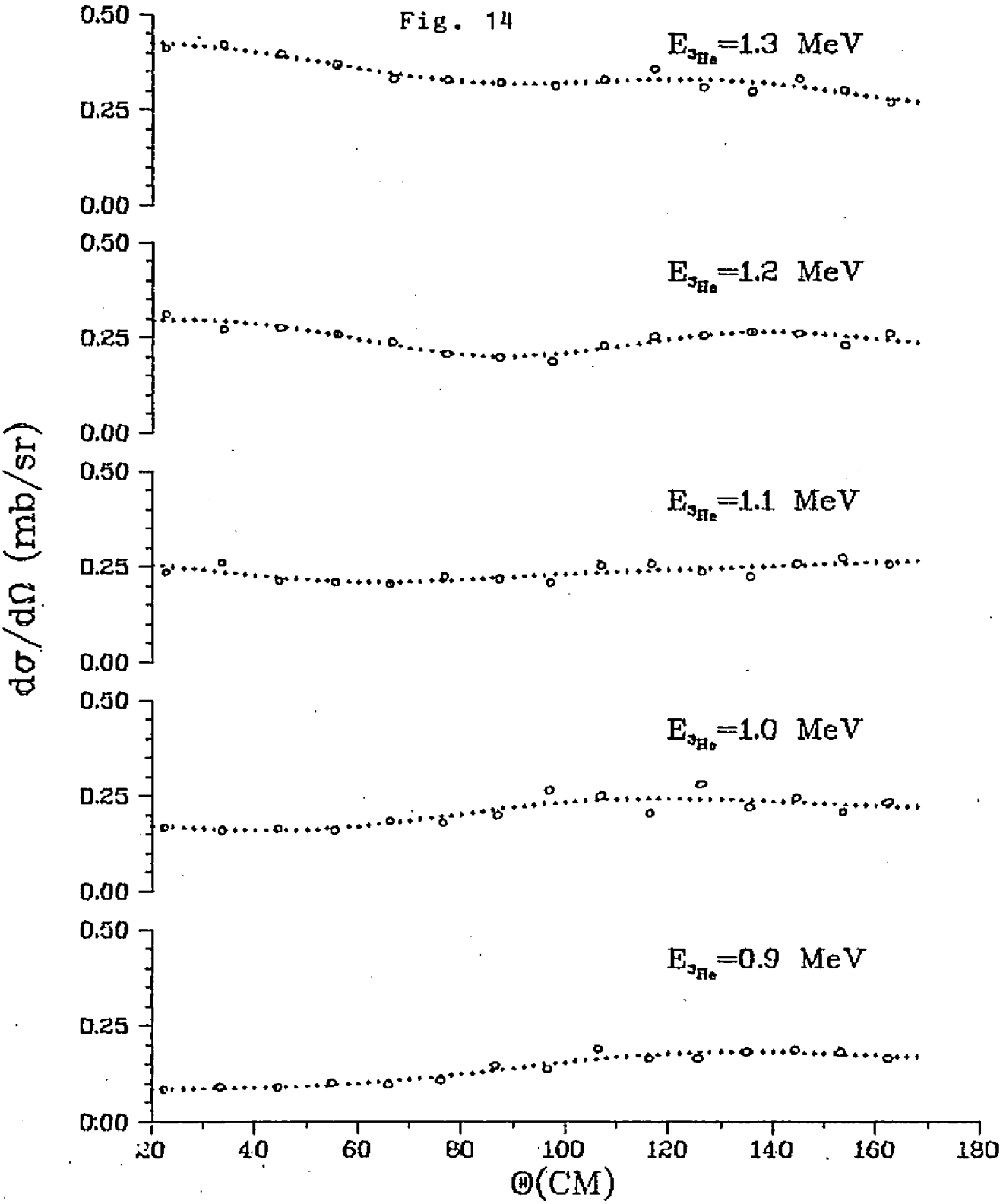

ANGULAR DISTRIBUTION FOR ^{6}LI(g.s.)

Fig. 15

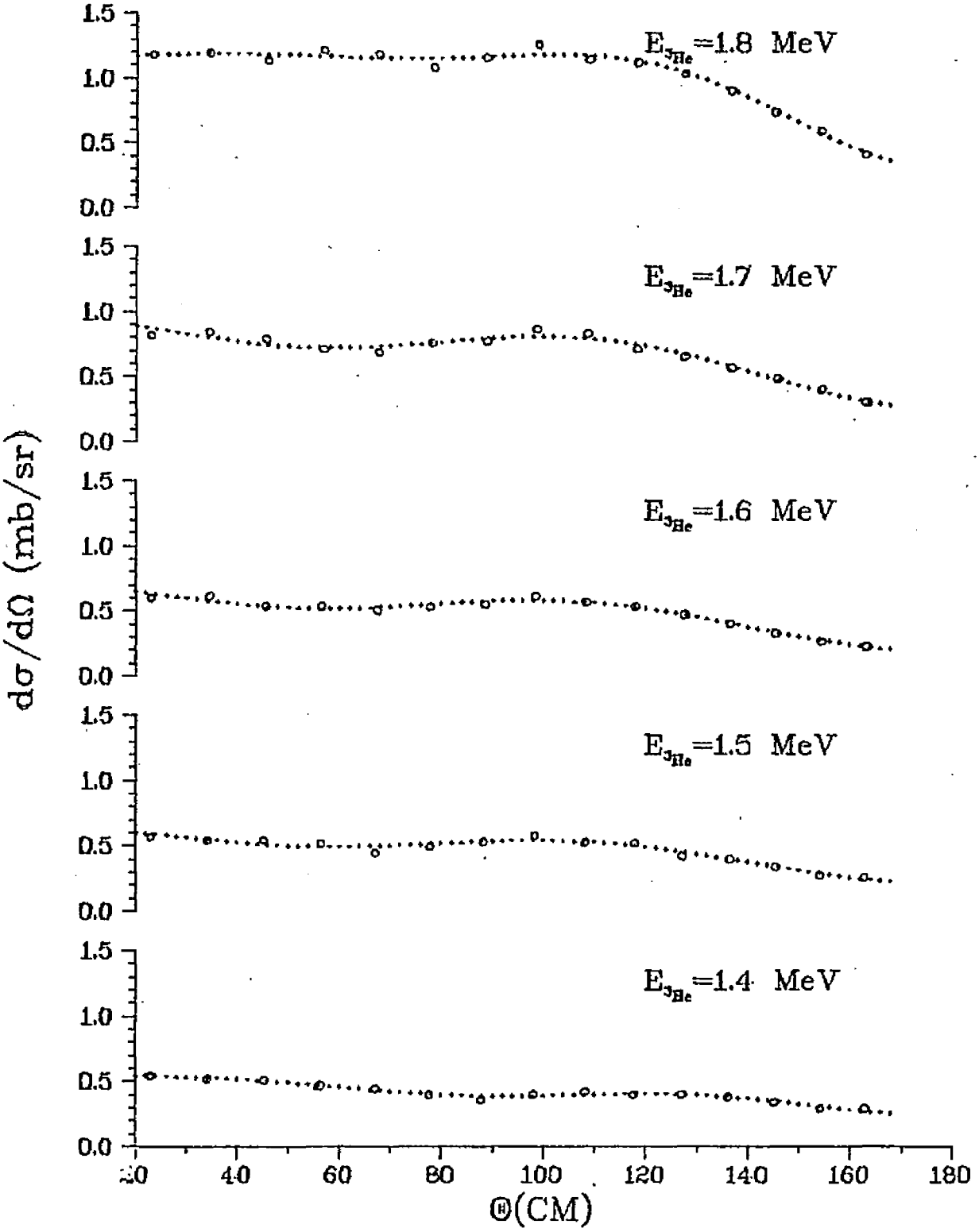

ANGULAR DISTRIBUTION FOR ^{6}LI(g.s.)

Fig. 16

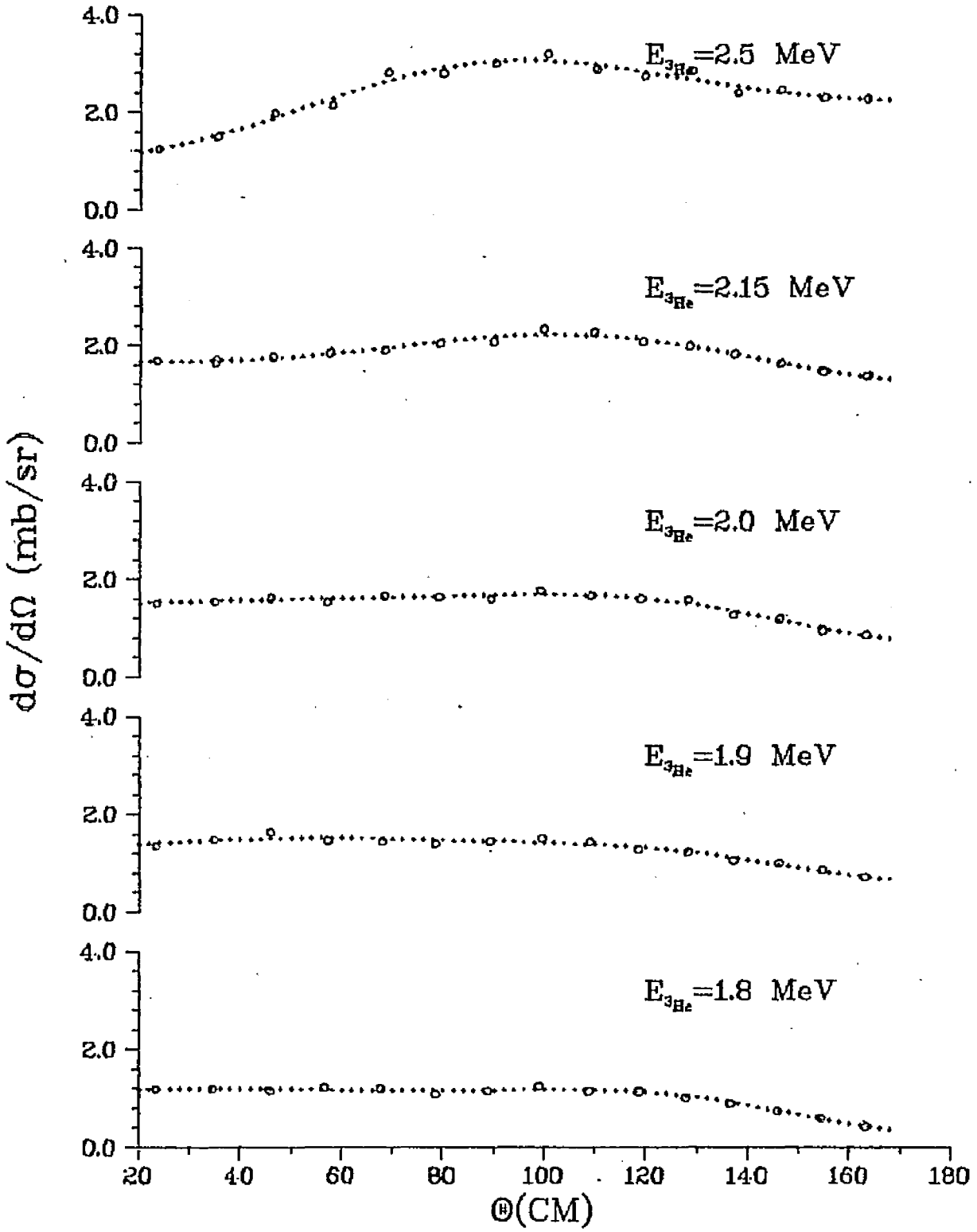

ANGULAR DISTRIBUTION FOR ^{6}LI(2.18)

Fig. 17

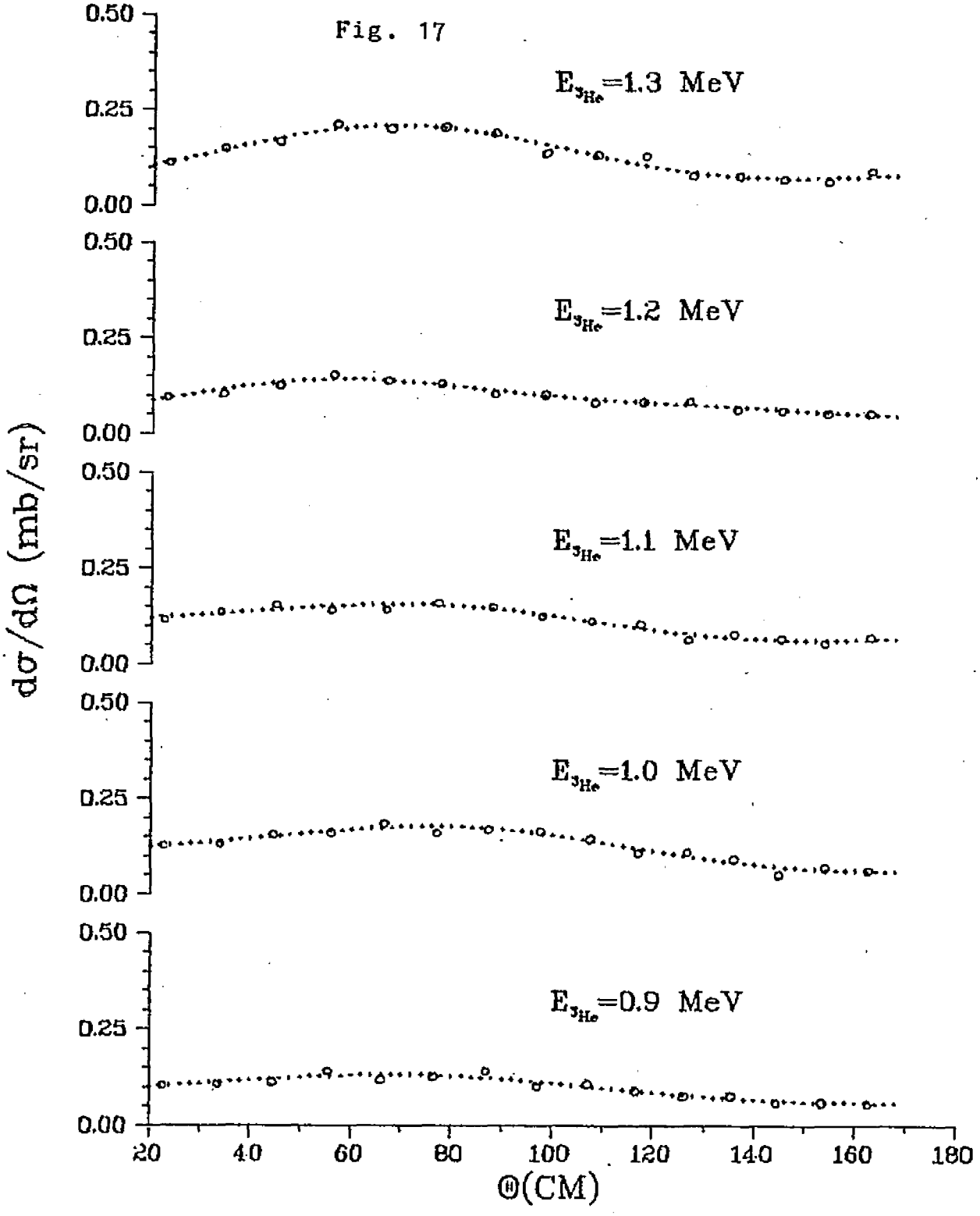

ANGULAR DISTRIBUTION FOR ^{6}LI(2.18)

Fig. 18

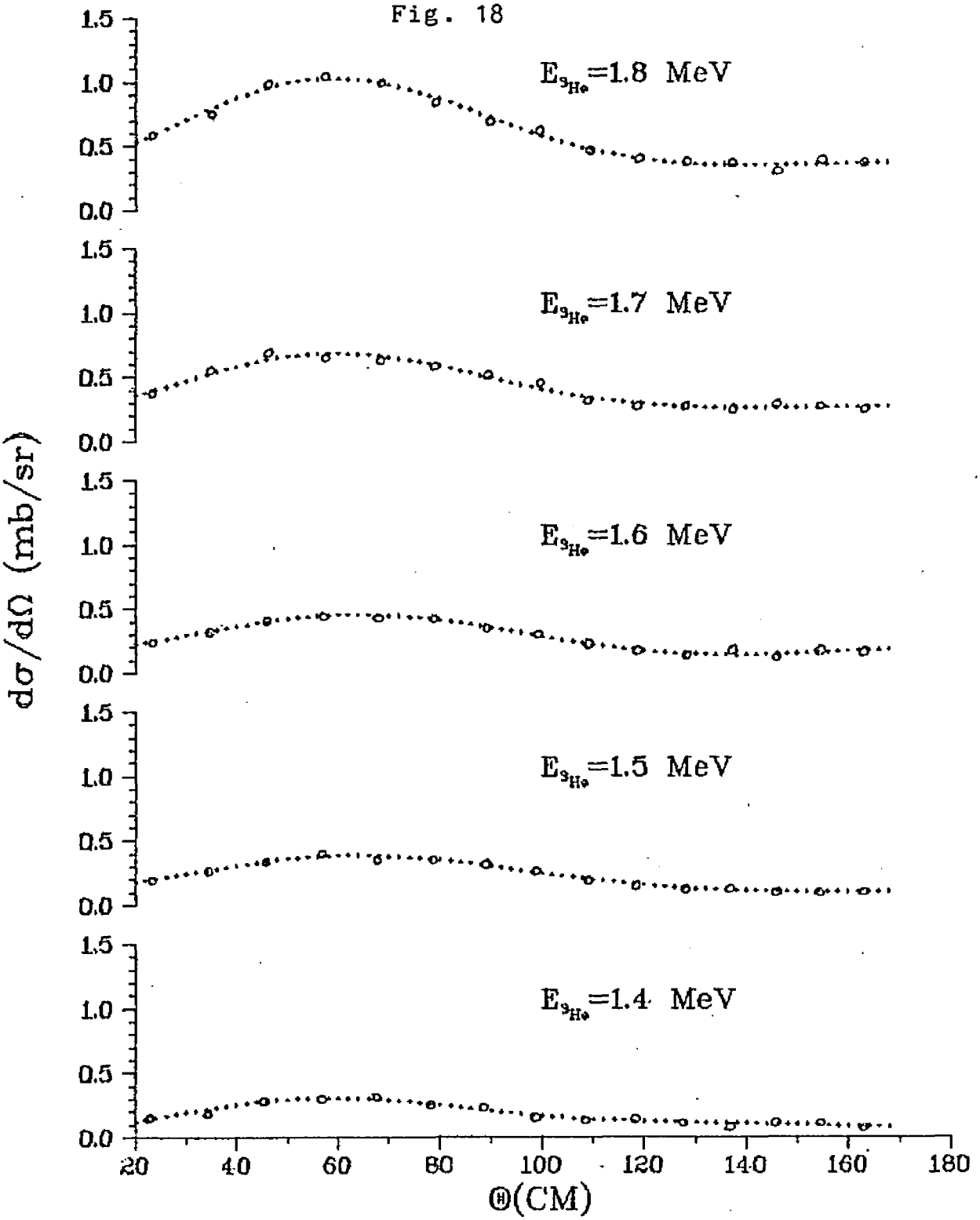

ANGULAR DISTRIBUTION FOR ^{6}LI(2.18)

Fig. 19

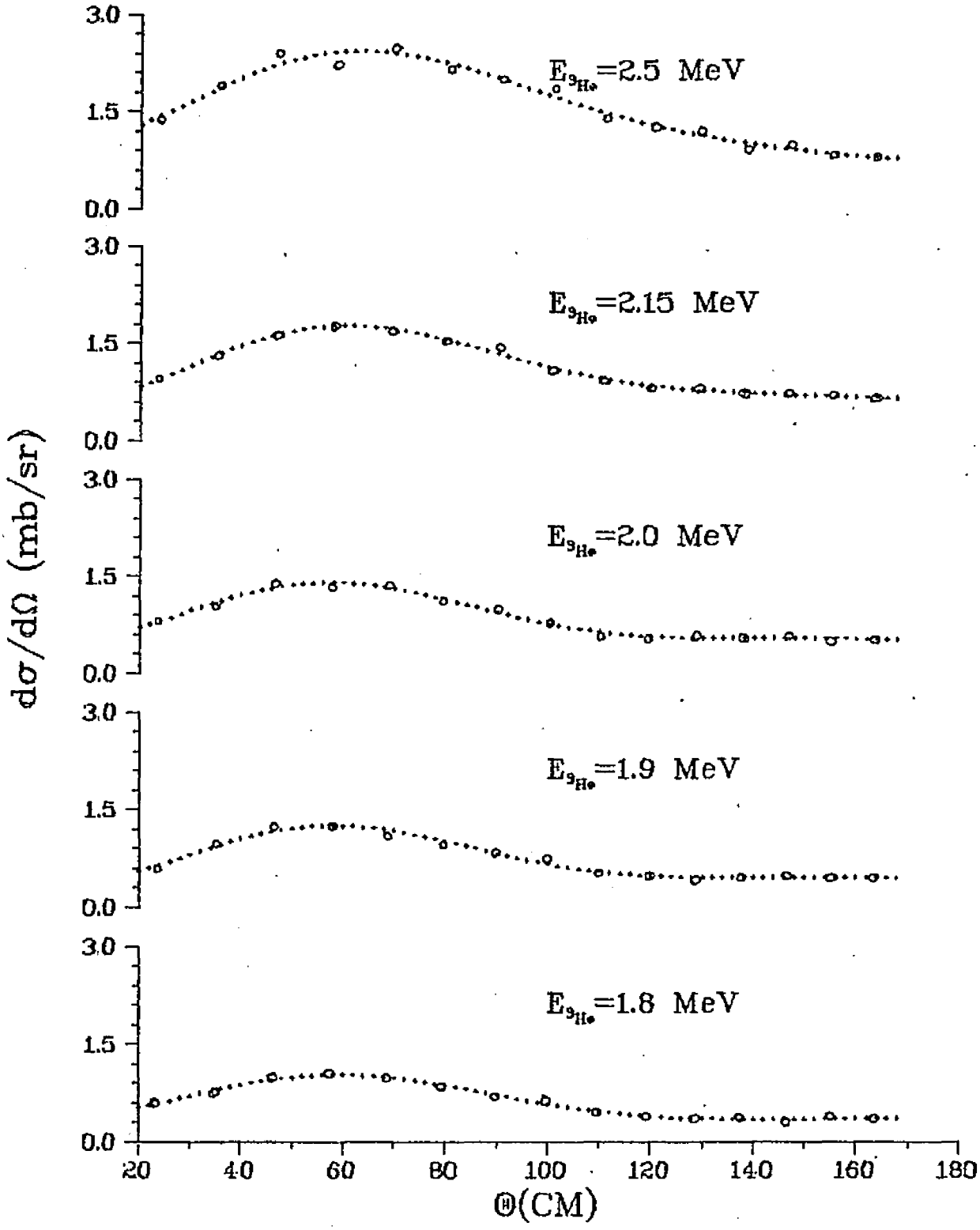

change appreciably throughout the range of energies studied. The a_2 angular distribution has a bell shape throughout all the energies. It at first peaks at 90° for energies up to 1.4 MeV, then shifts to 100° for energies between 1.5 MeV and 2.0 MeV and finally tends to peak at backward angles as the energy goes towards 2.5 MeV.

The angular distributions for the ground state and the first two excited states are generally in very good agreement with those previously measured by Forsyth et al(Ref.39). The only discrepancy is that a slightly rising at backward angles at 1.2 MeV of Paul's data(Ref.11) has not observed in the present measurements.

The angular distributions for the 5.37 MeV state are nearly isotropic at 1.1 and 1.4 MeV, exhibit a higher degree of symmetry about 90° CM angle in the vicinity of 2.1 MeV and show enhancement at backward angles. All these features indicate that the reaction proceeds predominately by compound nucleus mechanism which supports the conclusion drawn by the excitation functions. The angular distributions of 5.37 MeV state presented here are the first data available in the literature.

The total cross sections were obtained by fitting the angular distributions with a Legendre polynomial expansion and determing the zero order coefficient. These are plotted as a function of the bombarding energies from 0.9 to 2.5 MeV

ANGULAR DISTRIBUTION FOR ^{6}LI(3.56)

Fig. 20

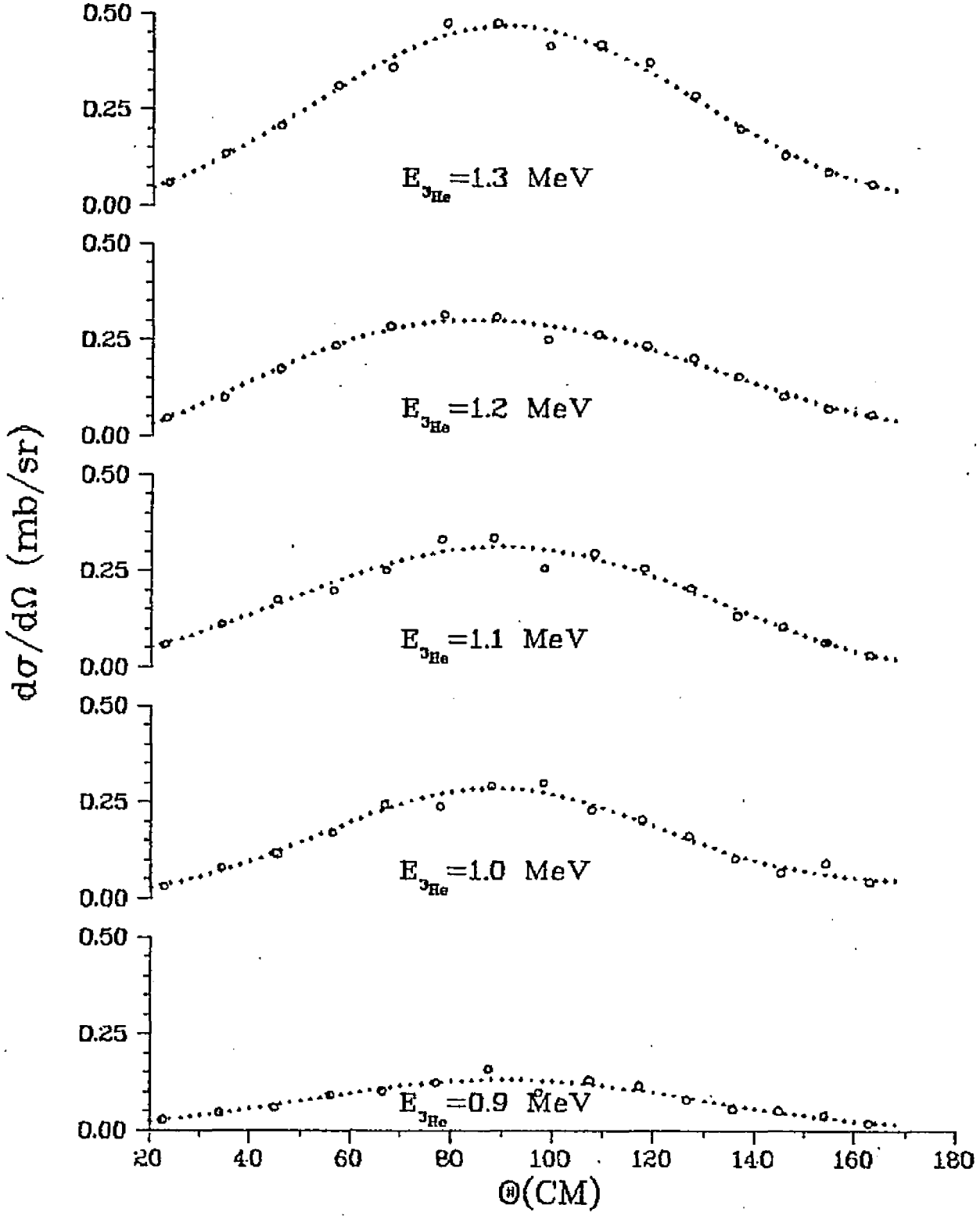

ANGULAR DISTRIBUTION FOR ^{6}LI(3.56)

Fig. 21

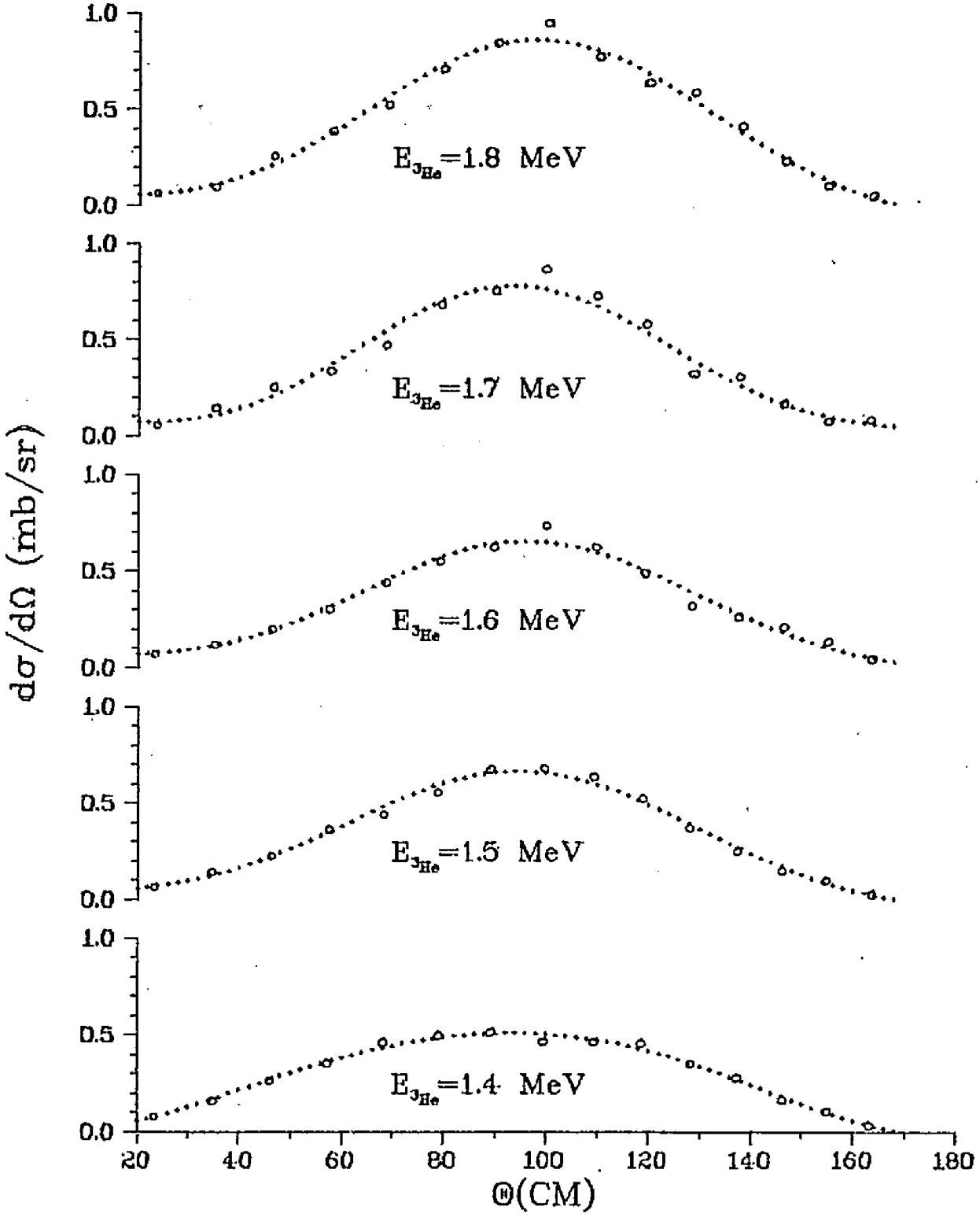

ANGULAR DISTRIBUTION FOR ^{6}LI(3.56)

Fig. 22

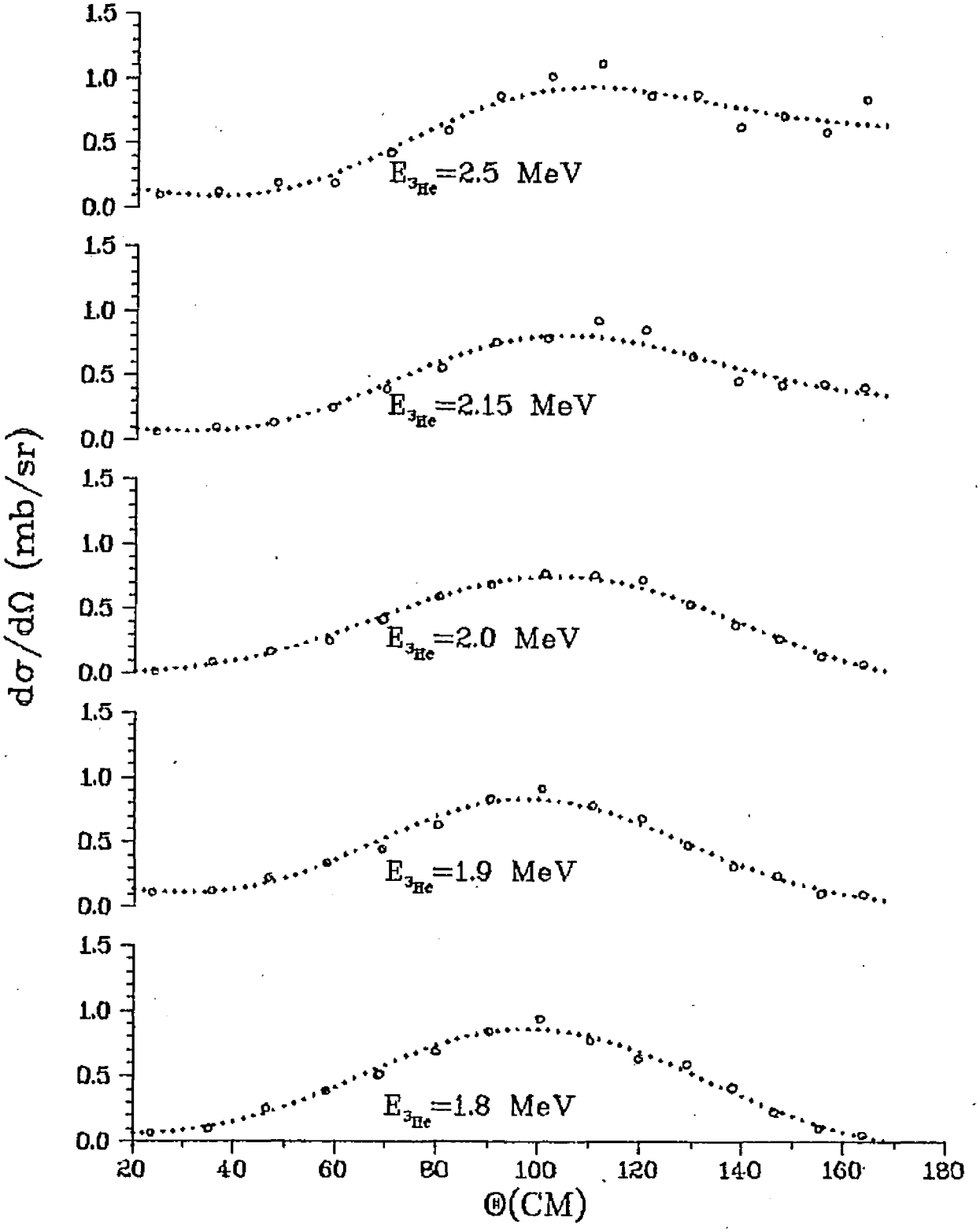

ANGULAR DISTRIBUTION FOR ^{6}LI(5.37)

Fig. 23

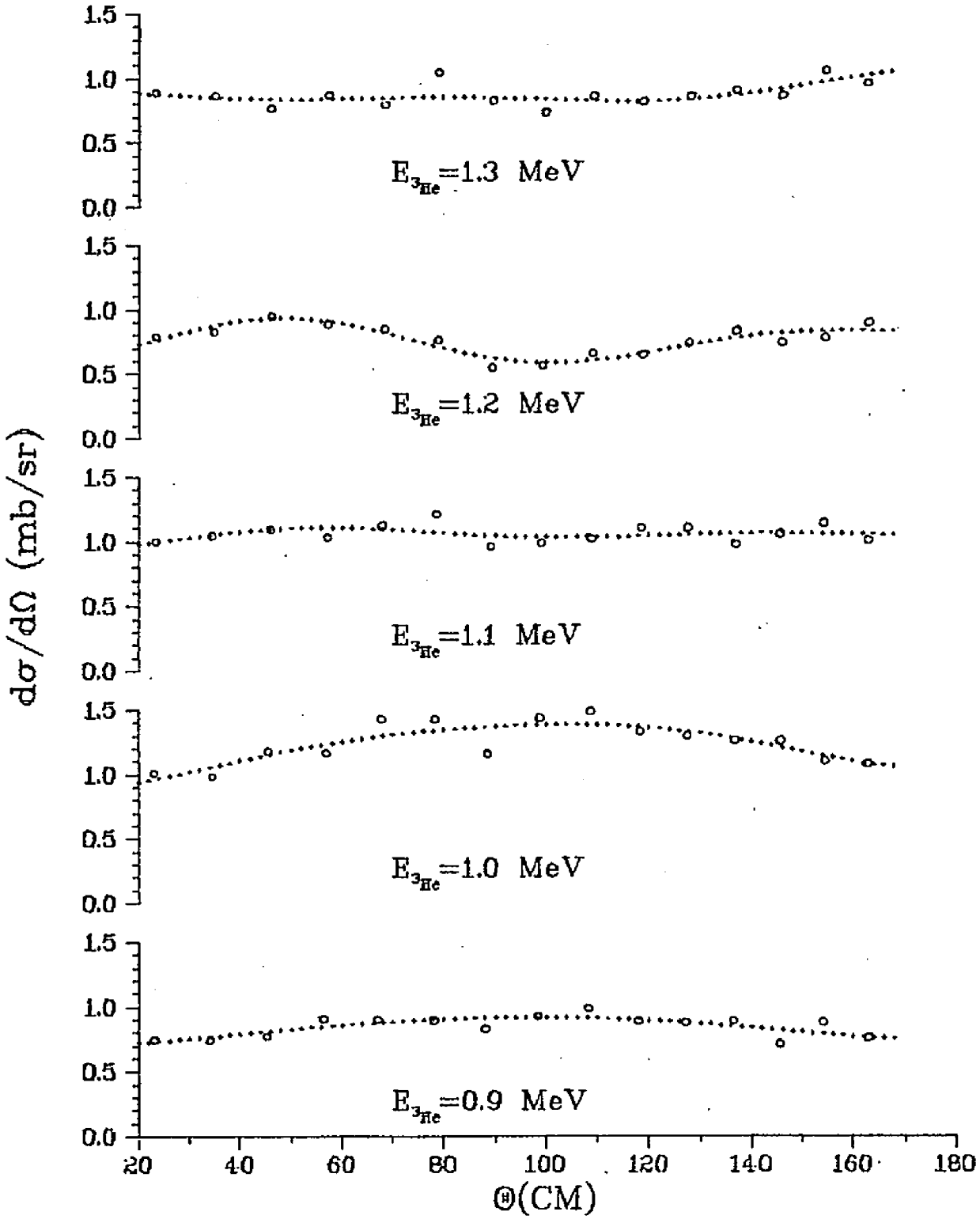

ANGULAR DISTRIBUTION FOR ^{6}LI(5.37)

Fig. 24

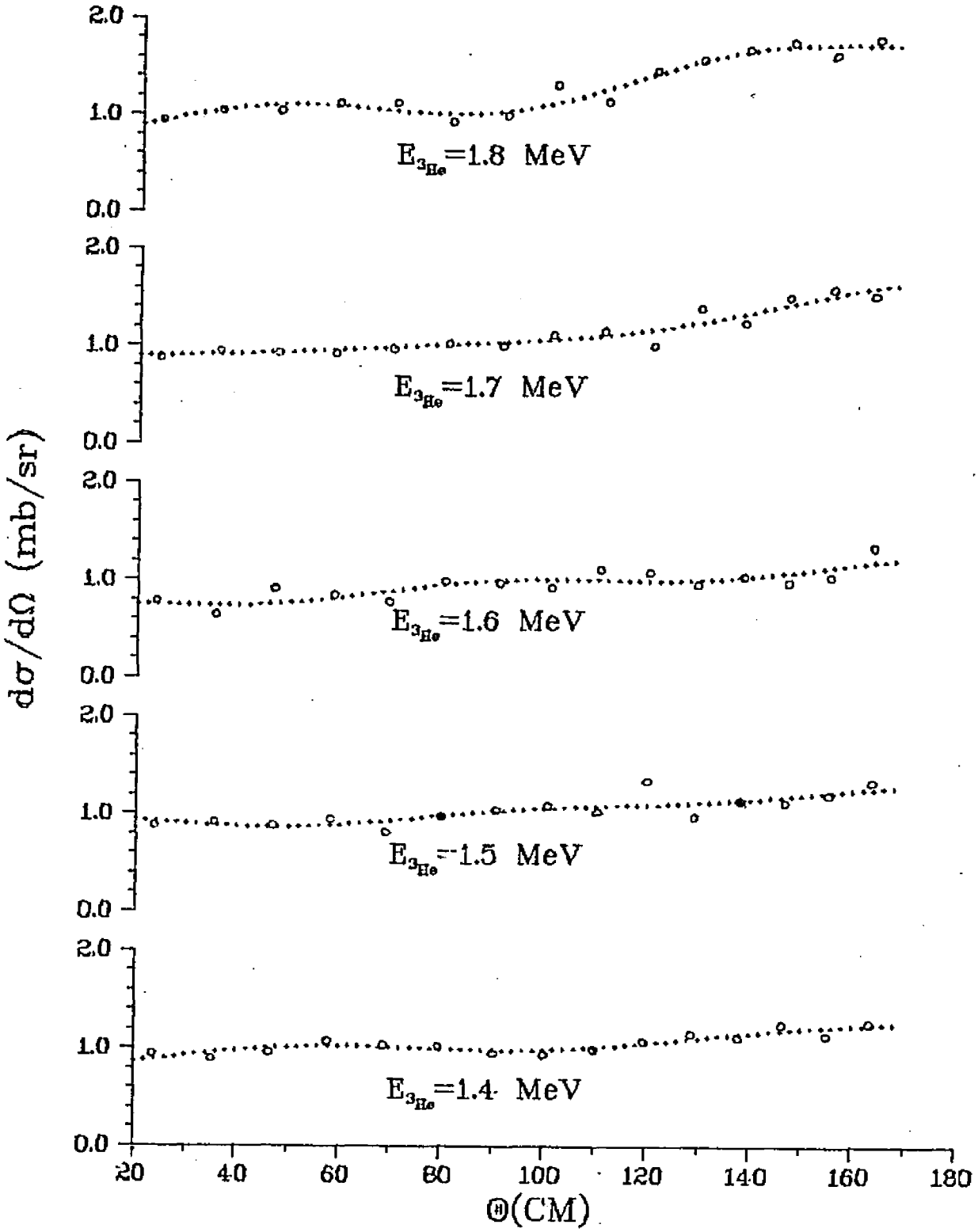

ANGULAR DISTRIBUTION FOR ^{6}LI(5.37)

Fig. 25

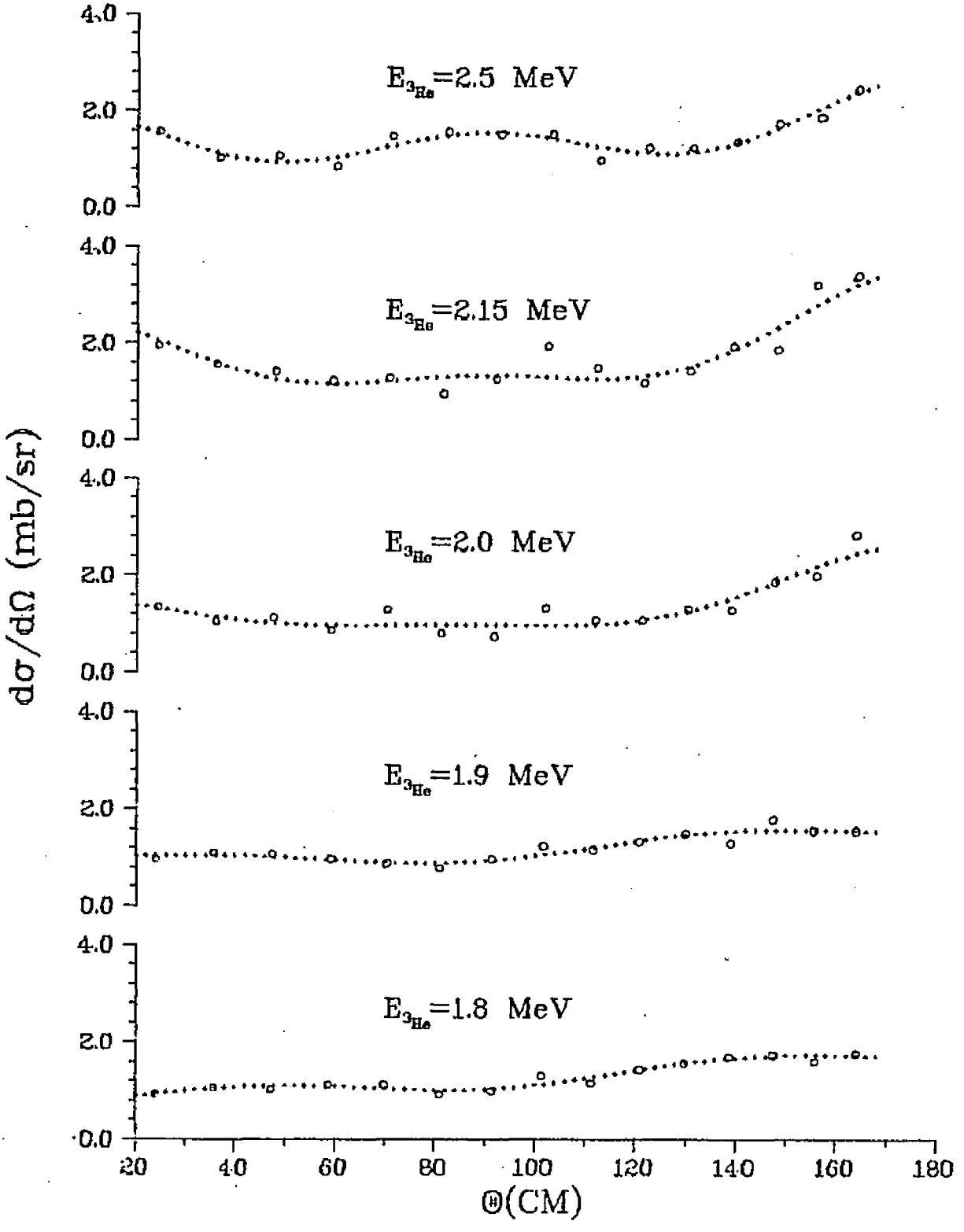

Energy Dependence of the A_l defined by

$d\sigma/d\Omega=\sum A_l P_l(\cos\theta)$

for the ^{6}Li(g.s.) state

Fig. 26

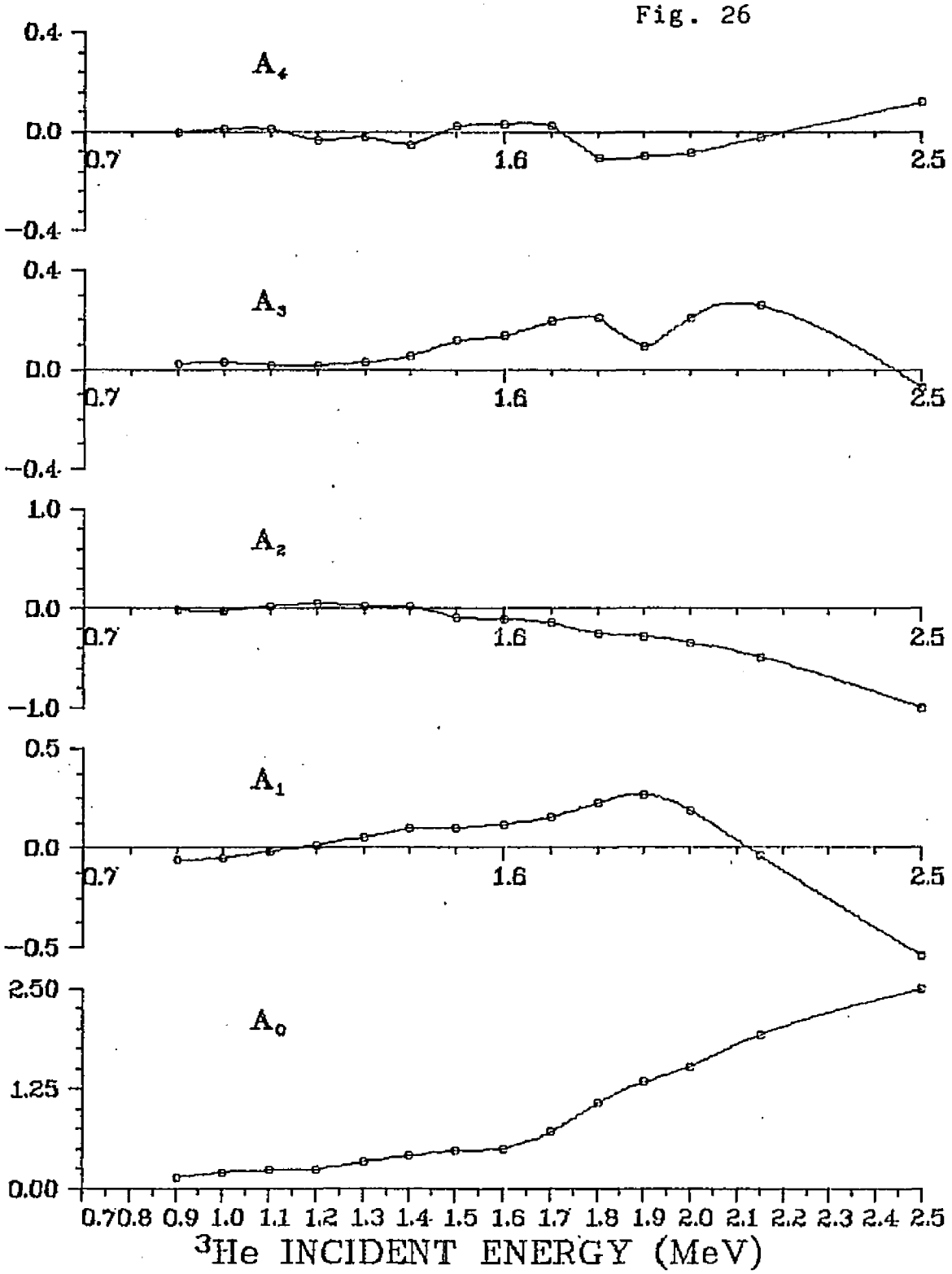

Energy Dependence of the A_l defined by

$d\sigma/d\Omega=\sum A_l P_l(\cos\theta)$

for the ^{6}Li(2.18) state

Fig. 27

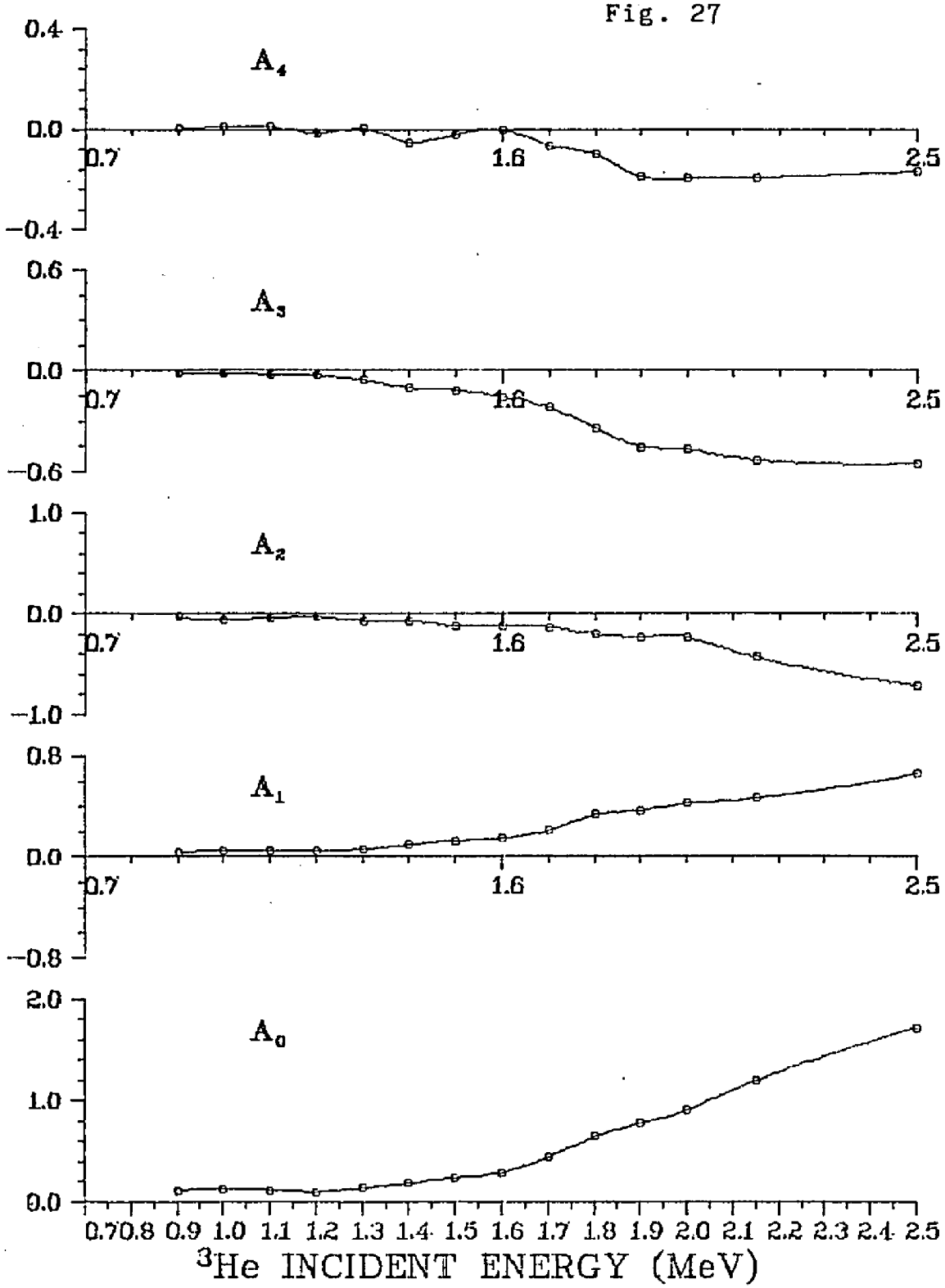

Energy Dependence of the A_l defined by

$d\sigma/d\Omega=\sum A_l P_l(\cos\theta)$

for the ^{6}Li(3.56) state

Fig. 28

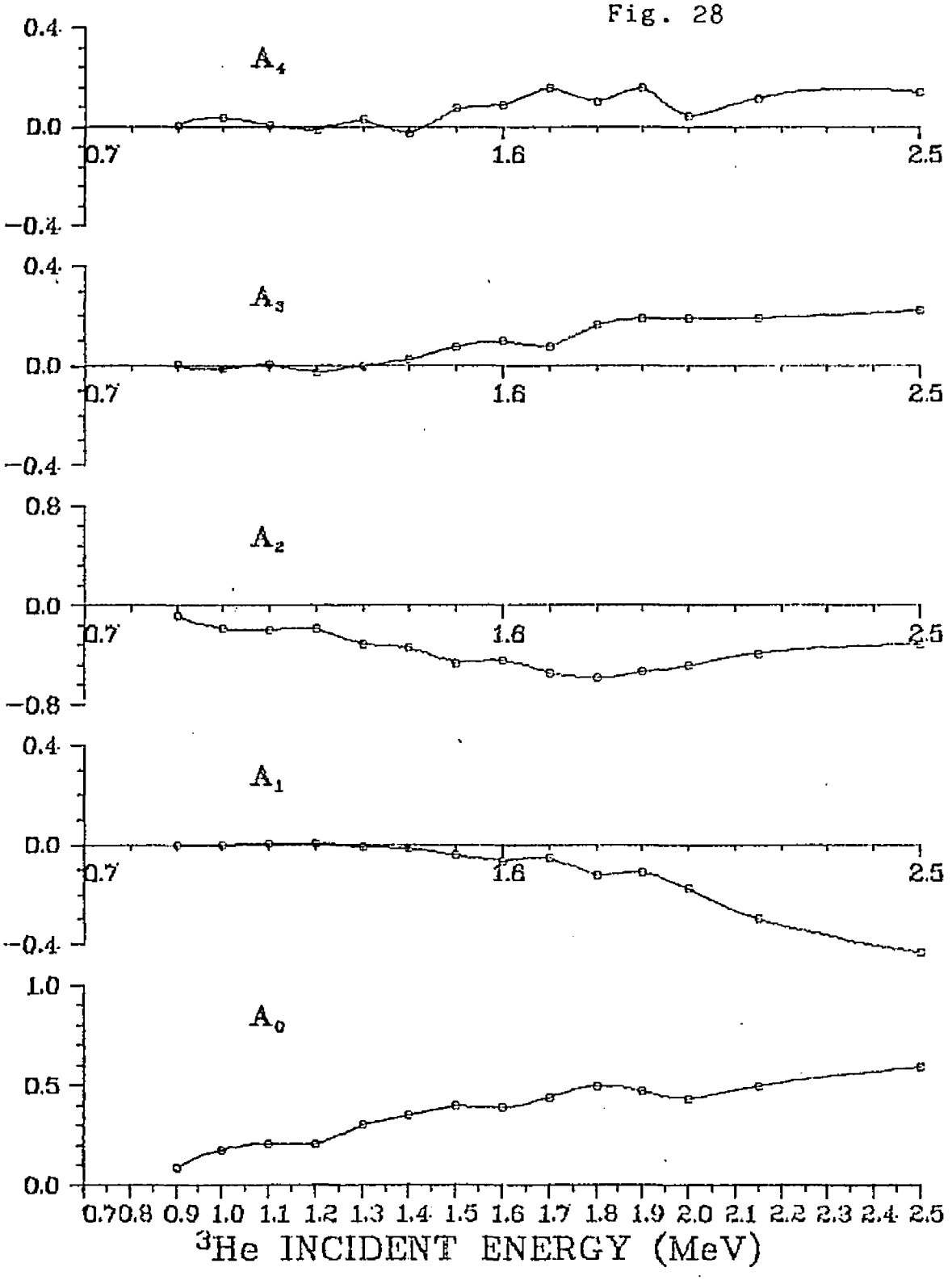

Energy Dependence of the A_l defined by

$d\sigma/d\Omega = \sum A_l P_l(\cos\theta)$

for the ^{6}Li(5.37) state

Fig. 29

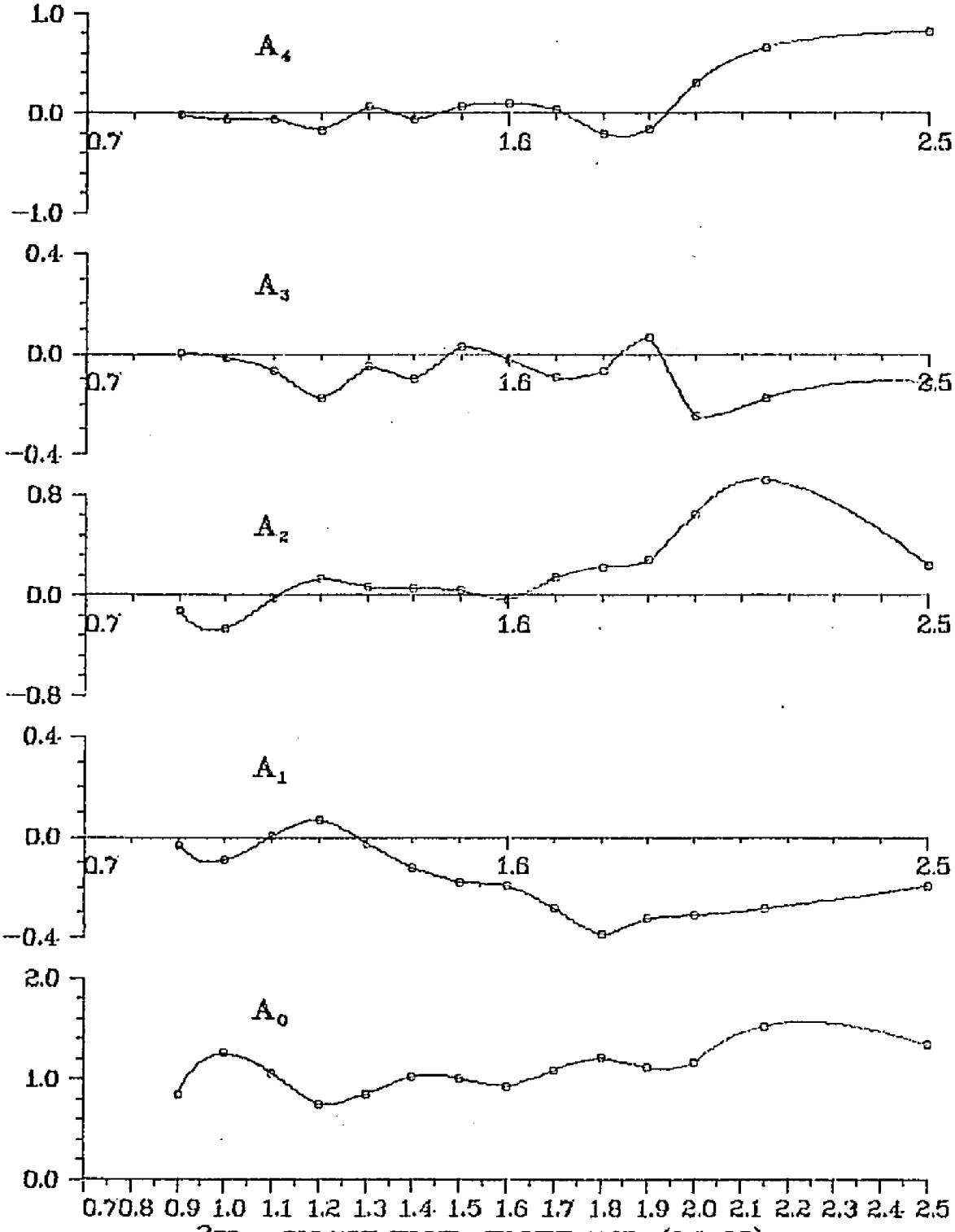

and are shown in Fig.26-29. Curves are drawn smoothly by hand and are merely meant to guide the eye. The total cross sections of the ground state and the first two excited states yield no unambiguous evidence for resonances. However, the total cross section of the 5.37 MeV excited state does show evidence of resonances at 1.0, 1.45 and 2.15 MeV and possibly around 1.8 MeV as well.

The Legendre polynomial coefficients $A_0, A_1 \text{---} A_4$ obtained from a least squares fit to the angular distributions, and plotted in Fig.26-29, can be compared with those of Paul et al(Ref.11) for the g.s. and first two excited states. The overall agreement between the present data and that of Ref.11 is very good, lending support to the accuracy of the new data obtained for the 5.37 MeV state. The numerical values of these coefficients are listed in Table 22-25.

C. DWBA Calculations

The (^{3}He,α) reaction is conventionally treated as a neutron transfer process at bombarding energies which are free from compound nucleus contributions. Classically, the physical interpretation assumed is that the projectile interacts with the target nucleus principally via a valence neutron, forming the outgoing alpha-particle and thereby tends to maintain the same direction(forward) as the projectile.

For all excited states of ^{6}Li populated in the present experiment, the J^{π} values have been well established leaving no ambiguity in determing the angular momentum carried by the transferred nucleon for the DWBA calculations.

The angular momentum carried by the transferred neutron in the direct pick-up process for the various ^{6}Li states transitions are listed in Table 1.

The bound state wave function for the transferred nucleon was determined by calculating cross sections for several different sets of bound state well parameters as well as for different sets of optical model parameters until the best overall reproduction of the cross sections at forward angles was reached.

After obtaining the best set of parameters for the bound state form factor the next step was to search the optical model parameters which could best reproduce the magnitude as well as the shape of the measured differential cross sections. In these calculations, the contributions from different transferred angular momentum were added incoherently.

The optical potential in the entrance channel was obtained from an anlysis of $^{7}Li + ^{3}He$ elastic scattering at 11 MeV by Scheklinski et al(Ref.45) and listed in Table 2. The DWBA calculations were not particularly sensitive to the entrance channel potential. The results were more sensitive to the exit channel potential. Since no data exists for al-

Table 1

Bound-State Woods-Saxon Potential Parameters

System	Orbit	E_{se}	V_o	R(fm)	a(fm)
$n+^3He$	$1S_{1/2}$	20.578	60	1.10	0.50
$n+^6Li$	$1P_{1/2,3/2}$	7.253	65	1.30	0.60

Table 2

Optical-model parameters used in zero-range DWBA analysis

System	V_o	W_v	W_s	R_o	R_v	R_s	a_o	a_v	a_s
$^7Li+^3He$	180	20	6.0	1.7	2.3	1.7	0.65	0.60	0.65
$\alpha+^6Li$	194	20		1.8	2.0	1.8	0.55	0.43	0.55

Table 3

Spectroscopic Factor of Cohen and Kurath

Orbit	Ground State	5.37 MeV State
$1P_{1/2}$	0.29	0.27
$1P_{3/2}$	0.49	0.33

pha scattering on ^{6}Li at these energies, potentials from an analysis by Zander et al (Ref.47) at 16 MeV were tried. The optical model parameters so obtained are listed in Table 2 for both entrance and exit channels.

In order to fit the magnitude of the experimental cross section properly, a renormalization constant was found necessary to multiply the calculated cross section.

Throughout the entire parametrization procedure the coulomb radius and the spin-orbit geometry parameters were set equal to the corresponding real well parameters and were not allowed to vary otherwise. All attempts to obtain satisfactory agreement between the calculated and experimental data using volume Woods-Saxon potentials failed.

The $^{7}Li(^{3}He,\alpha)^{6}Li$ differential cross sections calculated with the parameters of Table 2 and a renormalization constant of R=10 were compared to the experimental data at 1.8, 2.15 and 2.5 MeV for both the ground state and 5.37 MeV state. The spectroscopic factors have been taken from Cohen and Kurath(Table 3). The normalization factor was varied to obtain the overall fit at 1.8 MeV for the ground state data, then was kept fixed for the rest of calculations. The results are shown in Fig.30 & 31. As can be seen from these figures, the DWBA calculations are in poor agreement with the experimental data especially at 2.15 MeV. The disagreement is most pronounced regarding the ratio of back angle to

ANGULAR DISTRIBUTION FOR ^{6}LI(g.s.) AND DWBA CALCULATION

Fig. 30

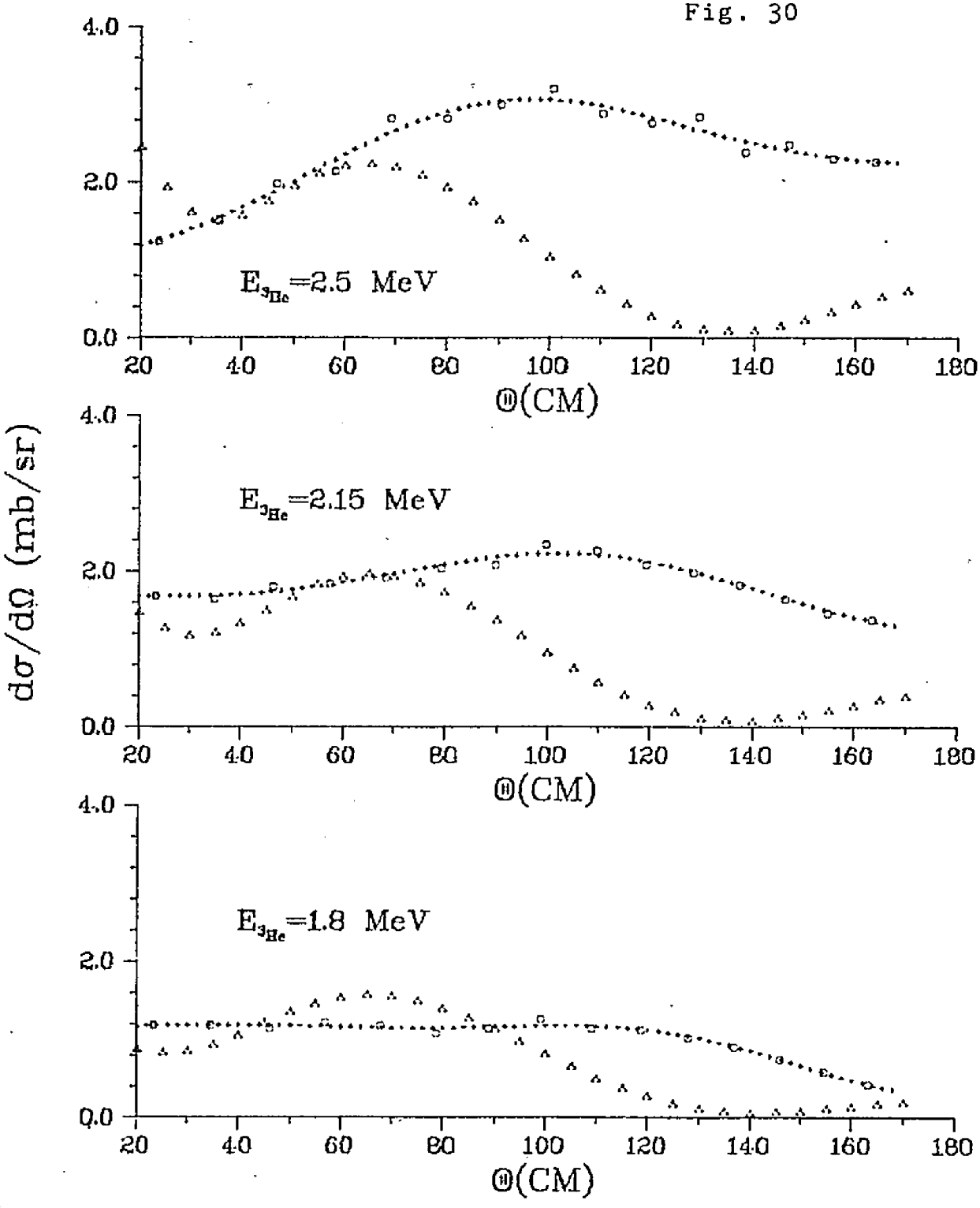

ANGULAR DISTRIBUTION FOR ^{6}LI(5.37) AND DWBA CALCULATION

Fig. 31

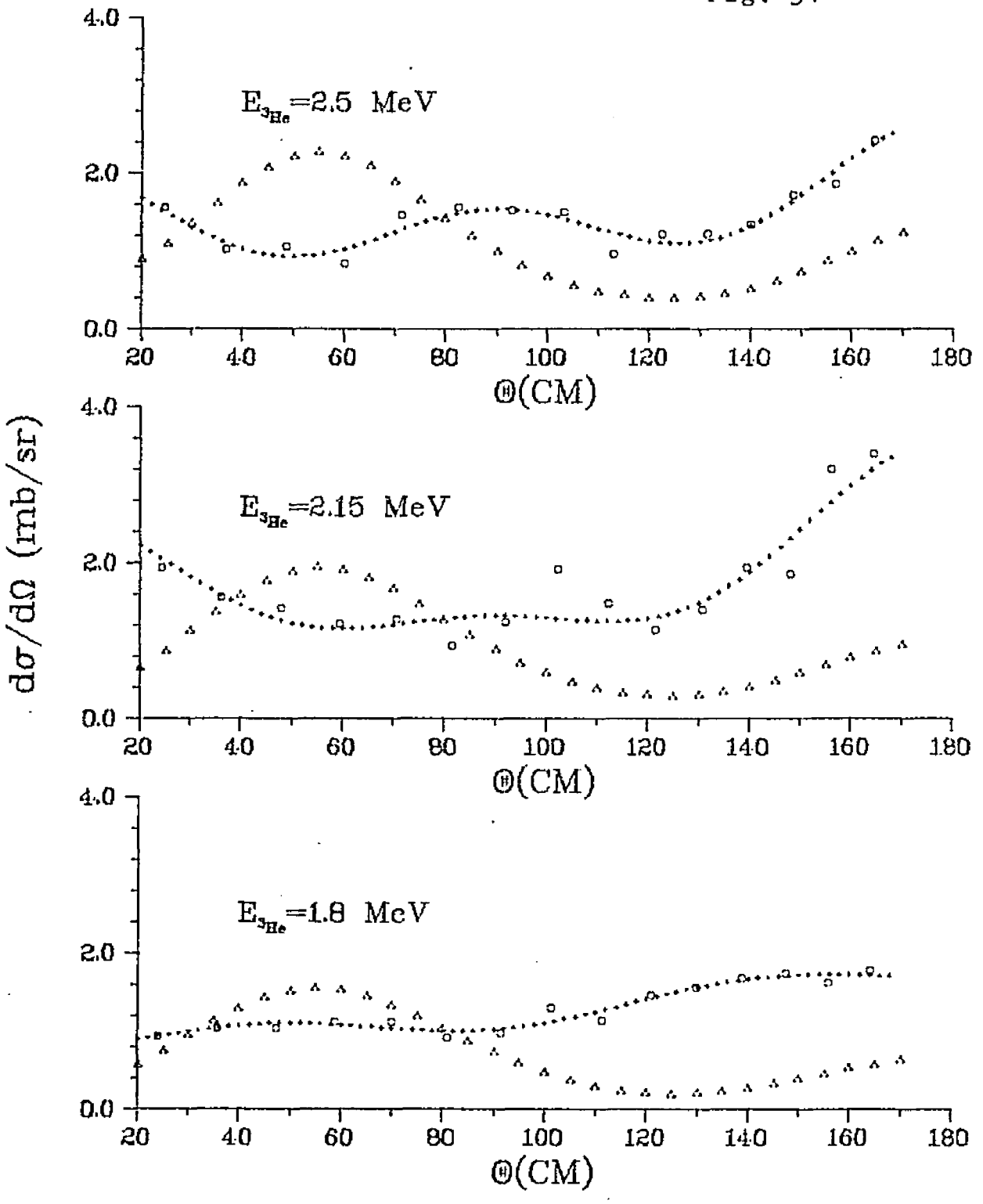

forward angle cross sections.

D. Decay of the 5.37 MeV State

For the α-α coincidence measurements, a 121 μm SB detector with 1/2 mil mylar foil in front of it was used to detect the first emitted alpha particle at 30° forming the 5.37 MeV excited state. A 22.7 μm SB detector, which can stop alpha particle energies up to 4.8 MeV, proton energies up to 1.22 MeV, deuteron energies up to 1.48 MeV, was used to detect the second emitted alpha particles from the decay of ^{6}Li. A 300 μm SB detector placed right behind it served as a reject detector to eliminate events corresponding to more energetic alpha particles passing through the 22.7 μm detector. The ensemble was collimated by a 5/32" X 5/16" aperature located 3.5" from the target. Decay alpha particles were measured at several angles in coincidence with the first emitted alpha particles at 30° and for a ^{3}He bombarding energy of 2.15 MeV.

Conventional fast-slow timing techniques were used as discussed in section III Fig. 8 describe the electronics except for the addition of a reject detector with associated spectroscopy amplifier and TSCA, supplying an anticoincidence pulse to the slow coincidence unit. A typical TAC spectrum taken during the run is shown in Fig.32. True to random ratios better than 10 to 1 and the FWHM is about 10

$\alpha - \alpha$ TAC Spectrum

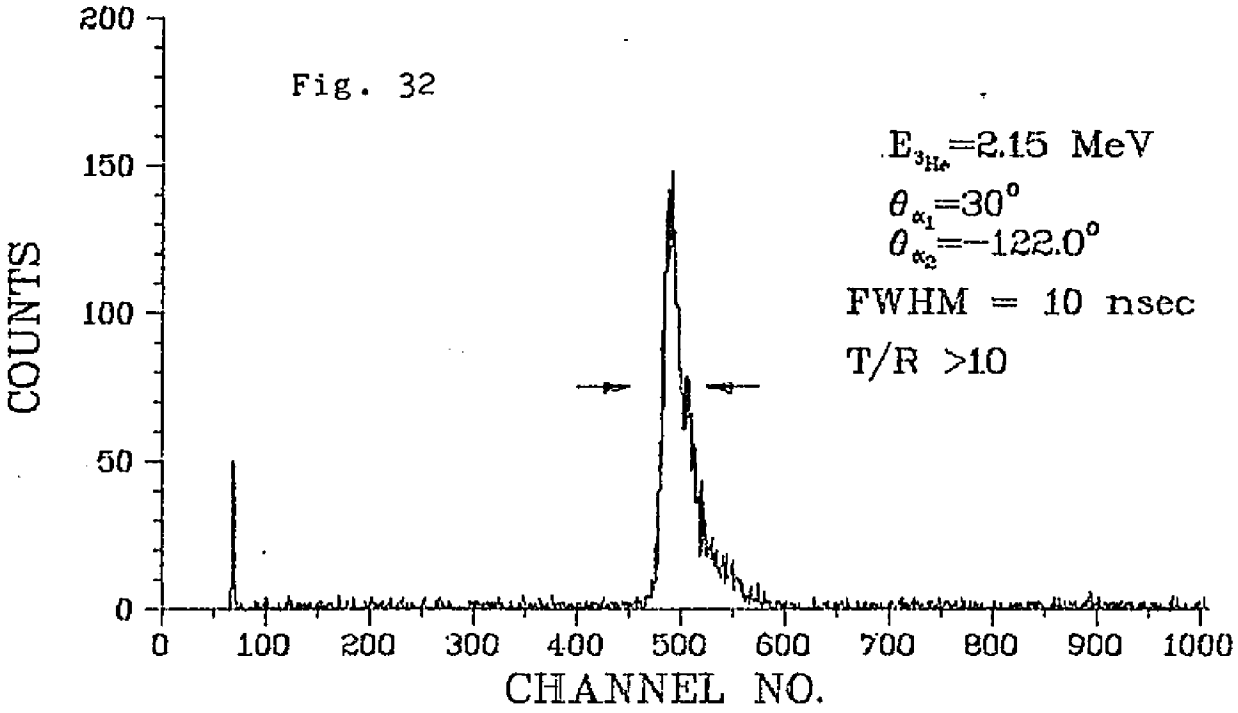

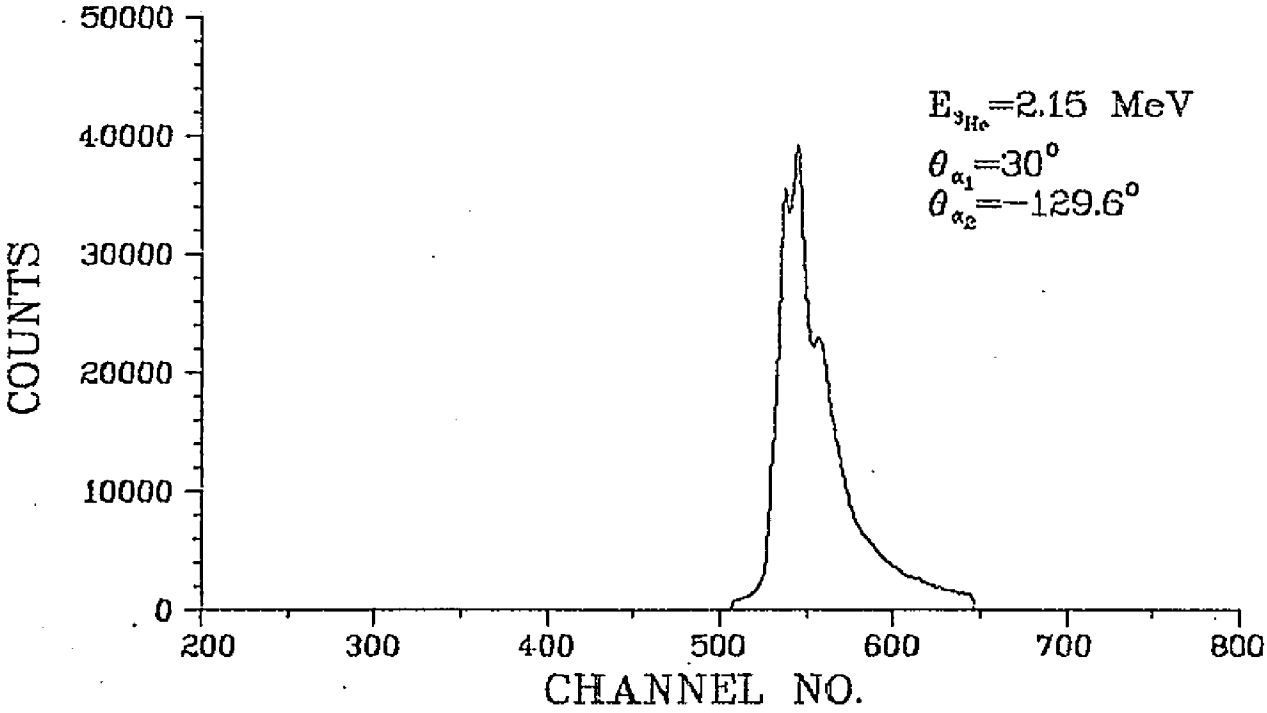

ns.

One expects to observe certain two body final state coincident events between α-particles and ^{6}Li nuclei stable with respect to particle decay. Since the ground state is stable and the 2.18 level is above only the α+d threshold, the $^{7}Li(^{3}He,\alpha)^{6}Li(g.s.)$ and $^{7}Li(^{3}He,\alpha)^{6}Li(2.18)\rightarrow\alpha+d$ reactions should be the dominant two- and three-body reactions respectively. It is also expected that, for the α-α coincidence, the indistinguishability of two identical particle will give rise to one more symmetric peak which results from the detection of the α-particles in opposite detectors.

Fig.33-39 shown the experimentally observed two-dimensional energy spectra at various angle pairs. The α-α kinematic curve is clearly seen and peaks in the yield along this curve are identified corresponding to the 2.18 MeV excited state of ^{6}Li. The decays into α + p + n are accumulated in a vertical band within the region of the four body final state. The curving shapes appear on the high energy end are due to the kinematic effect on the broad width of the 5.37 MeV state. Fig.40 shows the theoretically calculated kinematic curves with and without a mylar foil in front of the 30° detector.

Energy calibration was done using the four peaks appear in the recoil angle spectrum, α_1 energies were checked with the calibration of the singles spectrum at 30°. Back-

$\alpha - \alpha$ Coincidence Spectrum

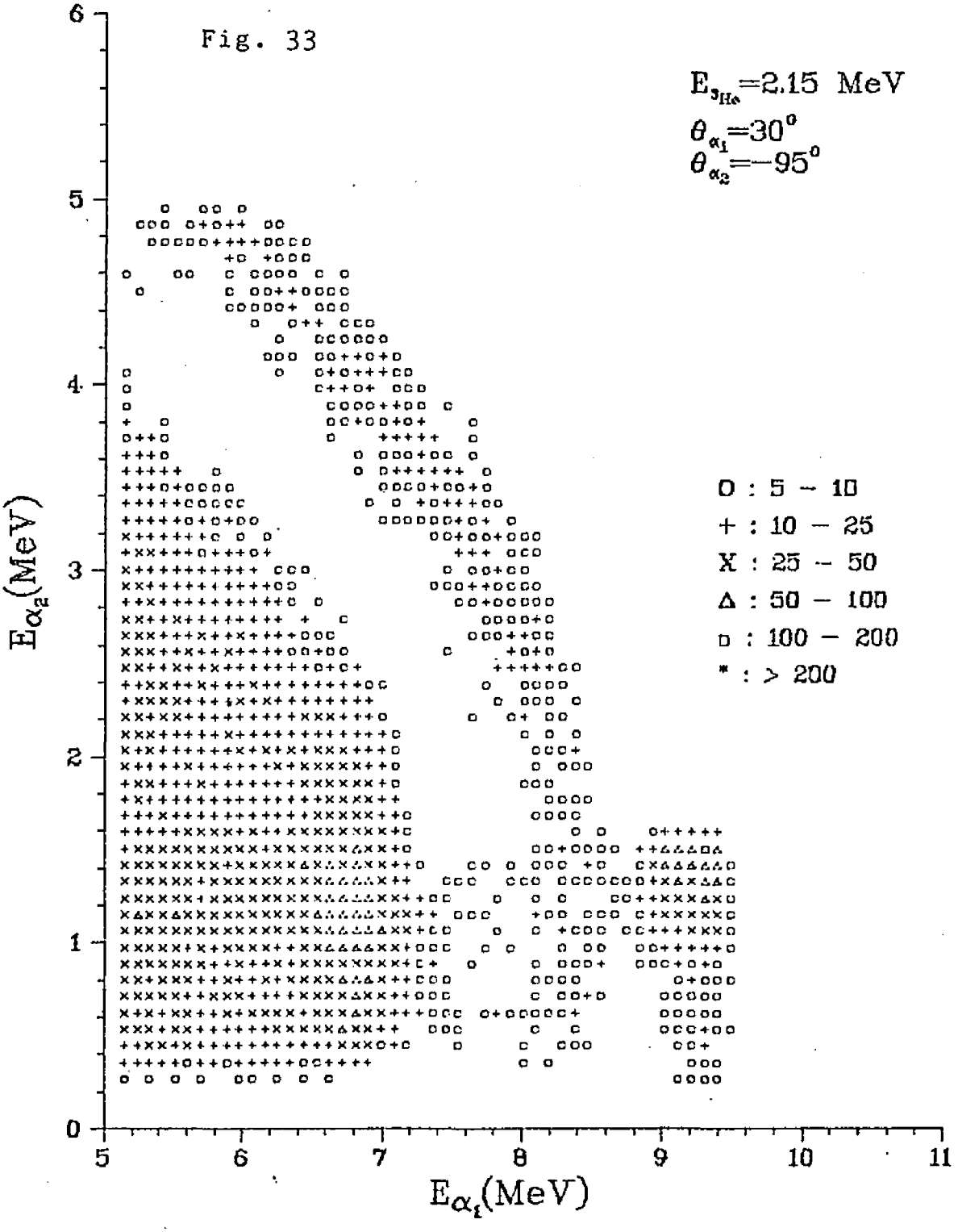

$\alpha - \alpha$ Coincidence Spectrum

Fig. 34

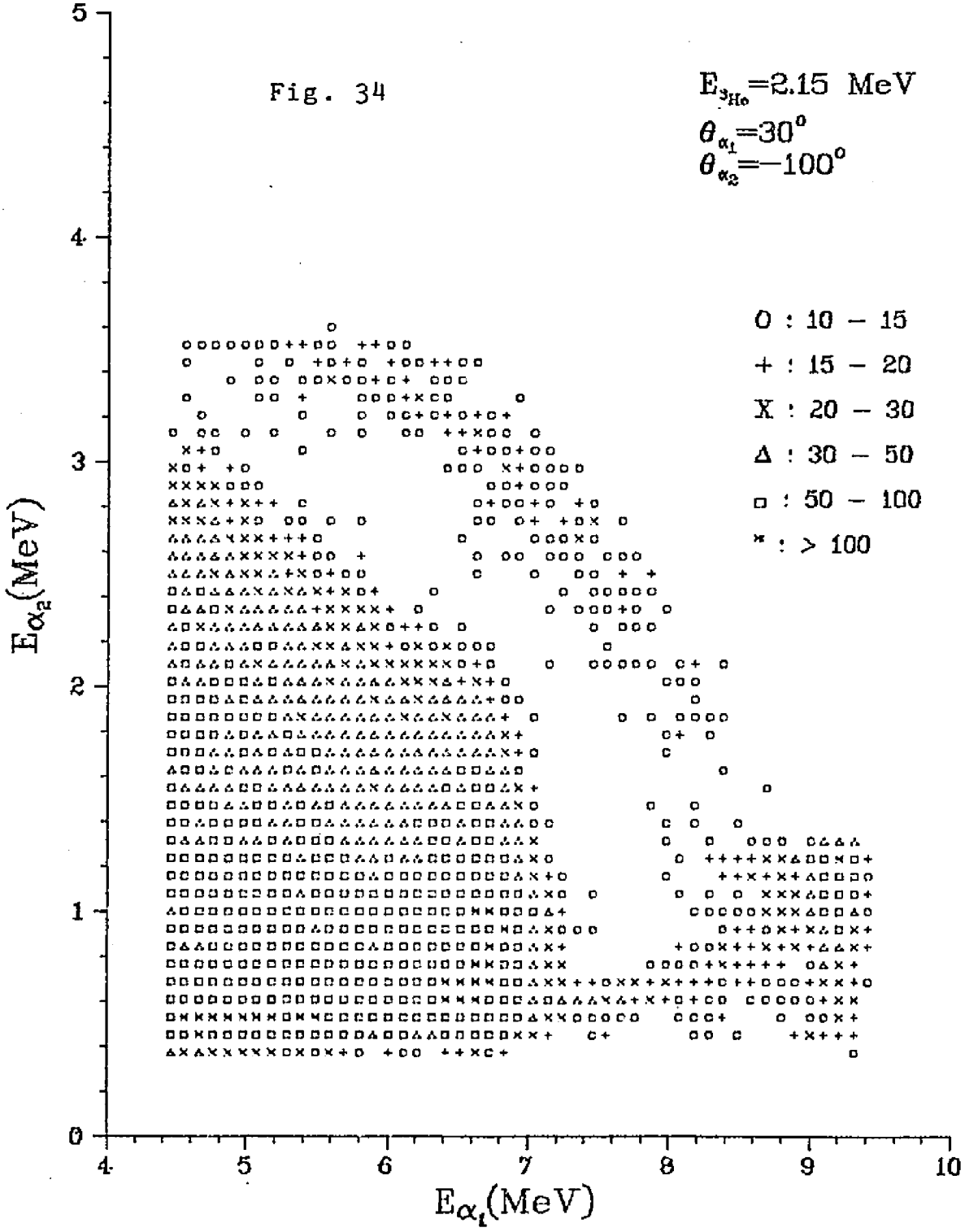

$\alpha - \alpha$ Coincidence Spectrum

Fig. 35

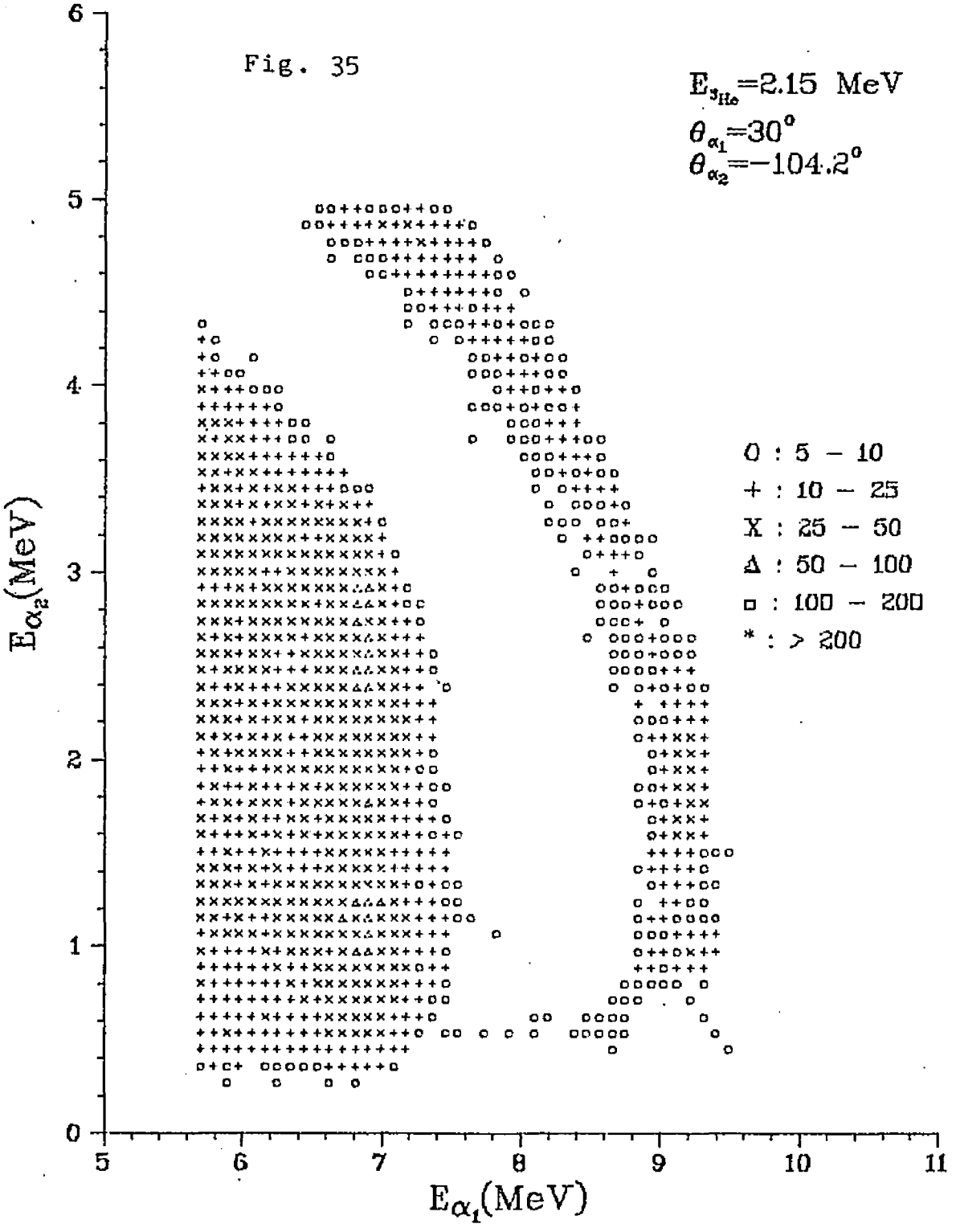

α − α Coincidence Spectrum

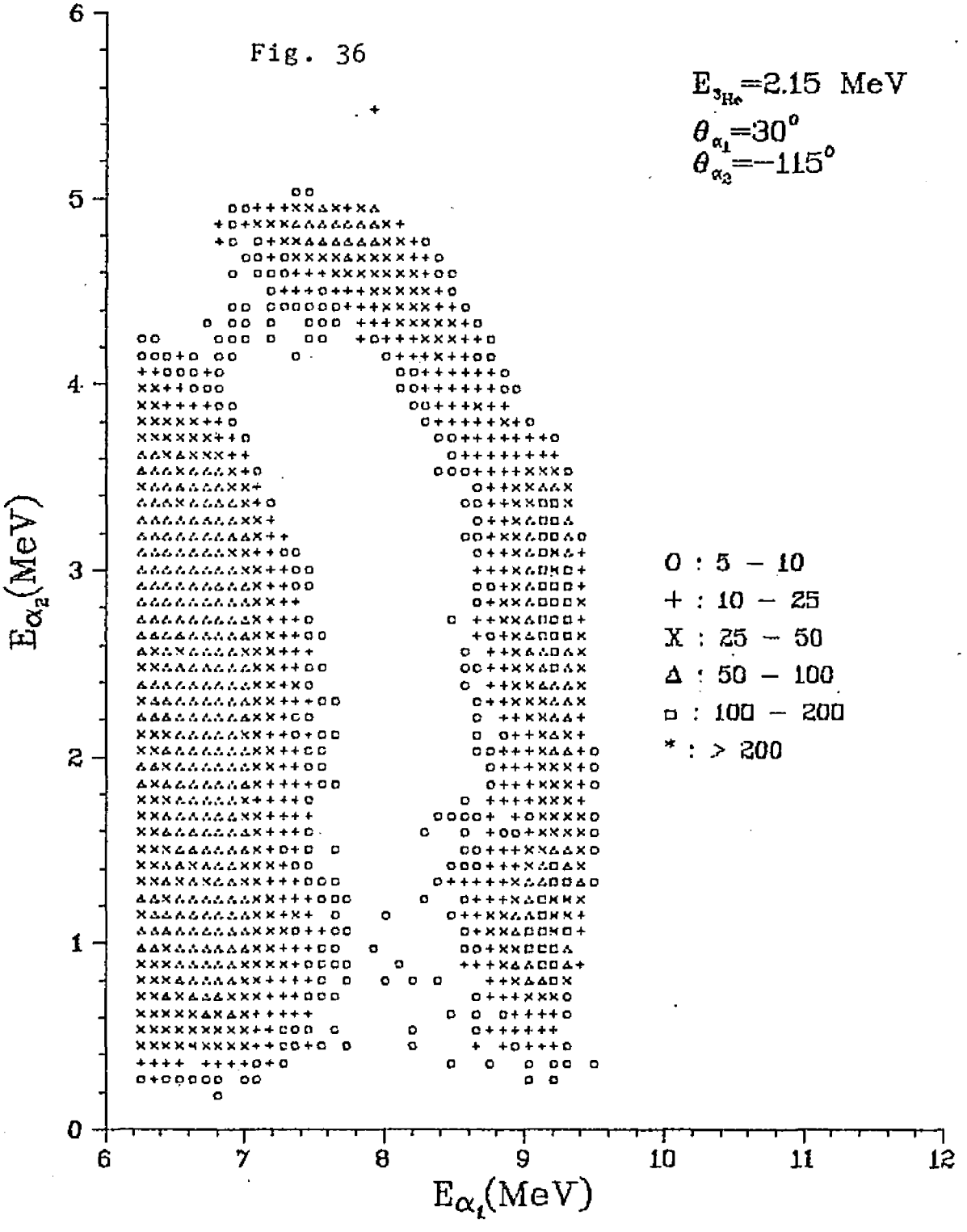

$\alpha - \alpha$ Coincidence Spectrum

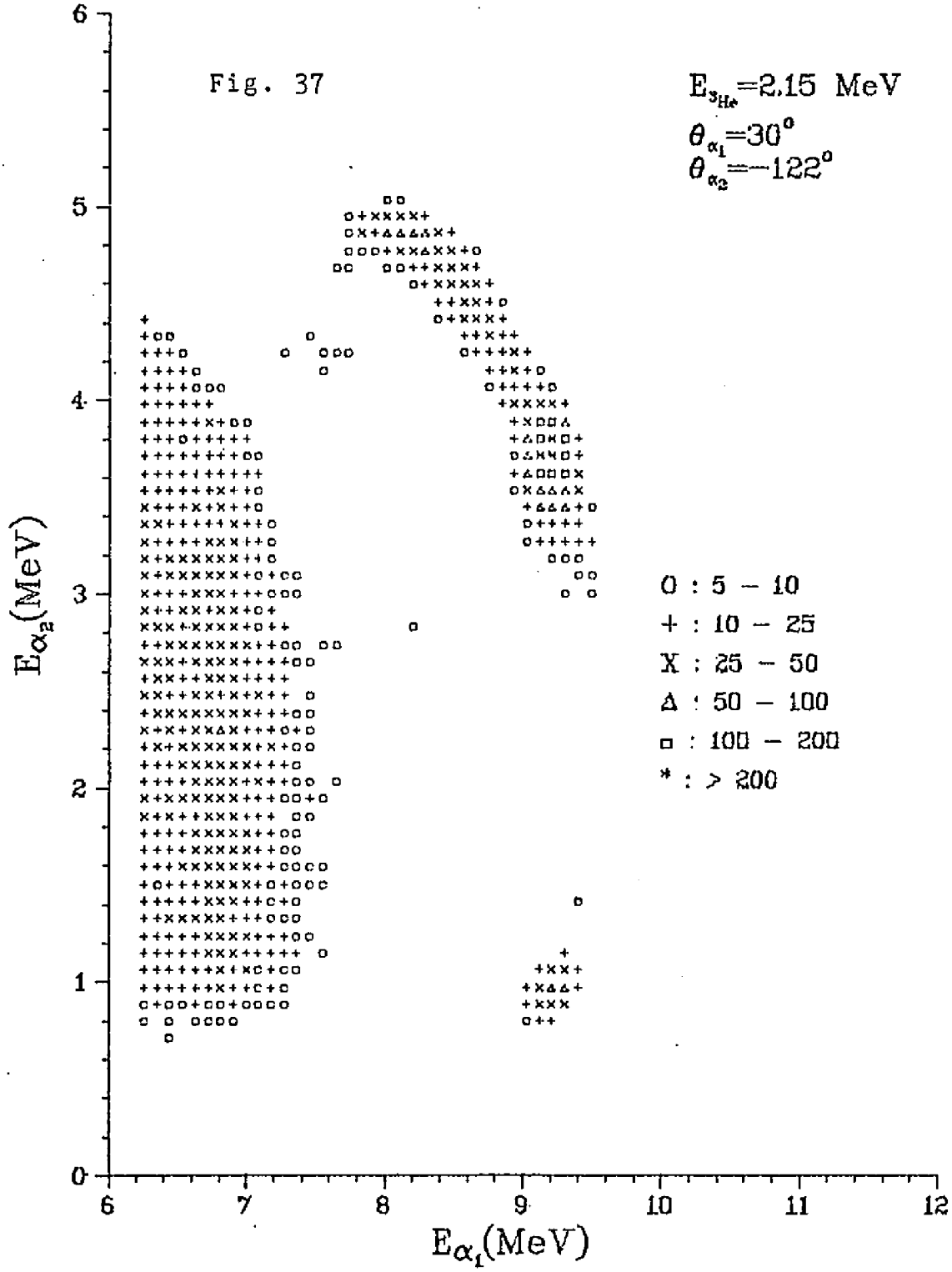

$\alpha - \alpha$ Coincidence Spectrum

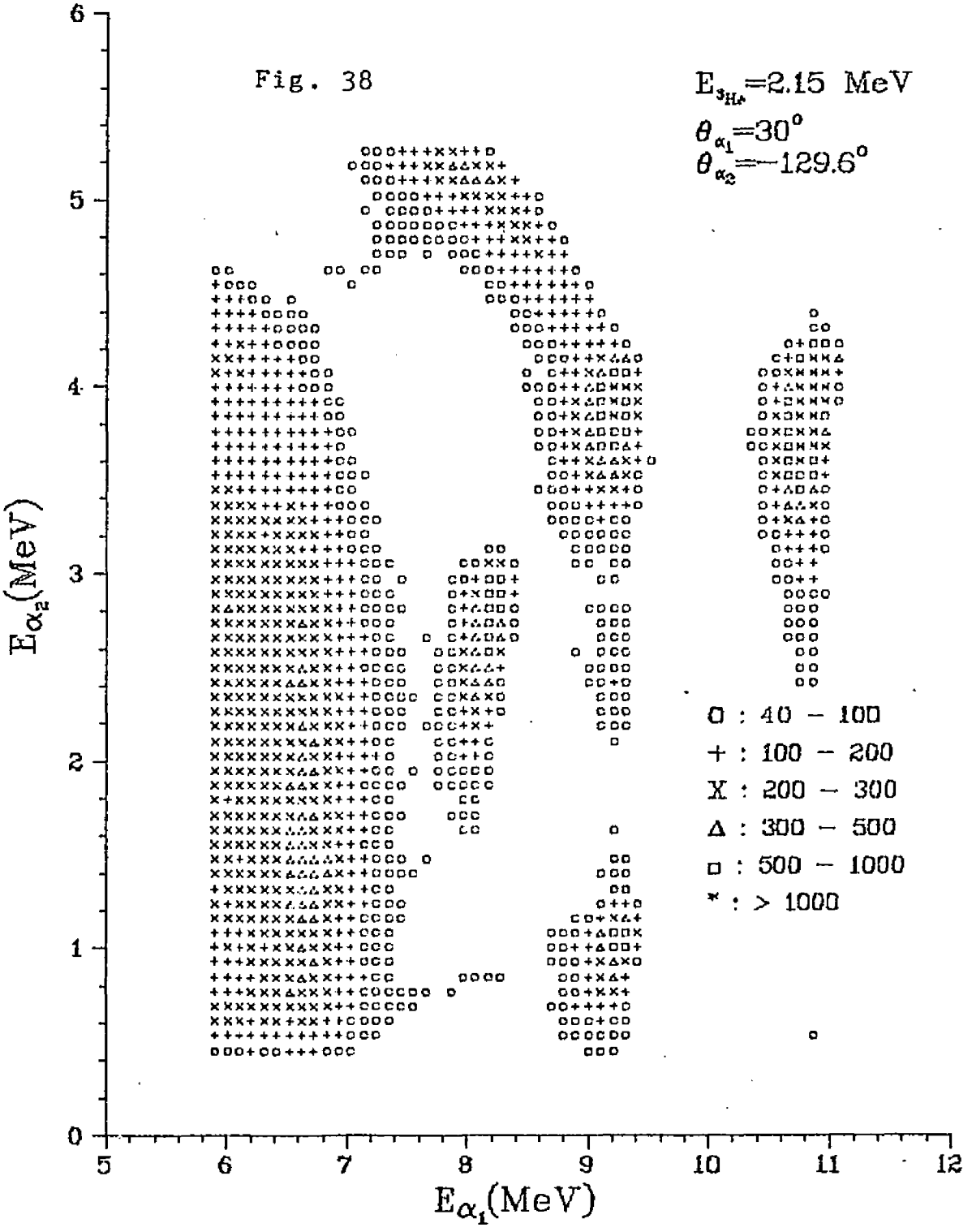

$\alpha - \alpha$ Coincidence Spectrum

Fig. 39

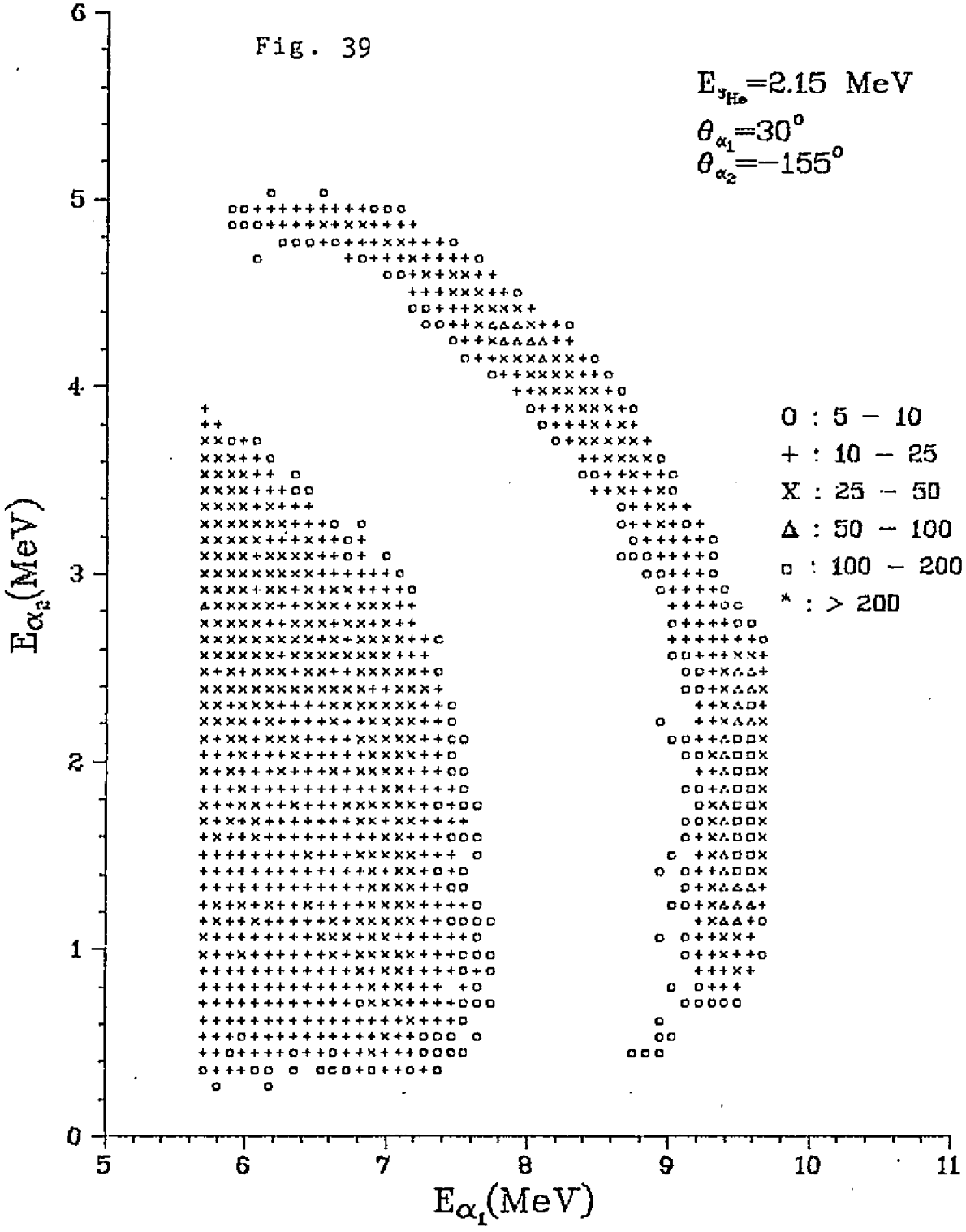

α–α Kinematic Curve for the Reaction $^{7}Li(^{3}He,\alpha d)\alpha$

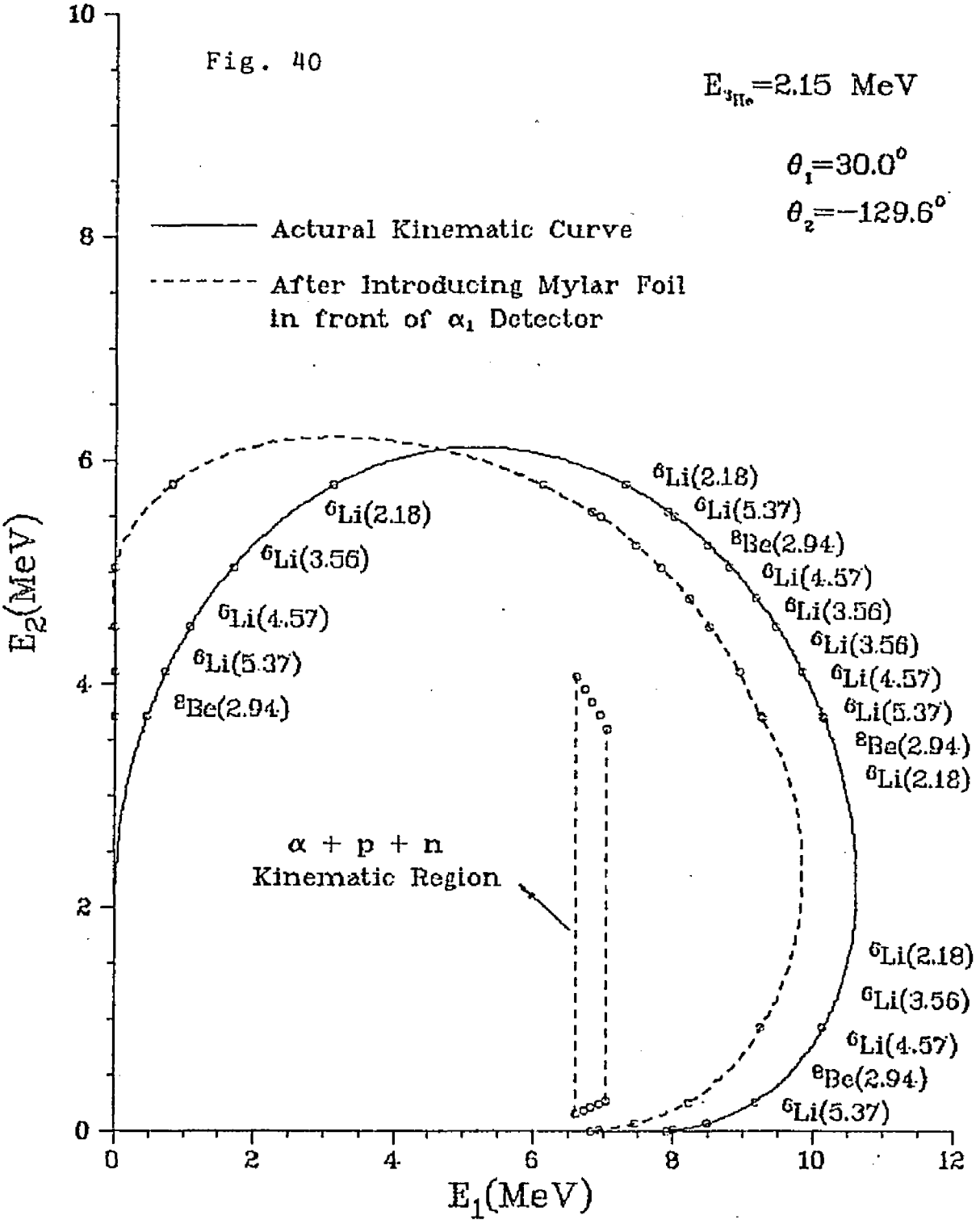

ground subtraction was done in a same manner as described before.

The α-α coincidence spectra were projected onto the α_2 axis and compared with the final state phase space distribution. These are plotted in Fig.41-43. All the yields have been normalized to the ground state and the phase space spectra were normalized in such a way as to have the same integrated yields as the data in the high energy region. The laboratory alpha particle energies corresponding to kinematic minimum and maximum energies in the ^{6}Li(5.37) CM system are indicated. The solid curves represent the phase space spectra which have been transformed into the laboratory system for comparison. The expression for the phase space distribution in the CM system $[E_\alpha(Q/3 - E_\alpha)]^{1/2}$ was taken from Geesaman et al(Ref.44).

As can be seen from the diagrams, the yield in the low energy part of the projected α_2 coincidence spectra is generally enhanced compared with the available phase space. However, the spectra at 104.2° and 155°, which angles are symmetrically placed relative to the recoil direction, show a reduction in counts in the low energy part of the spectrum.

The two-dimensional spectra were also projected onto the α_1 axis along the kinematic band corresponding to α+d decay to look for evidence of an isospin forbidden but

Coincidence and Phase Space Spectra

Fig. 41

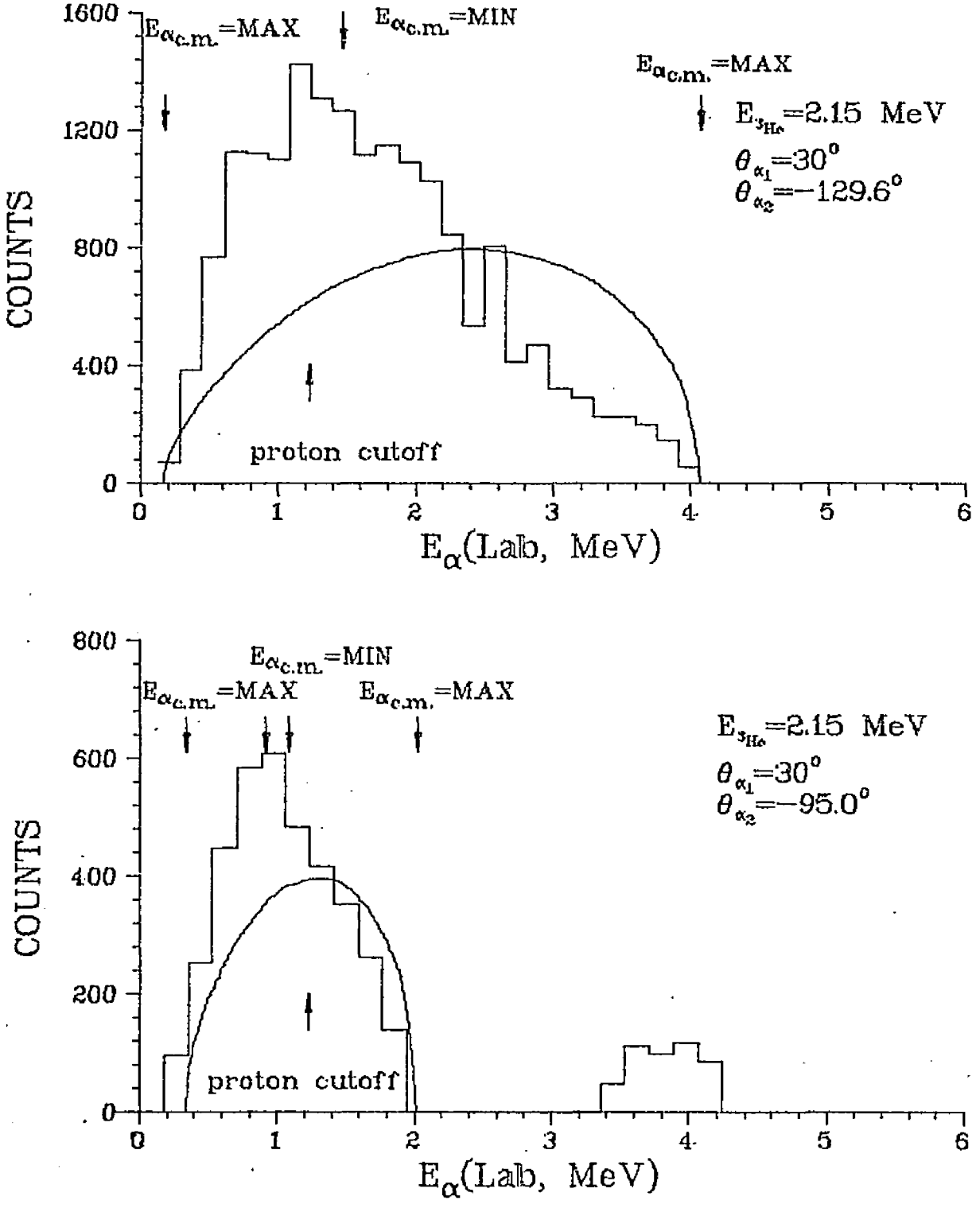

Coincidence and Phase Space Spectra

Fig. 42

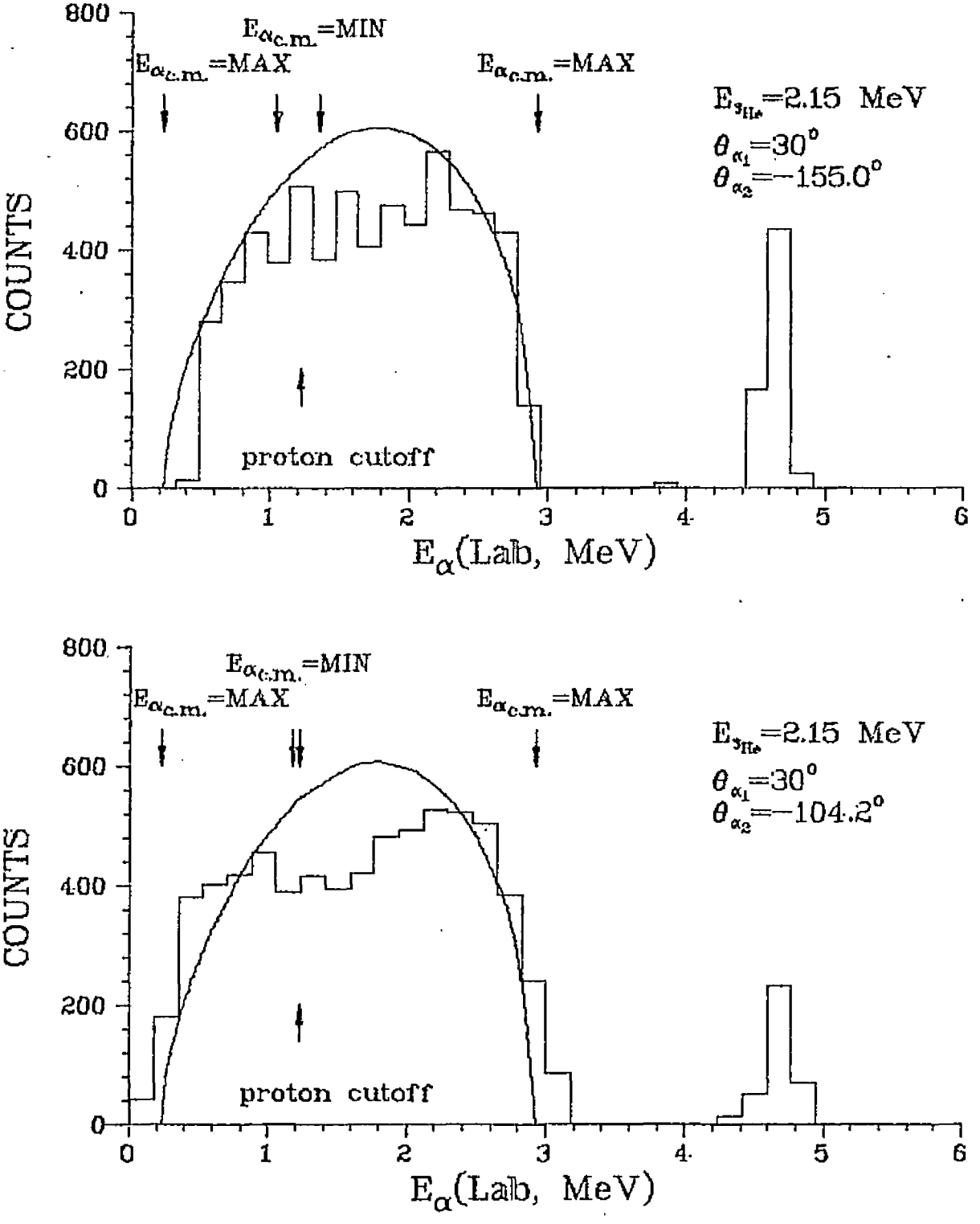

Coincidence and Phase Space Spectra

Fig. 43

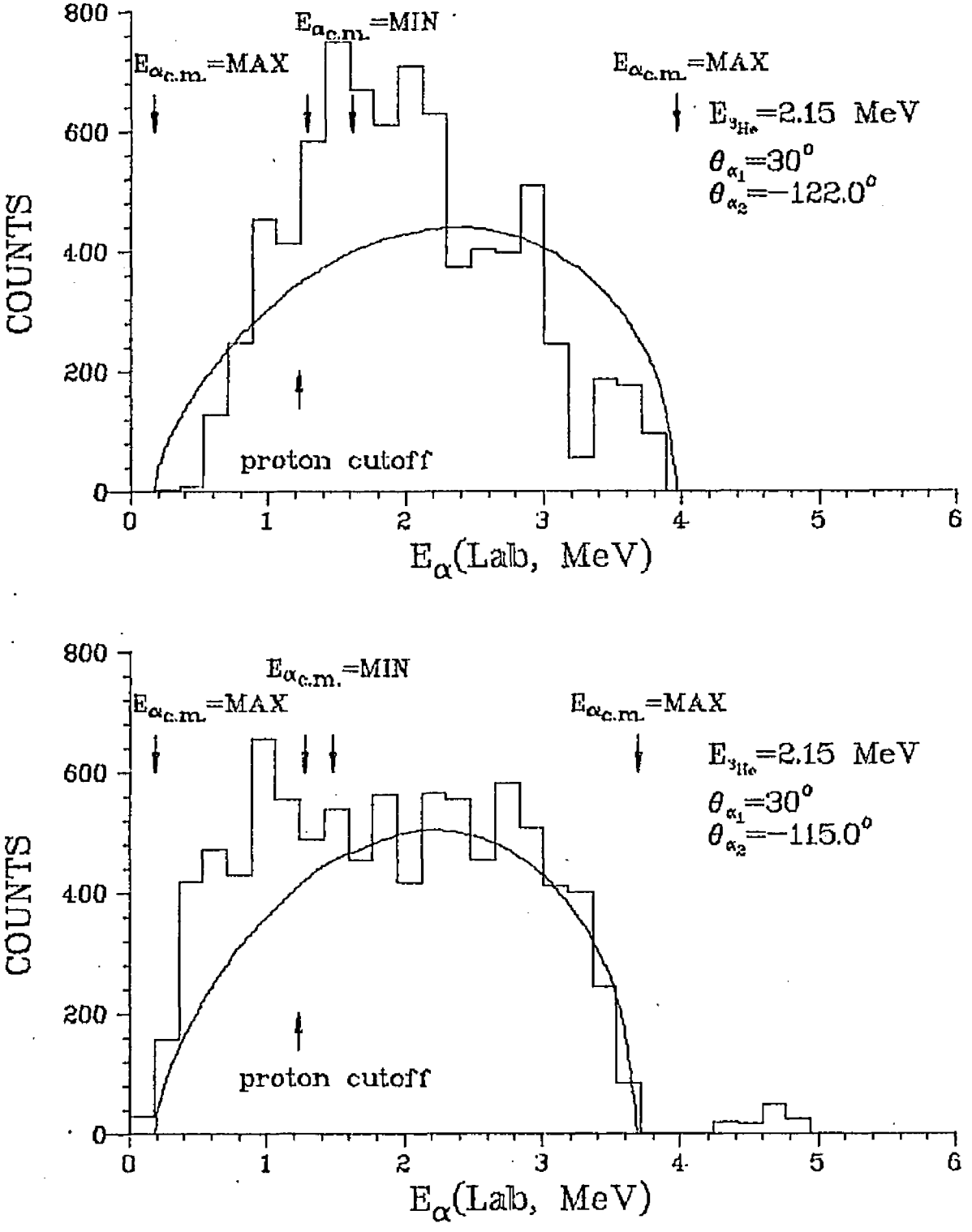

kinematically allowed decay of the 5.37 MeV state.(Fig.44)

The α-d coincidence spectra resulting from either of the two reactions $^{7}Li(^{3}He,\alpha)^{6}Li^{*} \rightarrow \alpha + d$ or $^{7}Li(^{3}He,d)^{8}Be(\alpha)(\alpha)$ were obtained with a particle identifier selecting the deuterons. Detector configurations were the same as that of the α-α coincidence measurements except the detector position was 1 and 1/16" away from the target. Thus the detector half angle was 4.21^{o} and the solid angle 43.25 msr. An α-d TAC spectrum is shown in Fig.45.

The deuterons were kinematically constrained to lie along the band which is shown in Fig.46-47. The intense peak at (9.25,2.92 MeV) results from the d-decay of the 2.18 MeV state in ^{6}Li. The sum along the kinematic band are projected onto both the alpha and deuteron axes and are plotted in Fig.48-49. States in ^{6}Li which appear as peaks in the singles spectra should also appear as peaks along the d-loci if they decay by d-emission. Strong d-decay from the 2.18 level is seen in channel 46 of Fig.48 and channel 53 of Fig.49 as would be expected, since this level is known to decay almost 100% by d-emission. The remaining d-yield spectrum shows disappointingly little structure. We expected contributions along this band from the 4.57 MeV level even though this level is not seen in the singles spectrum, but the broad width of this level and the 2.94 MeV level in ^{8}Be smear out the d-yield near the location of the 5.37 level. The absence of pronounced structure in the projected spectrum precludes

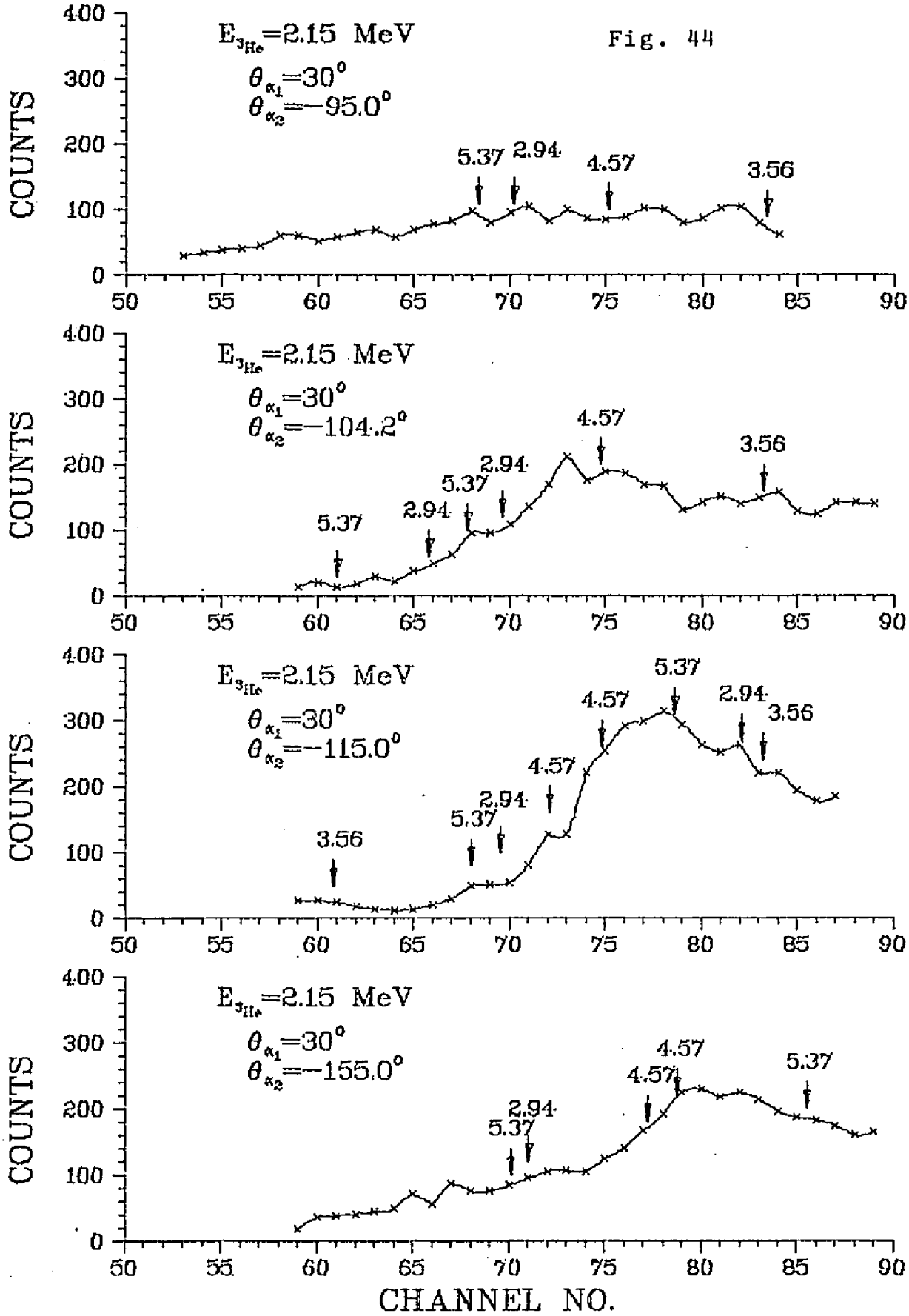
$E_{^3He}$=2.15 MeV
θ_{α_1}=30°
θ_{α_2}=−95.0°
5.37
2.94
4.57
3.56
$E_{^3He}$=2.15 MeV
θ_{α_1}=30°
θ_{α_2}=−104.2°
5.37
2.94
5.37
2.94
4.57
3.56
$E_{^3He}$=2.15 MeV
θ_{α_1}=30°
θ_{α_2}=−115.0°
3.56
5.37
2.94
4.57
4.57
5.37
2.94
3.56
$E_{^3He}$=2.15 MeV
θ_{α_1}=30°
θ_{α_2}=−155.0°
5.37
2.94
4.57
4.57
5.37
COUNTS
CHANNEL NO.
0
100
200
300
400
50
55
60
65
70
75
80
85
90

Fig. 44

α – d TAC Spectrum

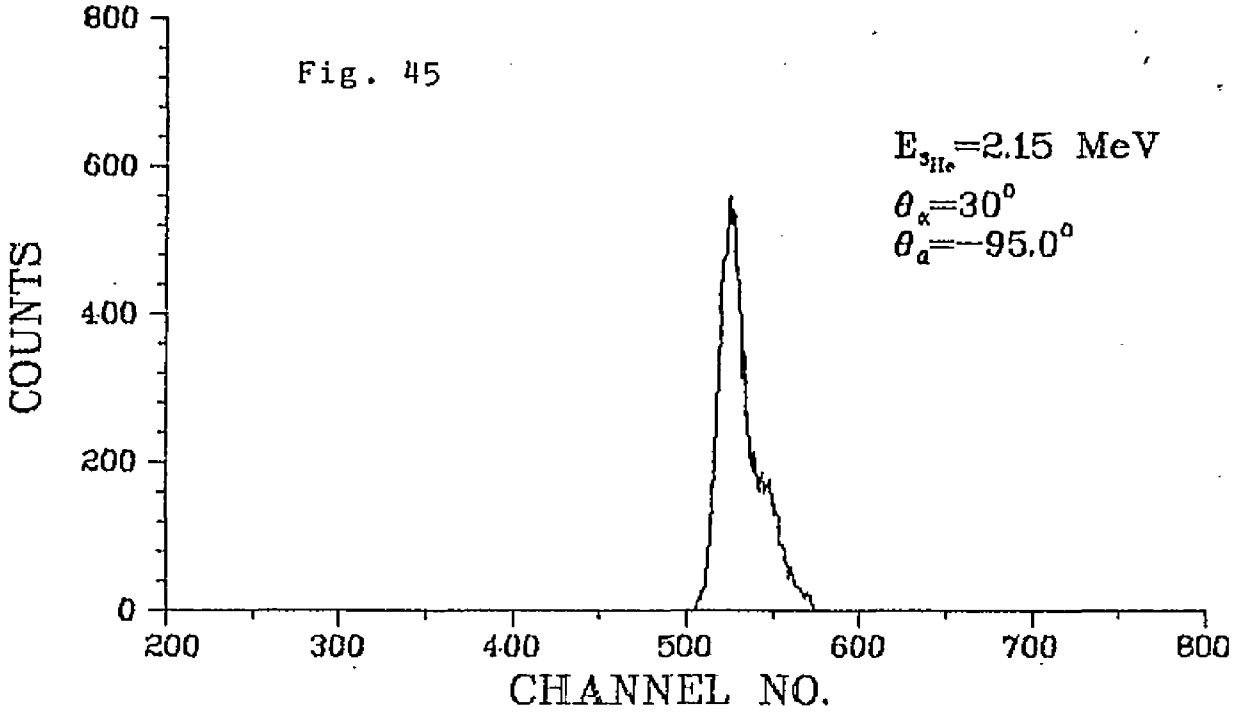

Fig. 45

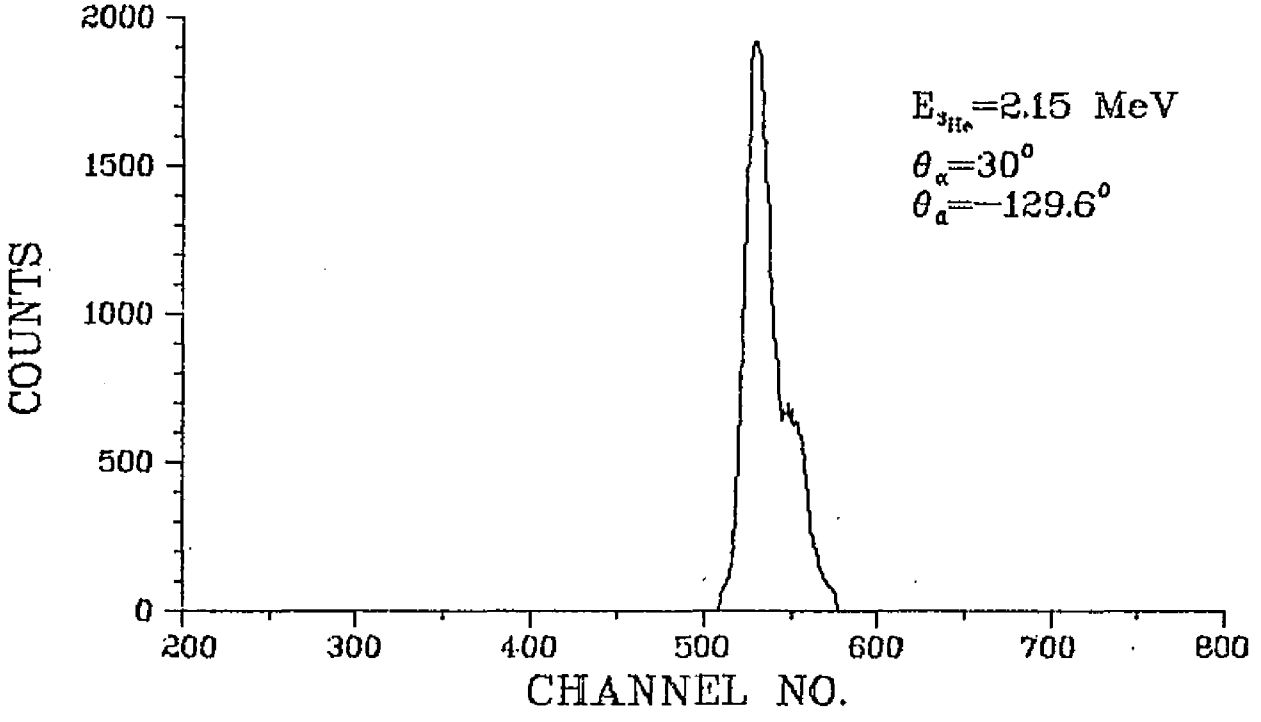

α – d Coincidence Spectrum

Fig. 46

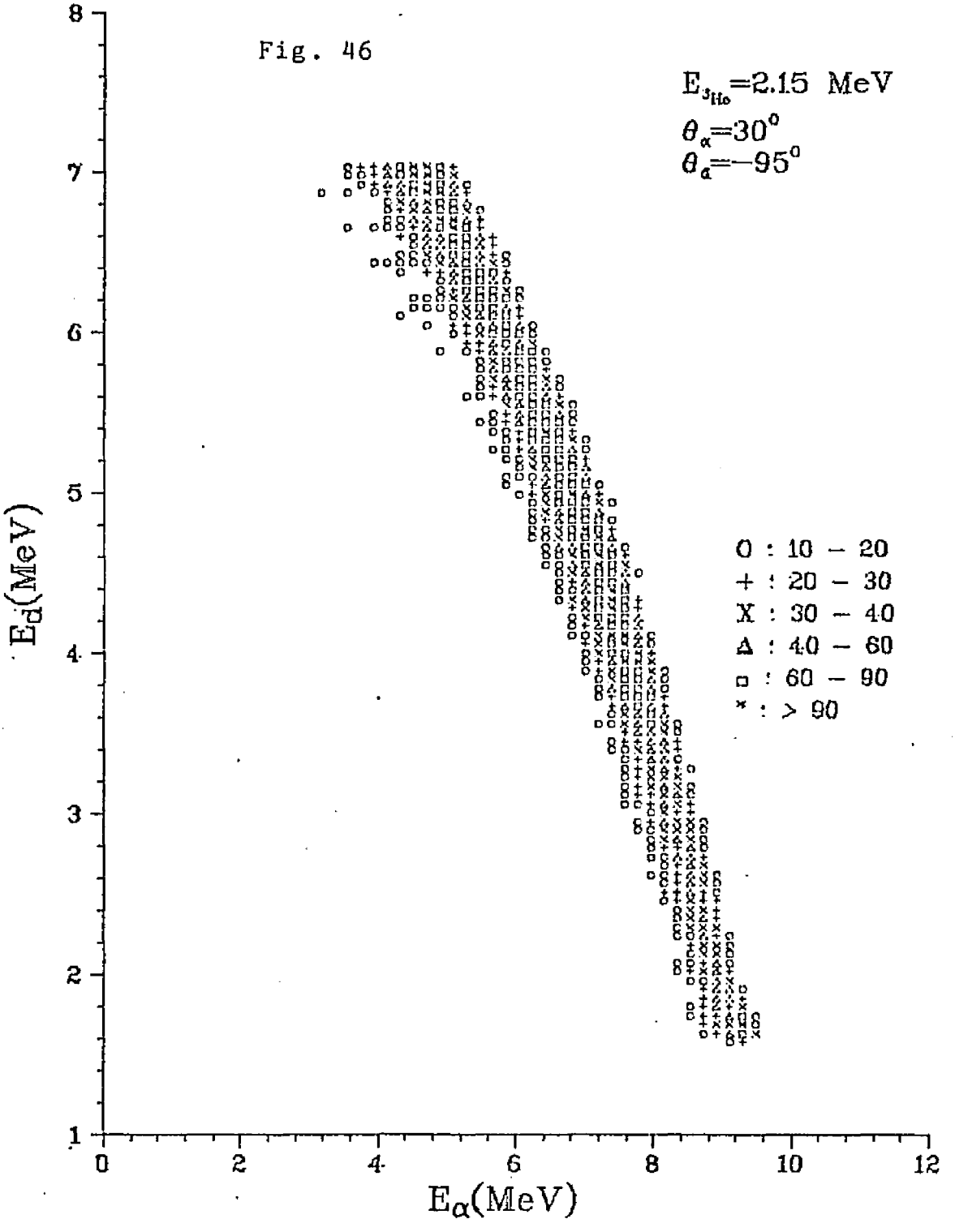

α – d Coincidence Spectrum

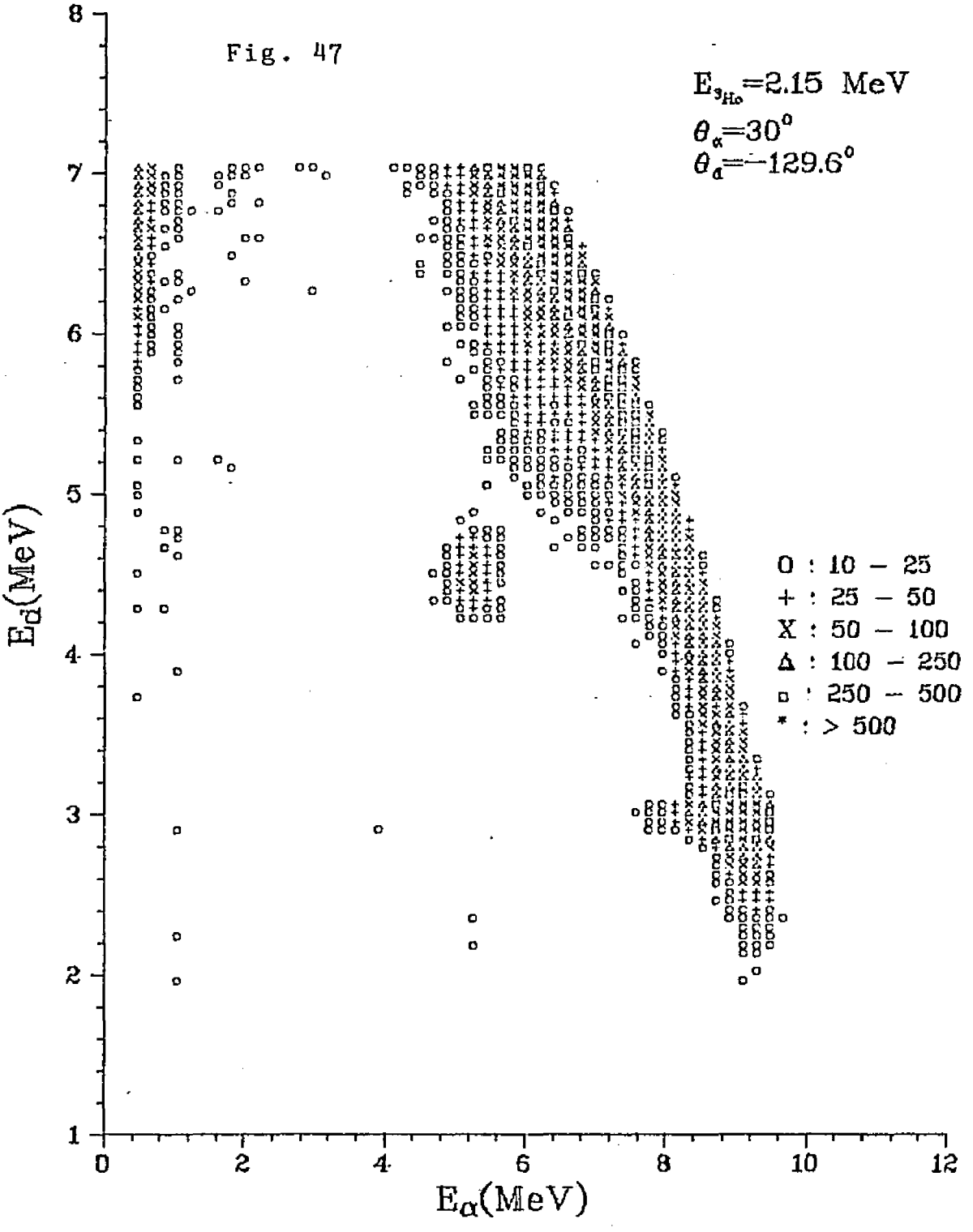

α – d Spectrum projected onto α–axis

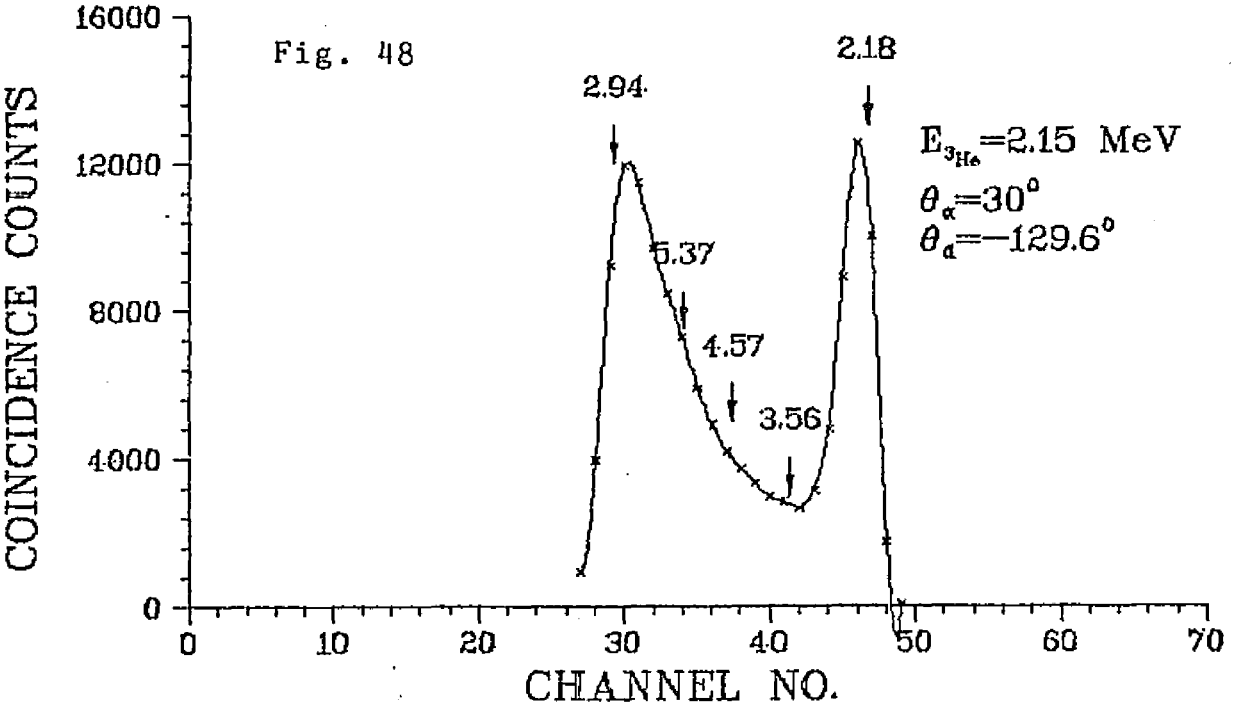

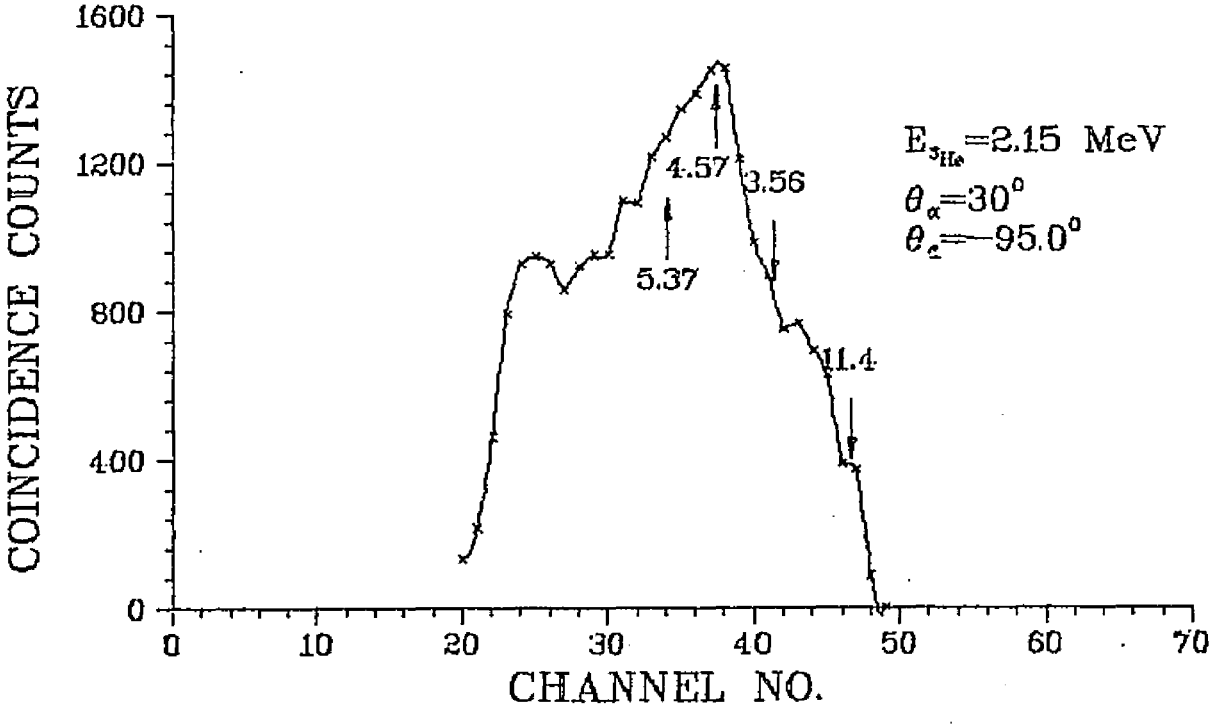

α – d Spectrum projected onto d–axis

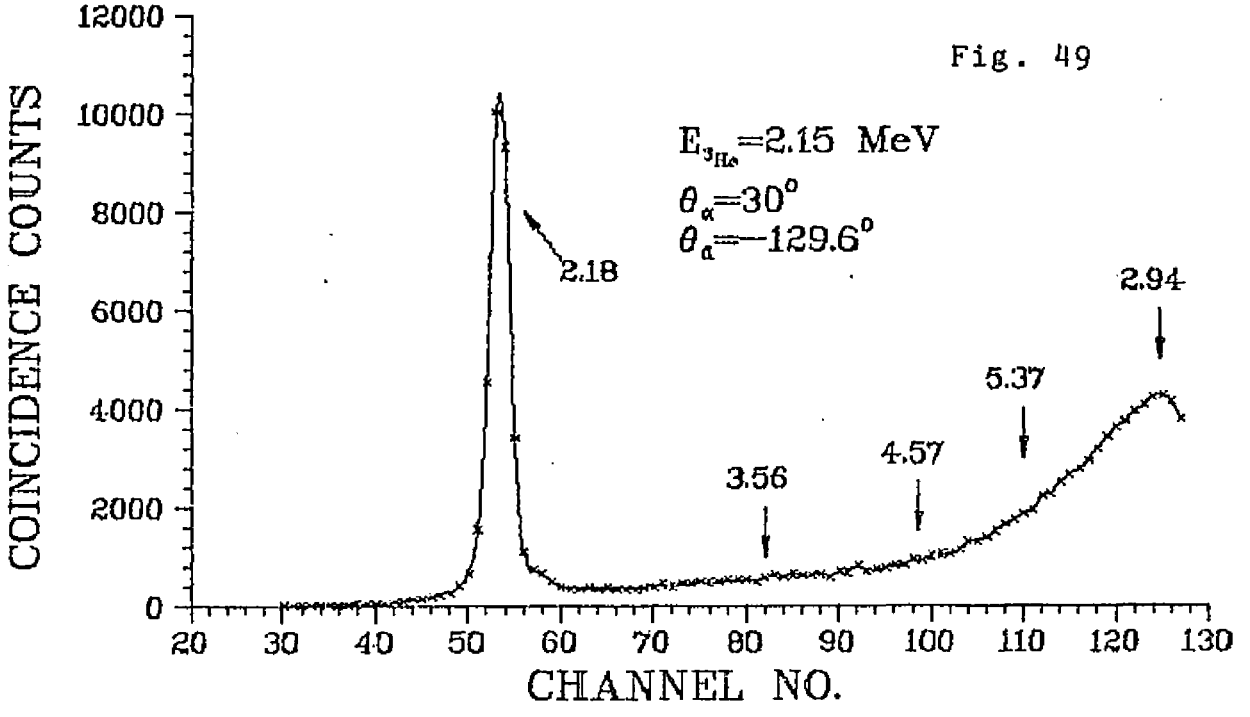

Fig. 49

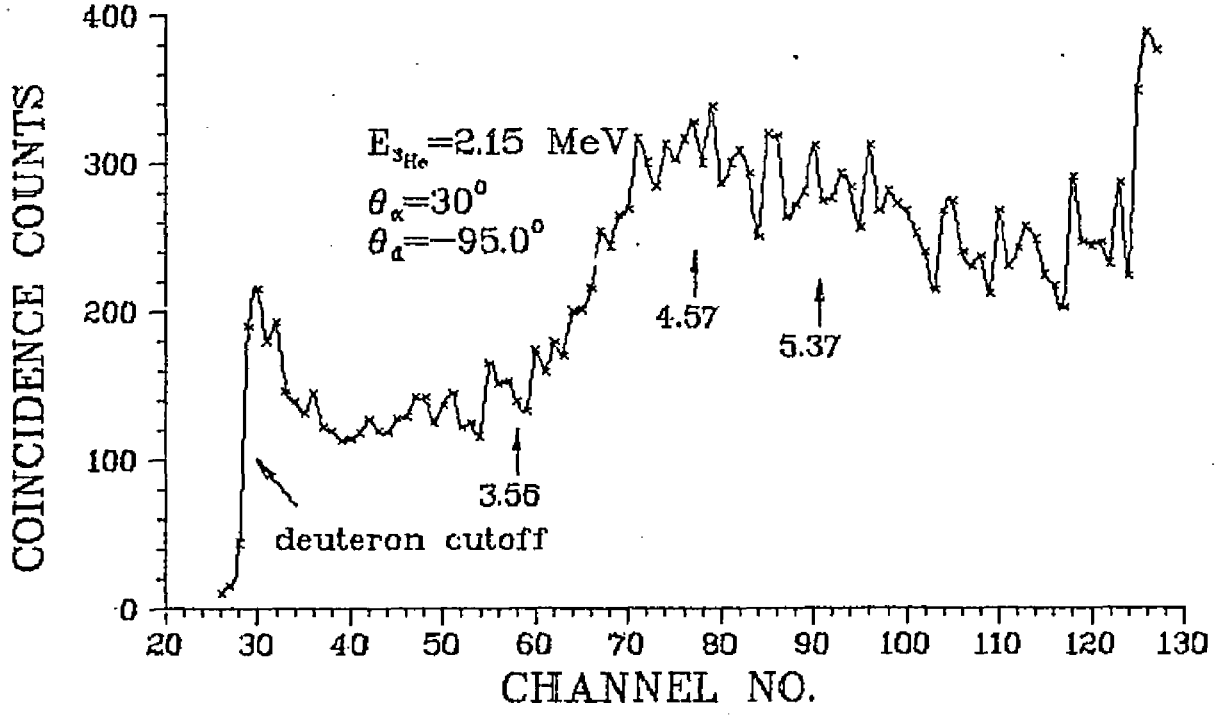

more definite extraction of a branching ratio for decay of $^{6}Li(5.37)$ into α+d.

The second value θ_d=-95° was chosen for the purpose of removing the large enhancement due to the formation and decay of the $^{8}Be(2.94)$ state. The large yield from the decay of 2.18 level seen at θ_d=-129.6° disappears at θ_d=-95° as it is no longer kinematically allowed. The projection of this coincidence spectrum shown in Fig.49 does not improve the separation good enough to extract the contributions from decay channel of α+d

It should be noted that there is a considerable populations of the kinematic locus in the vicinity of the 5.37 level and also some evidence for the occurrence of the 4.57 MeV state which was not seen in the singles spectra.

The measured α-d coincidence spectra do not show any possible evidence for decay of $^{6}Li(5.37)$ state into alpha -particle and a deuteron. The major decays from this level must therefore be either $p + {}^{5}He \dashrightarrow n + \alpha$ or direct breakup into $\alpha + p + n$. This leads to the α - p coincidence measurement.

The α-p coincidence spectrum was undertaken in an attempt to resolve the decays of the 5.37 level via the following two channels: a sequential decay through the broad ^{5}He ground state or a direct breakup into $\alpha + p + n$. Detector configurations were the same as those of α-α and

α-d measurements except particle identifier window set on proton rather than deuteron. Typical α-p TAC spectrum is shown in Fig.50.

The experimentally observed α-p coincidence spectrum is shown in Fig.51. A kinematically constrained curve is no longer seen as it is actually a four-body final state reaction. The kinematic region of the spectrum were projected onto the proton axis and were compared with the phase space distribution(Fig.52). Decaying protons forming the ^{5}He ground state is indicated. An enhancement at this location, compared with the available phase space, shows that a fair amount of contribution coming from the sequential decay channel of $p + {}^{5}He$.

α – p TAC Spectrum

Fig. 50

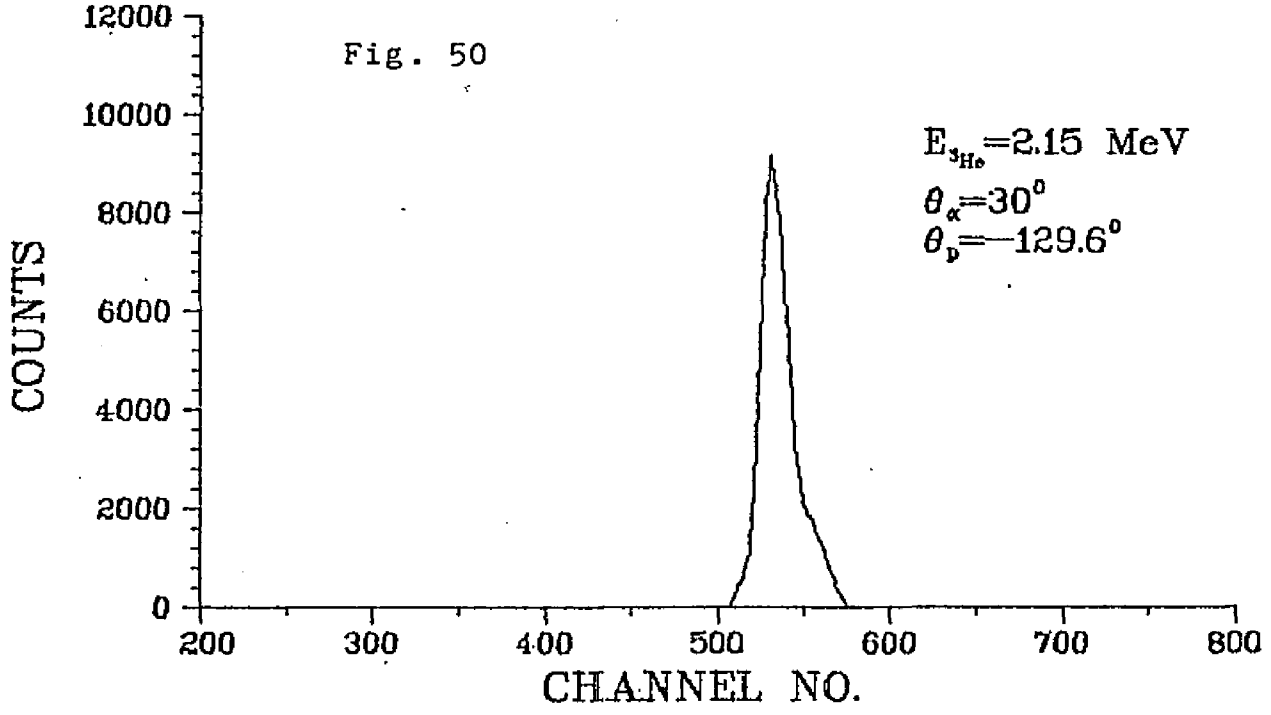

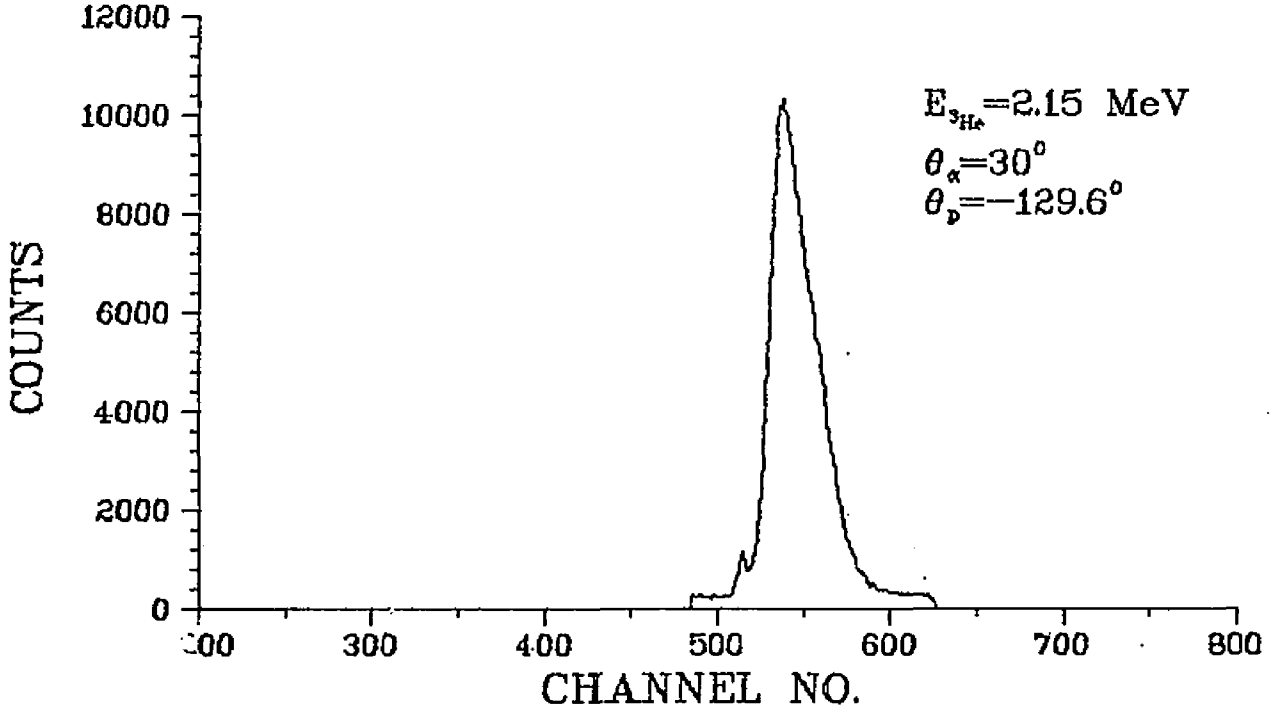

α − p Coincidence Spectrum

Fig. 51

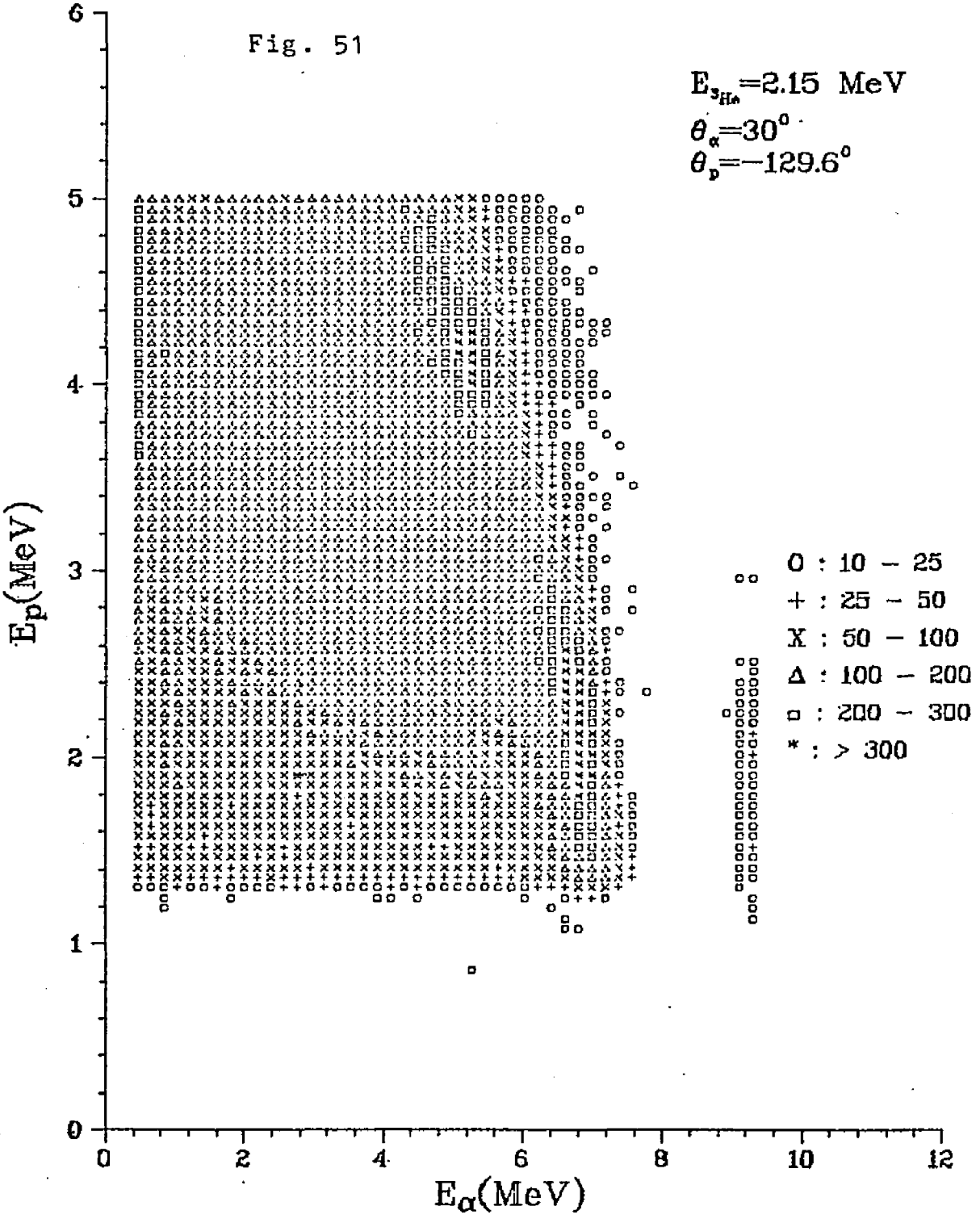

Coincidence and Phase Space Spectra

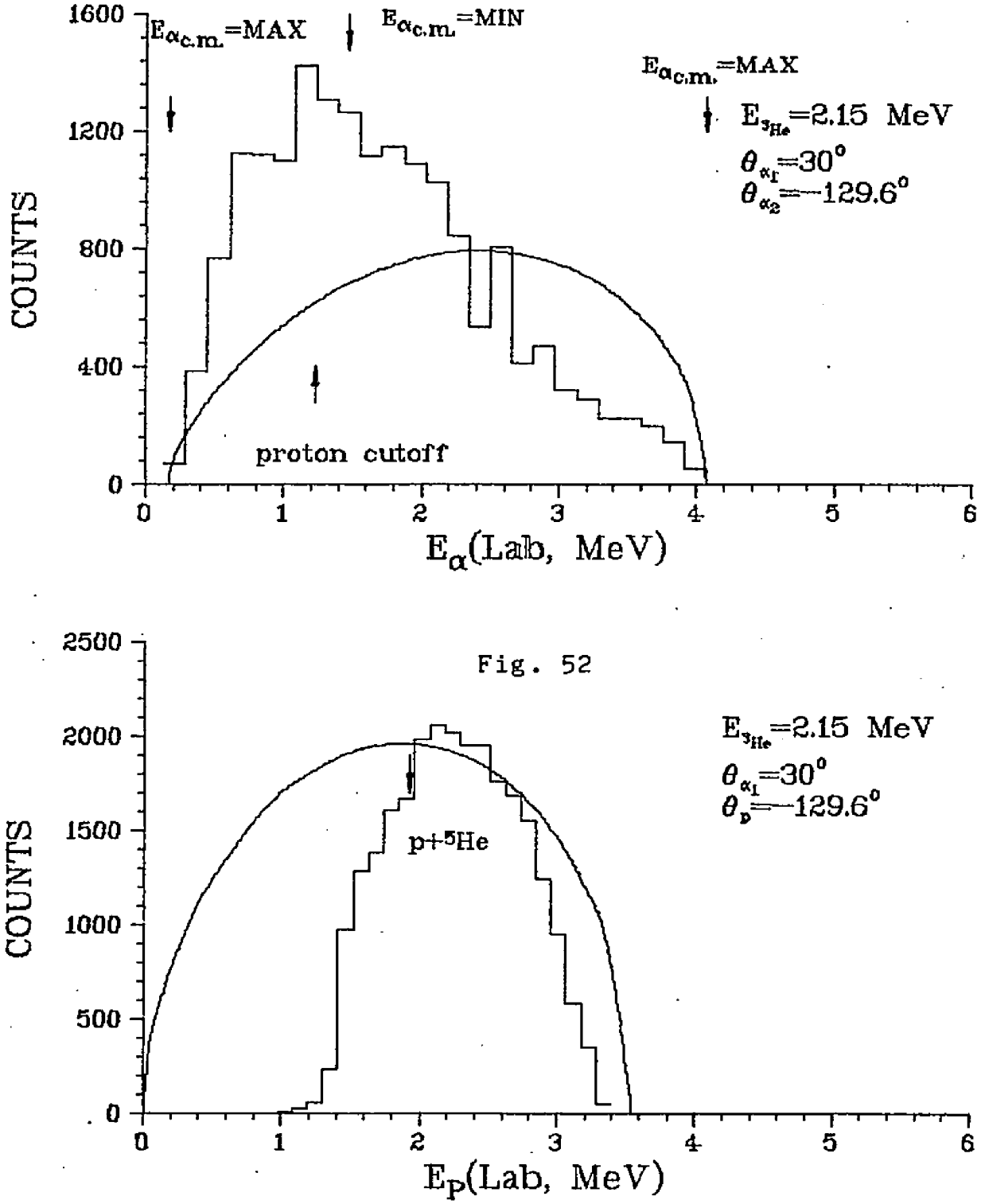

Fig. 52

RESULTS AND DISCUSSIONS

A. Mechanism of the First-Step Reaction

From the excitation curves(Fig.10-13) measured at laboratory angles of 30°, 90° and 150° and the total reaction cross sections(Fig.26-29), the 5.37 MeV state does show clear evidence of resonances at ^{3}He bombarding energies of 1.0, 1.45 and 2.15 MeV which correspond to the formation of the compound nucleus ^{10}B at excitation energies of 18.43, 18.8 and 19.3 MeV respectively, corresponding to known levels in ^{10}B. This resonance behavior is in contrast to the excitation functions for the ground and first two excited states of ^{6}Li which do not yield any evidence for resonances. The present data support T=1, isospin assignments for all three levels in ^{10}B, based on their α-decay to a T=1 level in ^{6}Li. The widths of these ^{10}B levels from the present data are also in good agreement with the compilation of Ajzenberg-Selove(Ref.4).

Both excitation functions and angular distributions for the ground and first two excited states are in very good agreement with those measured by Forsyth et al(Ref.39) and by Paul et. al(Ref.11). The angular distributions for the ground state and the first two excited states do not show any structure which can be clearly accounted for as a pure

mechanism(either direct or compound reaction). It is worth noting that the angular distributions for the ground state are much more energy dependent than those of the first and second excited states. The angular dstributions for the 5.37 MeV state are nearly isotropic at 1.1 and 1.4 MeV and exhibit a higher degree of symmetry about 90° CM angle in the vicinity of 2.1 MeV. This phenomenum supports the results of the excitation function with respect to a compound nucleus reaction mechanism.

B. DWBA Analysis

The DWBA calculations(Fig.30-31) cannot reproduce the measured angular distributions at 1.8, 2.15 and 2.5 MeV ^{3}He incident energies for either the ground state or the 5.37 MeV states. Previous DWBA calculations of this reaction performed by Zander(Ref.46) at ^{3}He incident energies of 16-18 MeV, where the data are relatively free from compound nucleus resonance structure, has shown that both front and back angle maxima in the measured ground state angular distributions can be reproduced by the conventional DWBA analysis, while the zero-range DWBA calculation is a factor of 25 smaller than the measured cross section. In our calculation, a renormalization factor of 10 has been employed in order to fit the measured cross sections at forward angles. Zander's work is so far the only example of successful fits

to the angular distributions for this reaction using DWBA calculations. Their data were taken at significantly higher ^3He bombarding energies than ours. The disagreement in our calculation is not surprising since the DWBA calculation is not expected to be suitable for the reactions involving light target nuclei, especially at relatively low bombarding energies.

C. Branching Ratios

The four-body kinematic region in the α-α coincidence spectra was projected onto the α_2 axis. The projected spectra, which are plotted in Fig.41-43, show enhancement at low(CM) α_2 energies relative to high α_2 energies, compared to the phase space calculations, for all angles measured except those of 104.2° and 155°. At these two angles, which are symmetric to the recoil direction, the reverse is true.

The spectra projected onto the α_1 axis along the α + d kinematic band are shown in Fig.44. These spectra reveal a small shoulder at the location of the 5.37 level but most of the contribution in this region comes from the ^8Be(2.94) and ^6Li(4.57) states, both of which are very broad. These shoulders, in the proper location for the 5.37 MeV state, were integrated after fitting a smooth background to the adjacent regions

Branching ratios for the isospin forbidden decay channel of α + d were then deduced from the projected spectra at 104° and 115°(Fig.44) by assuming that the decay is isotropic. The expression used for this calculation was

$$B.R. = \frac{4\pi N_d}{N_1(g.s.)} \times \frac{d\sigma(g.s.)}{d\sigma(5.37)} \times \frac{d\Omega_2(Lab)}{d\Omega_2(CM)} \times \frac{1}{\Delta\Omega_2(Lab)}$$

where N_d is the counts of the decay particle. The results are 1.1% and 0.95% from the 115° and 104.2° data respectively. Due to the fact that the assumption of isotropy is probably not adequate and that the statistics are very poor, it is possible only to deduce an upper limit for the α + d branch. An upper limit of (1 ± 1)% is therefore determined from the present measurement. This result can be compared with previous measurements(Ref.17,18), from which upper limits in the range of 10%(Artemov et al) to 2%(Cocke et al) have been deduced.

In extracting the ratios between the probabilities of decays via channels of ^{5}He + p and α + p + n, both the α-α projected spectra and the α-p projected spectrum were analyzed using different approaches. For the α-α analysis, the projected spectra were fitted with the phase space distribution

$$\frac{d^2\sigma}{dE_\alpha d\Omega_\alpha} = C_1[E_\alpha(Q/3-E_\alpha-E_o+2(E_oE_\alpha)^{1/2}z)]^{1/2}$$

plus a contribution coming from sequential decay

$C_{2g/m_\alpha}(g^2+u^2-2ugz)^{-1/2}$ derived by Morinigo(Ref.45). These expressions have been described earlier in section II.F.

After adjusting the two parameters C_1 and C_2 to get the best fit beyond the proton cutoff portion of the spectra, the results plotted in Fig. 54,55 were obtained.

For the α-p analysis, a simple Breit-Wigner resonance with the fixed centroid and width corresponding to the known parameters for the ^{5}He ground state was used to attribute for the p + ^{5}He channel and a phase space distribution was used to account for the α + p + n decay channel. This phase space distribution(for protons) has the form of $C_2[E_p(5Q/6-E_p-E_o+2(E_oE_p)^{1/2}z)]^{1/2}$. The results obtained using this procedure are shown in Fig.56.

Branching ratios for the decay channels ^{5}He + p and α + p + n were then deduced from these fits. The results are listed in Table 4 along with the data of Artemov et al(Ref.18).

D. Alpha - Alpha Angular Correlations

The measured α - α angular correlations have been transformed to the rest system of 5.37 MeV state of ^{6}Li and are shown in Fig.53 for various (CM)α_2 energies. The angular correlation function $W(\theta) = \sum_{n=0}^{4} A_n P_n(\cos\theta)$ has been fitted

Analysis of the $\alpha - \alpha$ Coincidence Spectrum projected onto α–axis

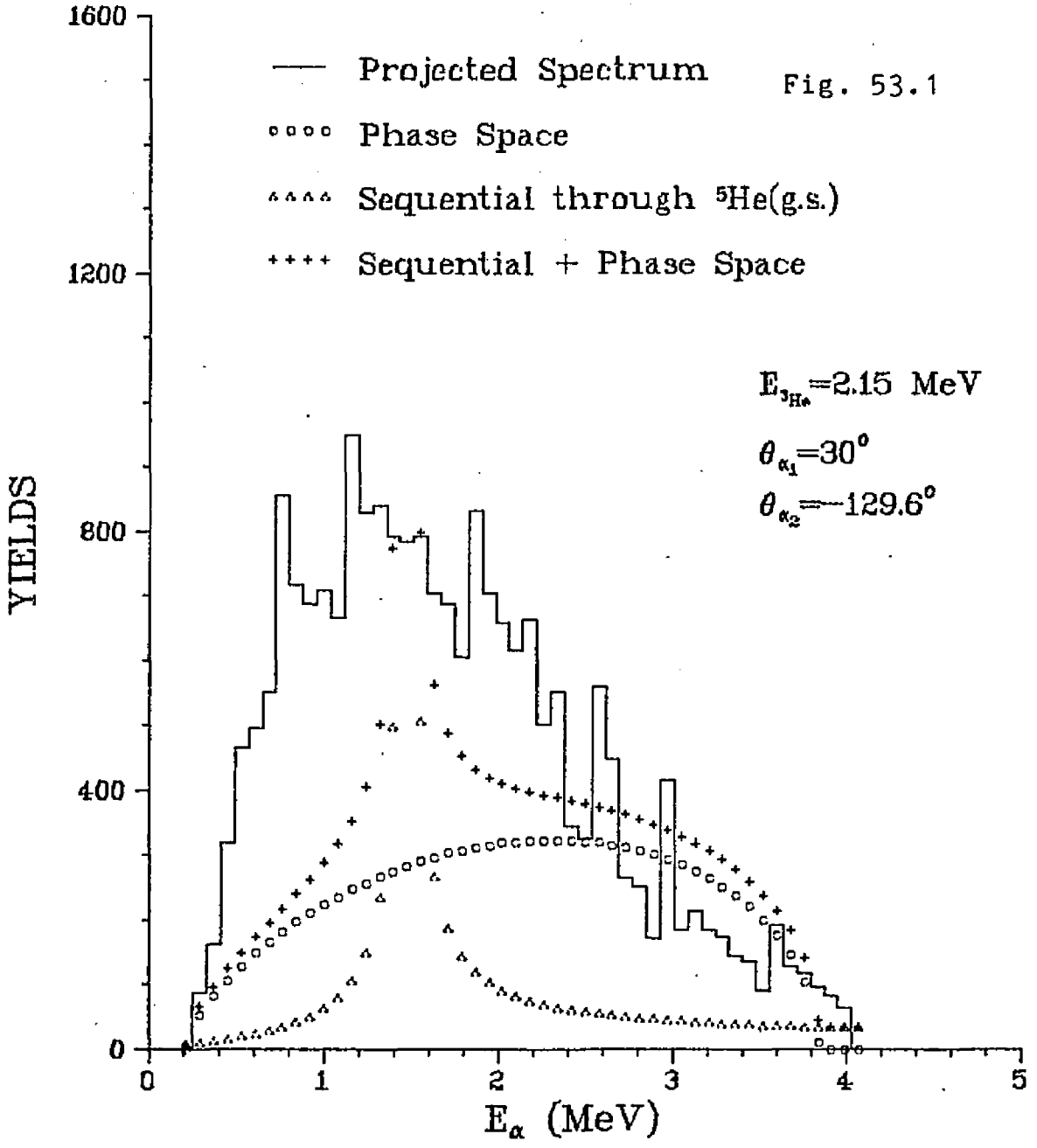

Fig. 53.1

Analysis of the $\alpha - \alpha$ Coincidence Spectrum projected onto α-axis

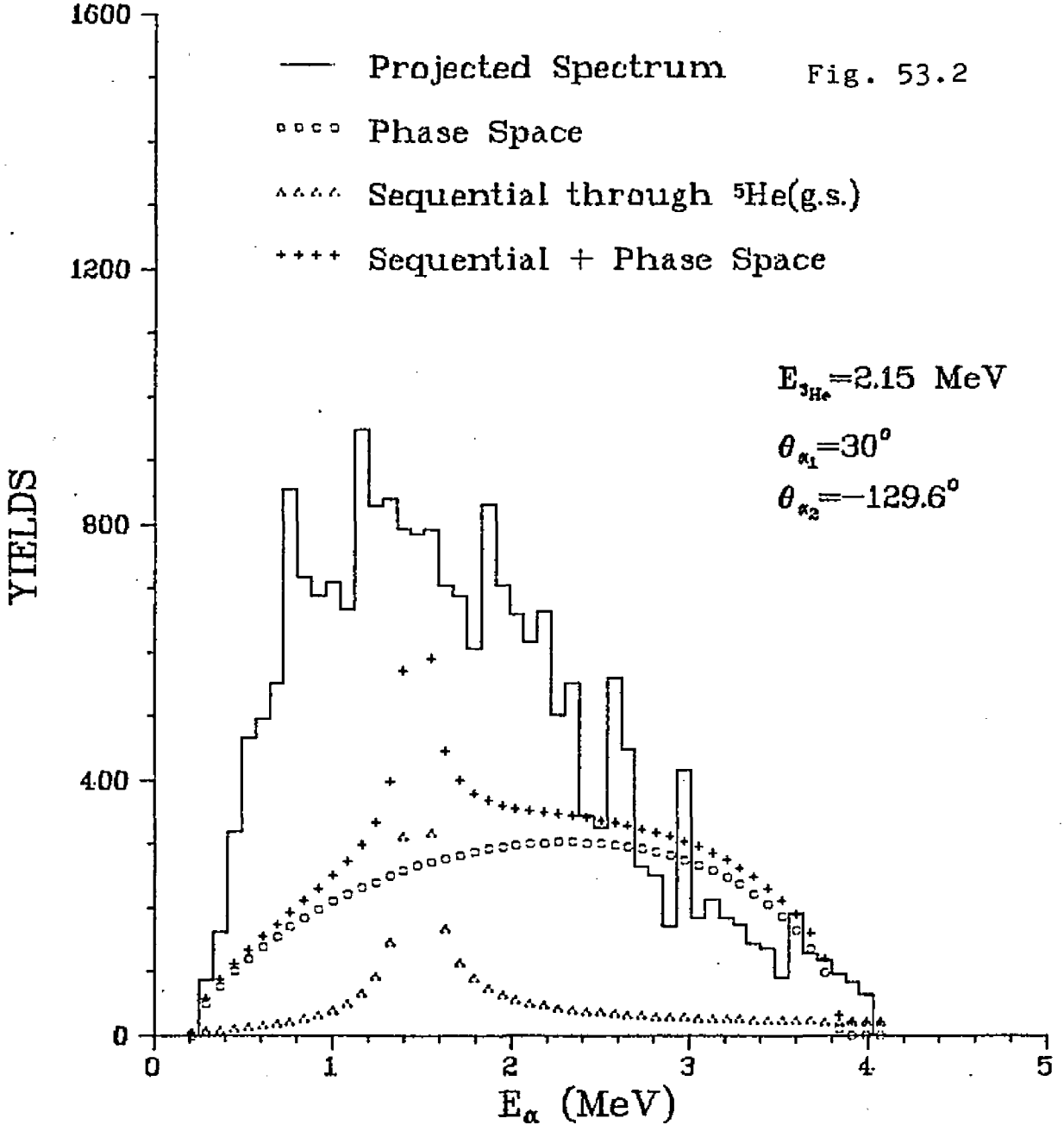

Fig. 53.2

Analysis of the $\alpha - \alpha$ Coincidence Spectrum projected onto α–axis

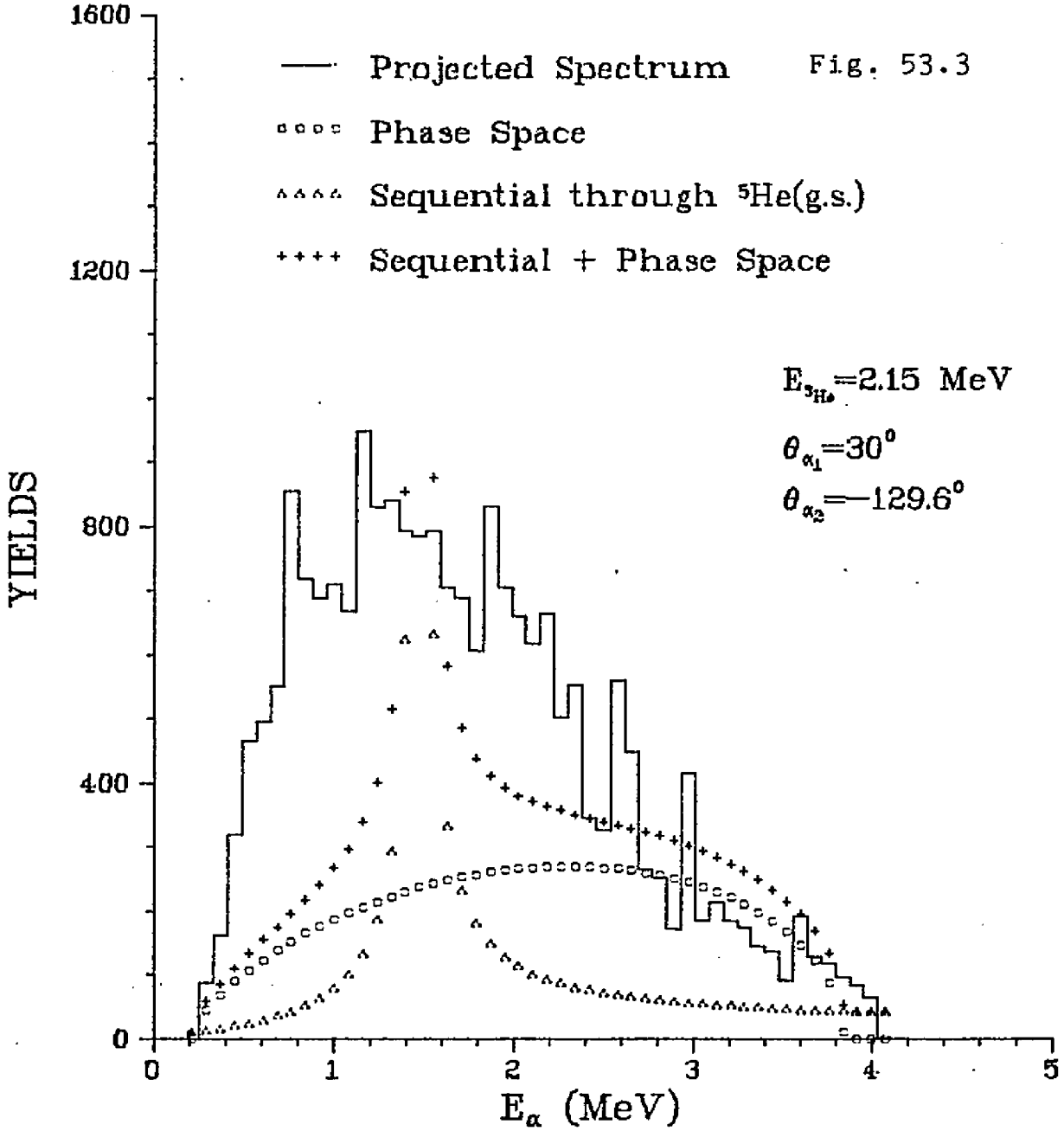

Fig. 53.3

Analysis of the $\alpha - \alpha$ Coincidence Spectrum projected onto α-axis

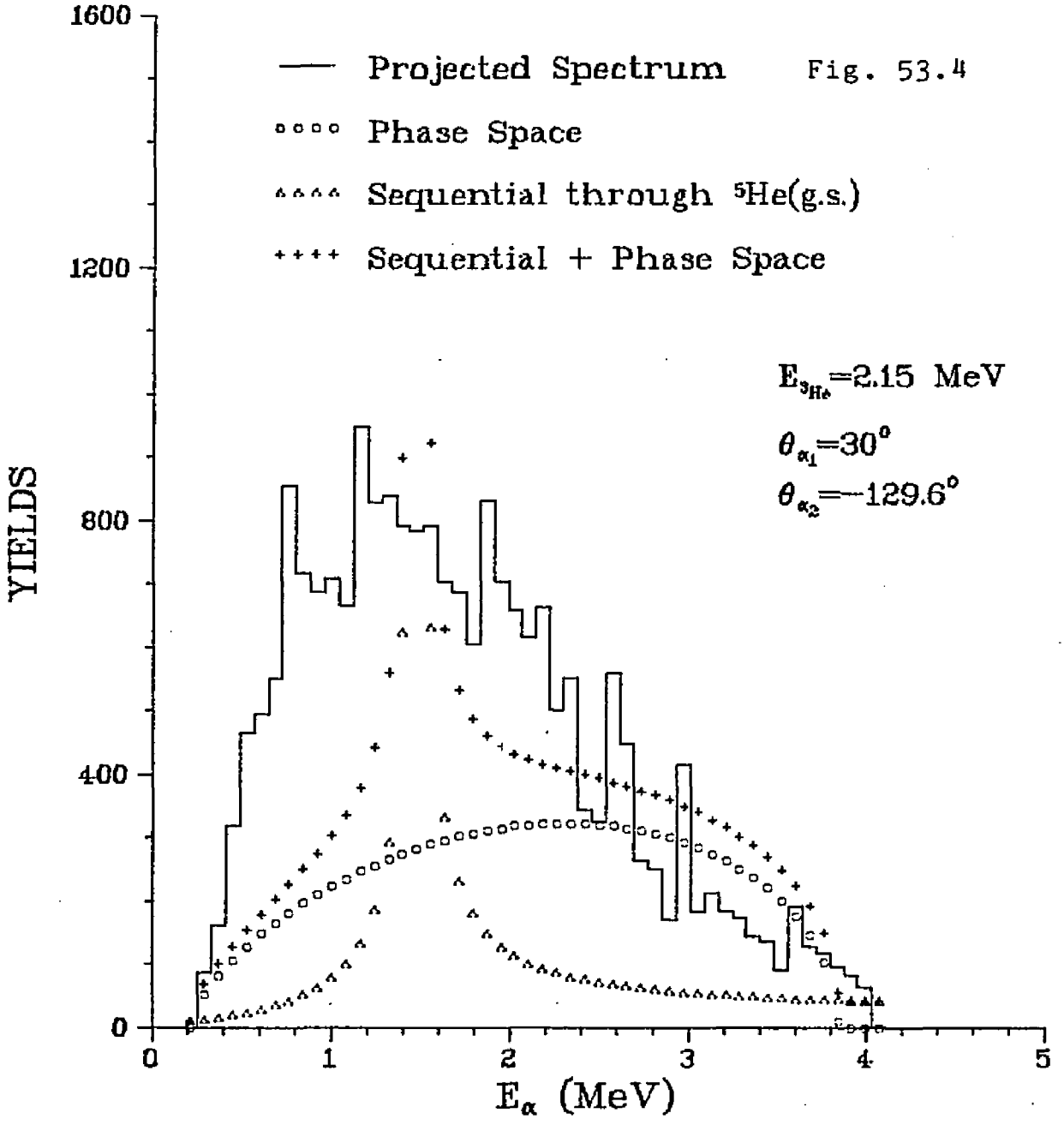

Fig. 53.4

Analysis of the $\alpha - \alpha$ Coincidence Spectrum projected onto α–axis

Fig. 54.1

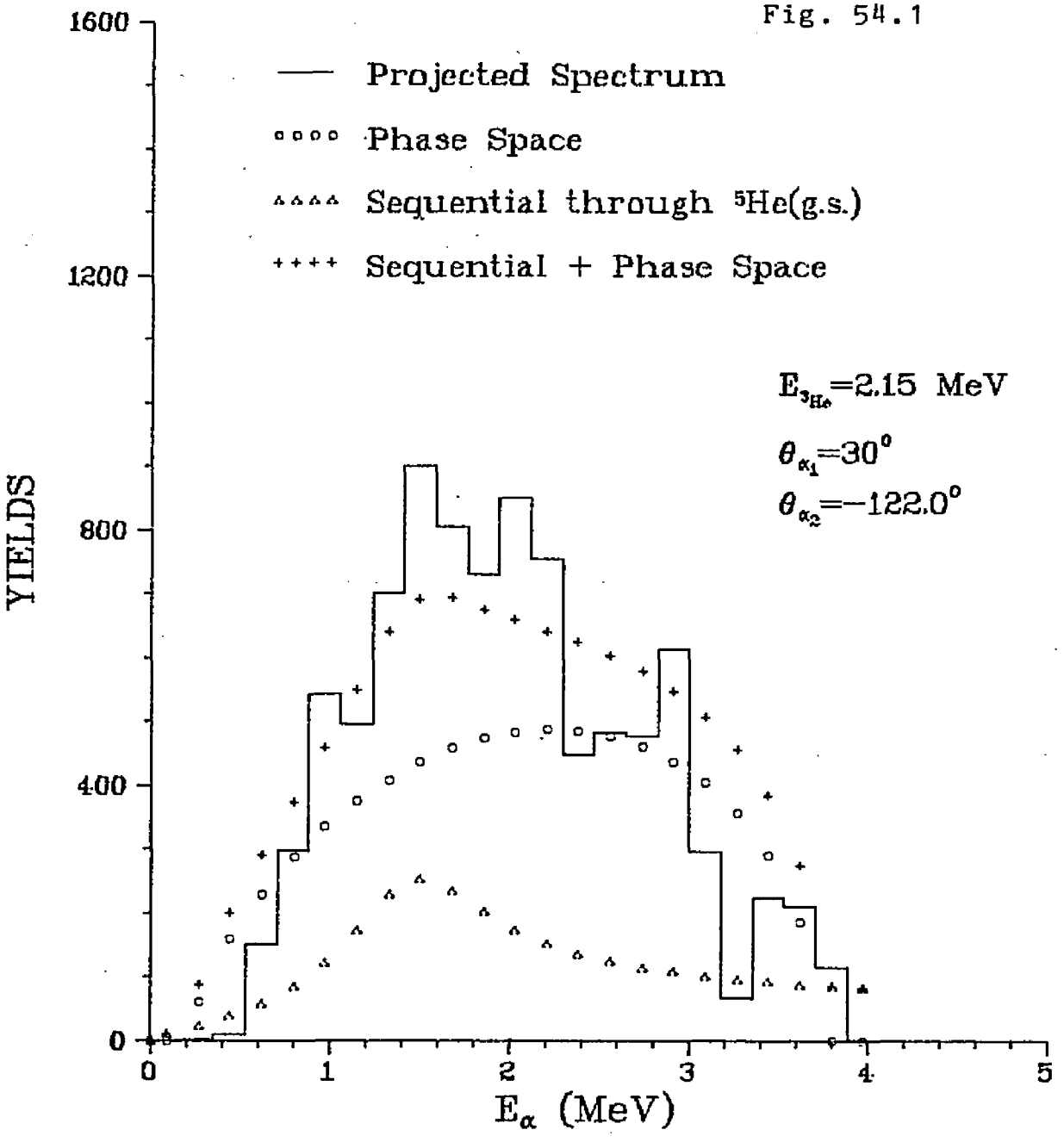

Analysis of the $\alpha - \alpha$ Coincidence Spectrum projected onto α–axis

Fig. 54.2

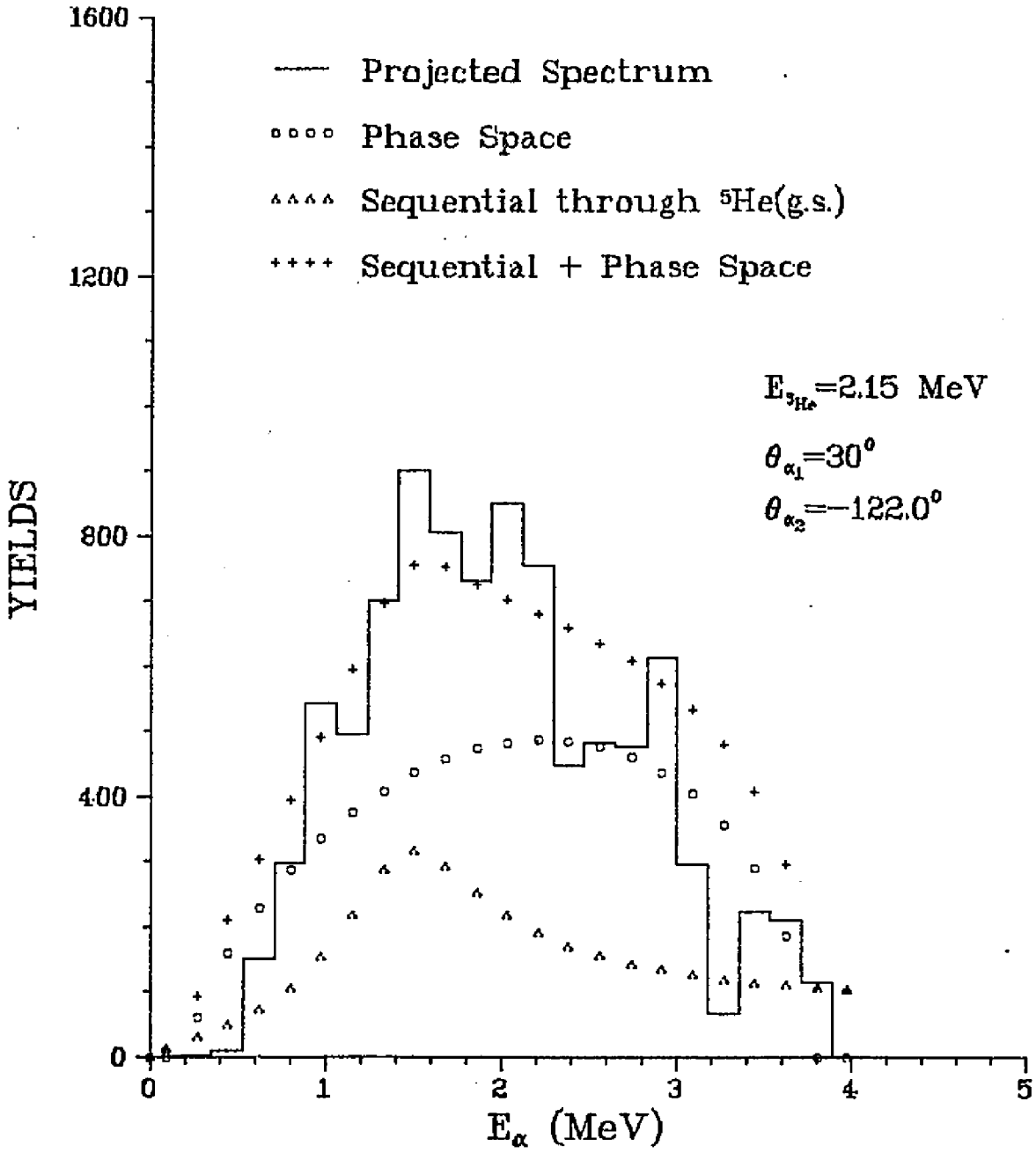

Analysis of the $\alpha - \alpha$ Coincidence Spectrum projected onto α–axis

Fig. 54.3

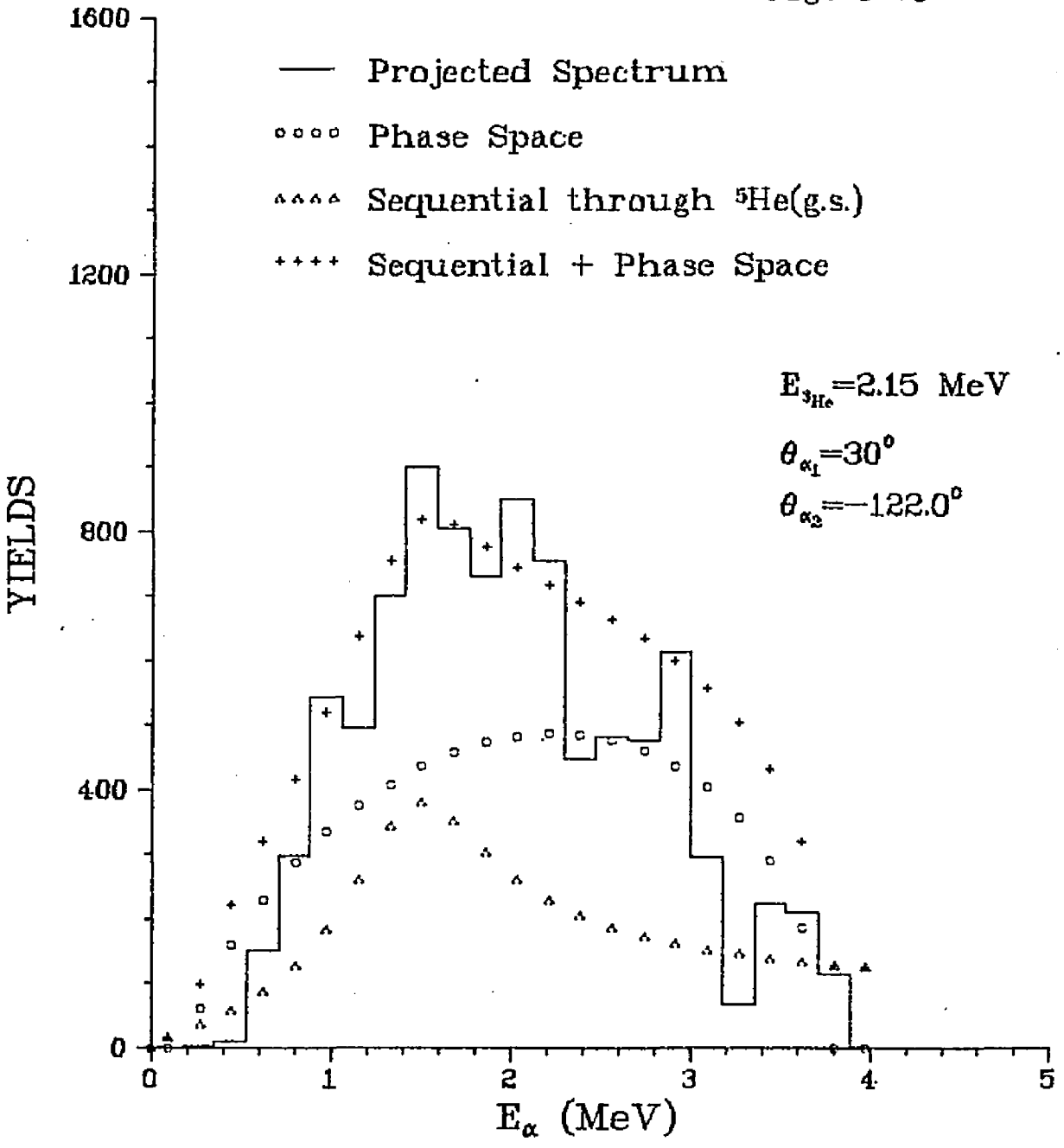

Analysis of the $\alpha - \alpha$ Coincidence Spectrum projected onto α–axis

Fig. 54.4

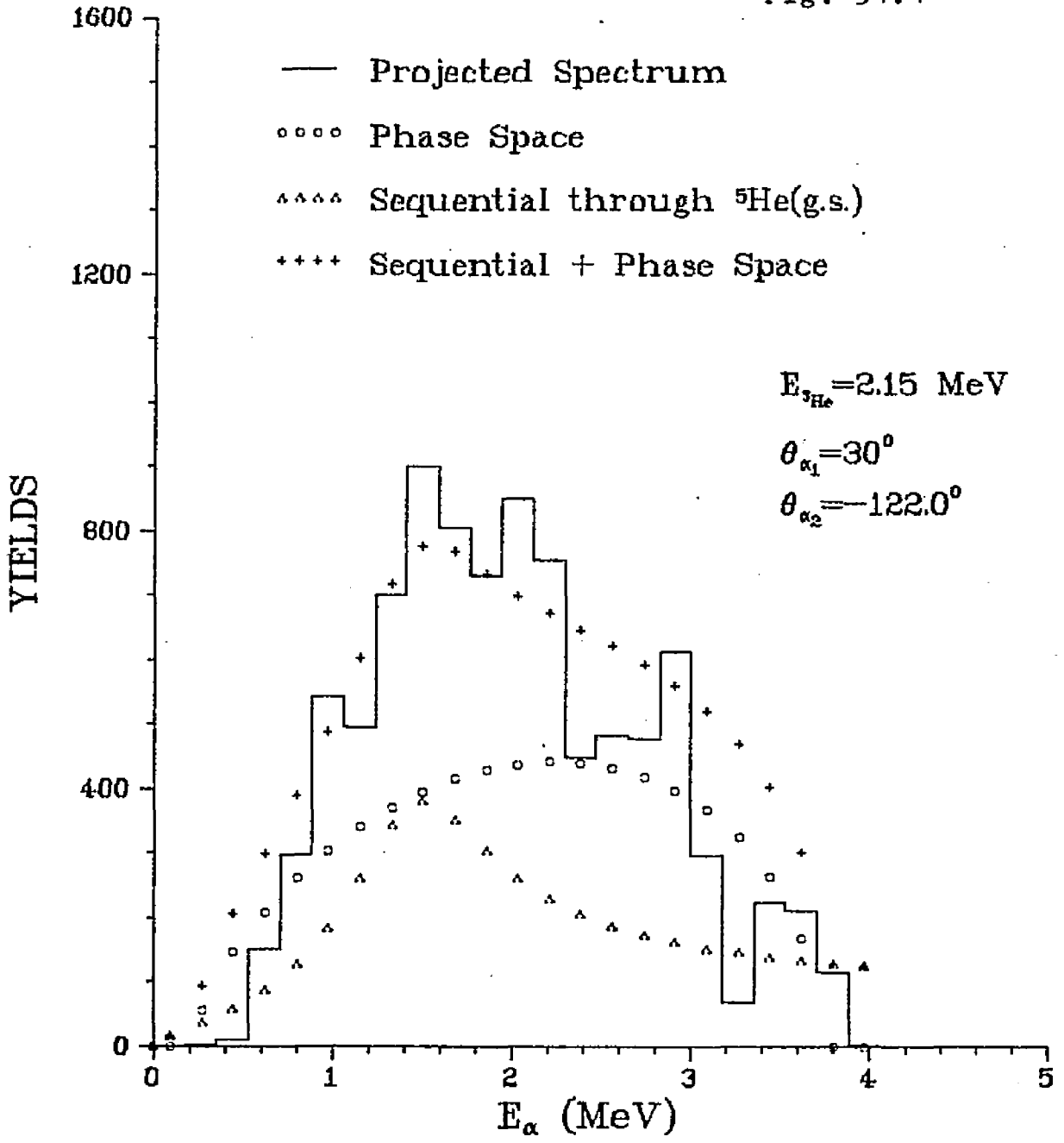

Analysis of the α − p Coincidence Spectrum projected onto p–axis

Fig. 55.1

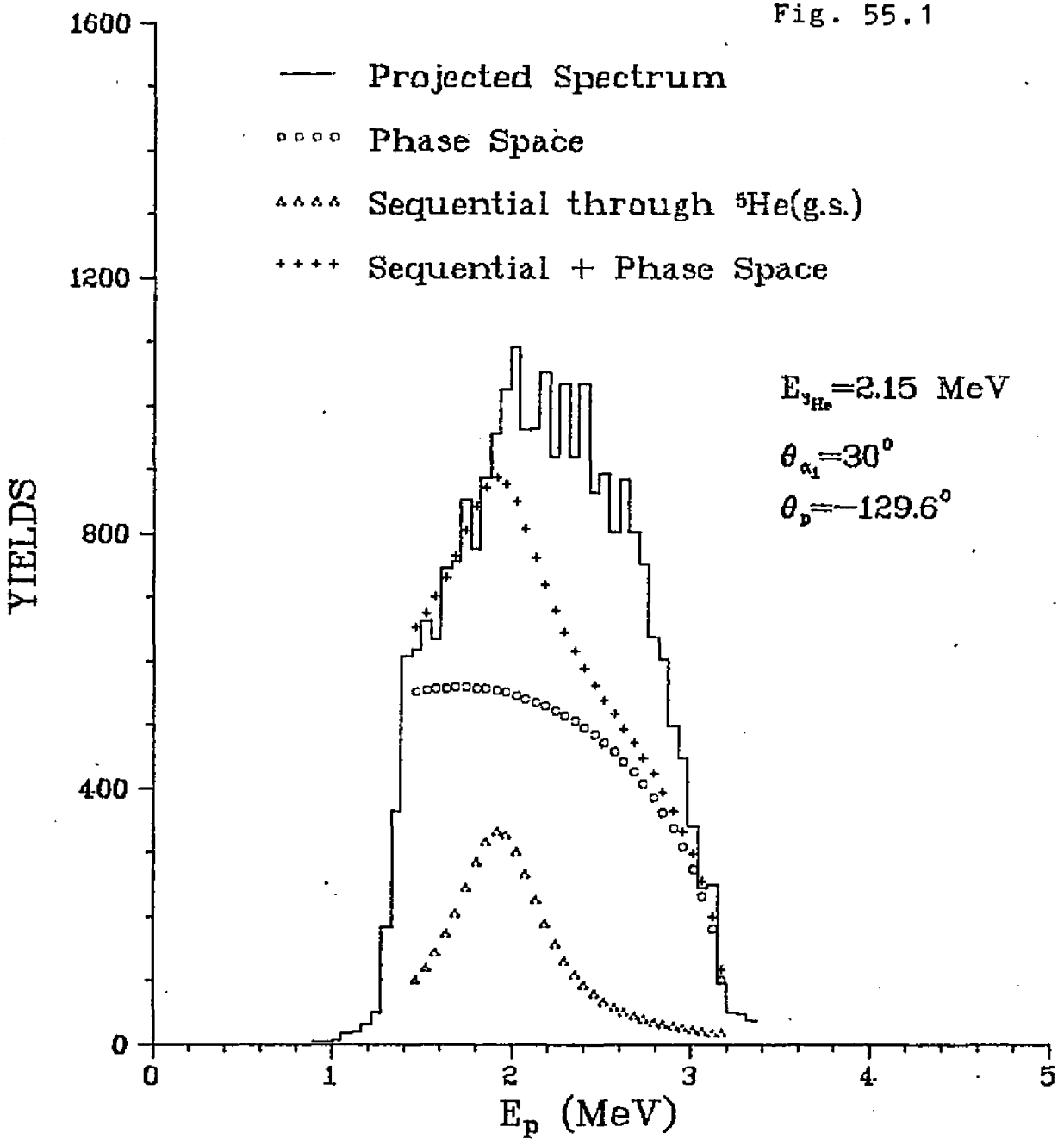

Analysis of the α – p Coincidence Spectrum projected onto p–axis

Fig. 55.2

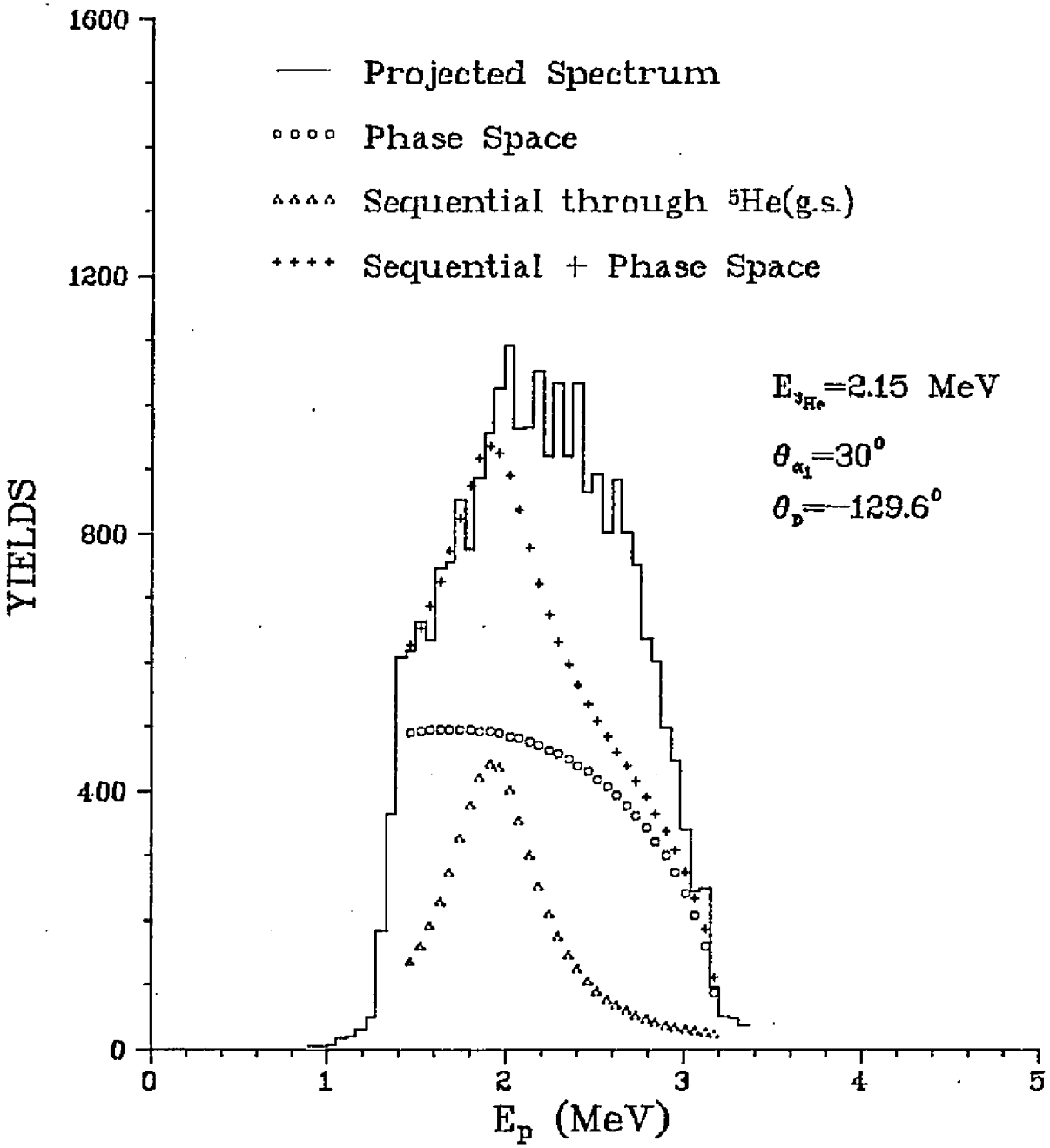

Analysis of the α − p Coincidence Spectrum projected onto p−axis

Fig. 55.3

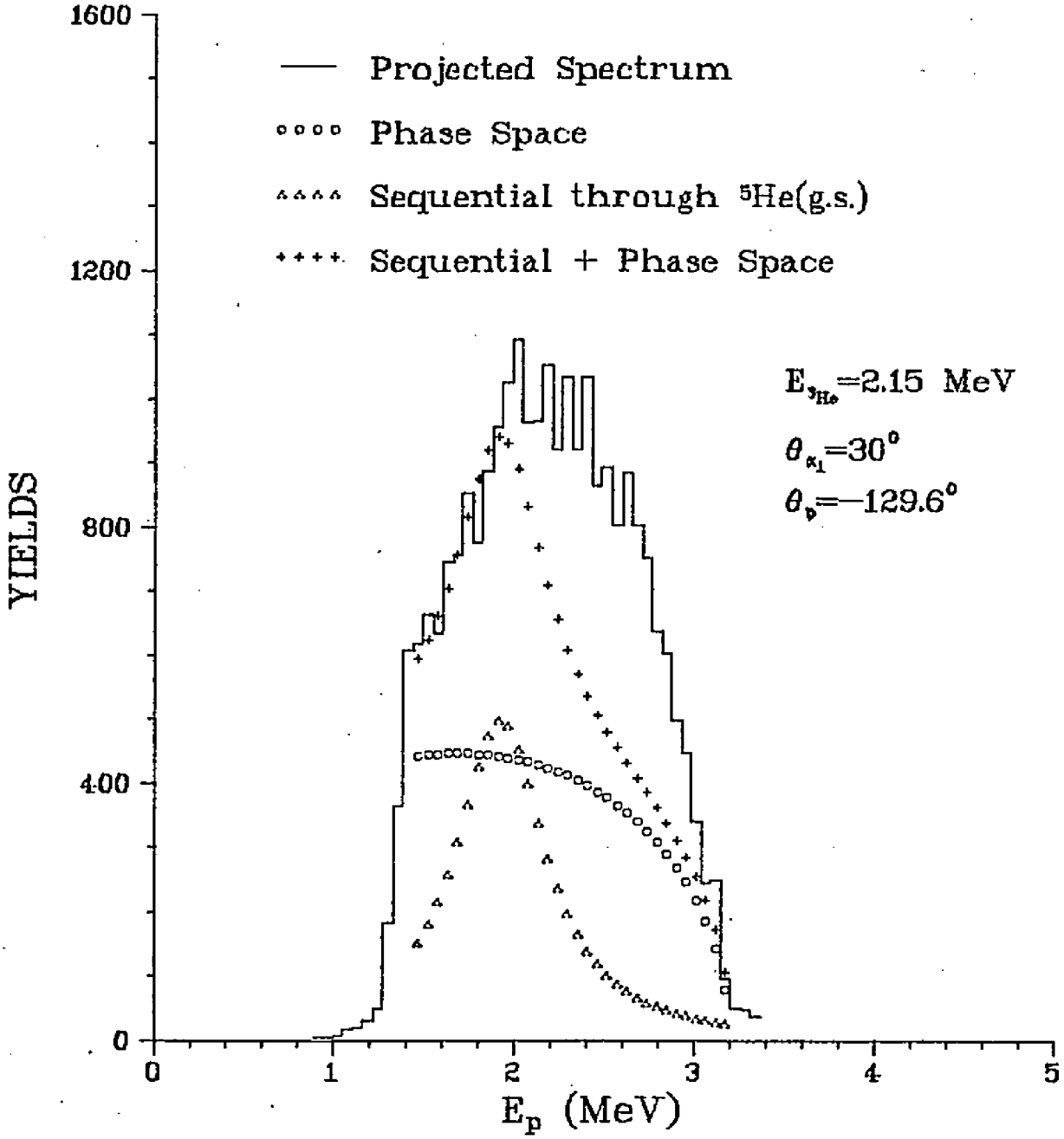

Table 4

Branching Ratios of the Decays from $^{6}Li^{*}(5.37)$

Channels	Present Data	Artemov et al.
$\alpha + d$	$< (0.01 \pm 0.01)$	< 0.1
$p + {}^{5}He \rightarrow \alpha + n$	0.20 ± 0.10	0.35 ± 0.10
$\alpha + p + n$	0.80 ± 0.10	0.65 ± 0.10

Parameters used in extracting the branching ratios

Spectrum	C_1	C_2	B.R.($p+^{5}He$)	Figure
$\alpha - \alpha$ (129.6^{o})	480	80	0.16	53.1
	450	50	0.10	53.2
	400	100	0.20	53.3
	480	100	0.20	53.4
$\alpha - \alpha$ (122.0^{o})	750	200	0.27	54.1
	750	250	0.34	54.2
	750	300	0.41	54.3
	680	300	0.41	54.4
$\alpha - p$	30	450	0.16	55.1
	40	400	0.21	55.2
	45	360	0.24	55.3

Table 5

Coefficients of the α-α Angular Correlation Function

$W(\theta)=A_o+A_2P_2(\cos\theta)+A_4P_4(\cos\theta)$ for $^{6}Li^{*}(5.37)$ state

$E_{\alpha_{cm}}$	A_o	A_2	A_4
0.65--0.55	109.5	-26.2	-78.7
0.55--0.45	227.6	-141.0	-80.9
0.45--0.35	272.0	-167.4	-106.3
0.35--0.25	233.0	-130.1	-46.7
0.25--0.15	297.4	-143.8	-82.1
0.15--0.05	321.2	-135.5	-4.7

$\alpha - \alpha$ Angular Correlations

Fig. 56

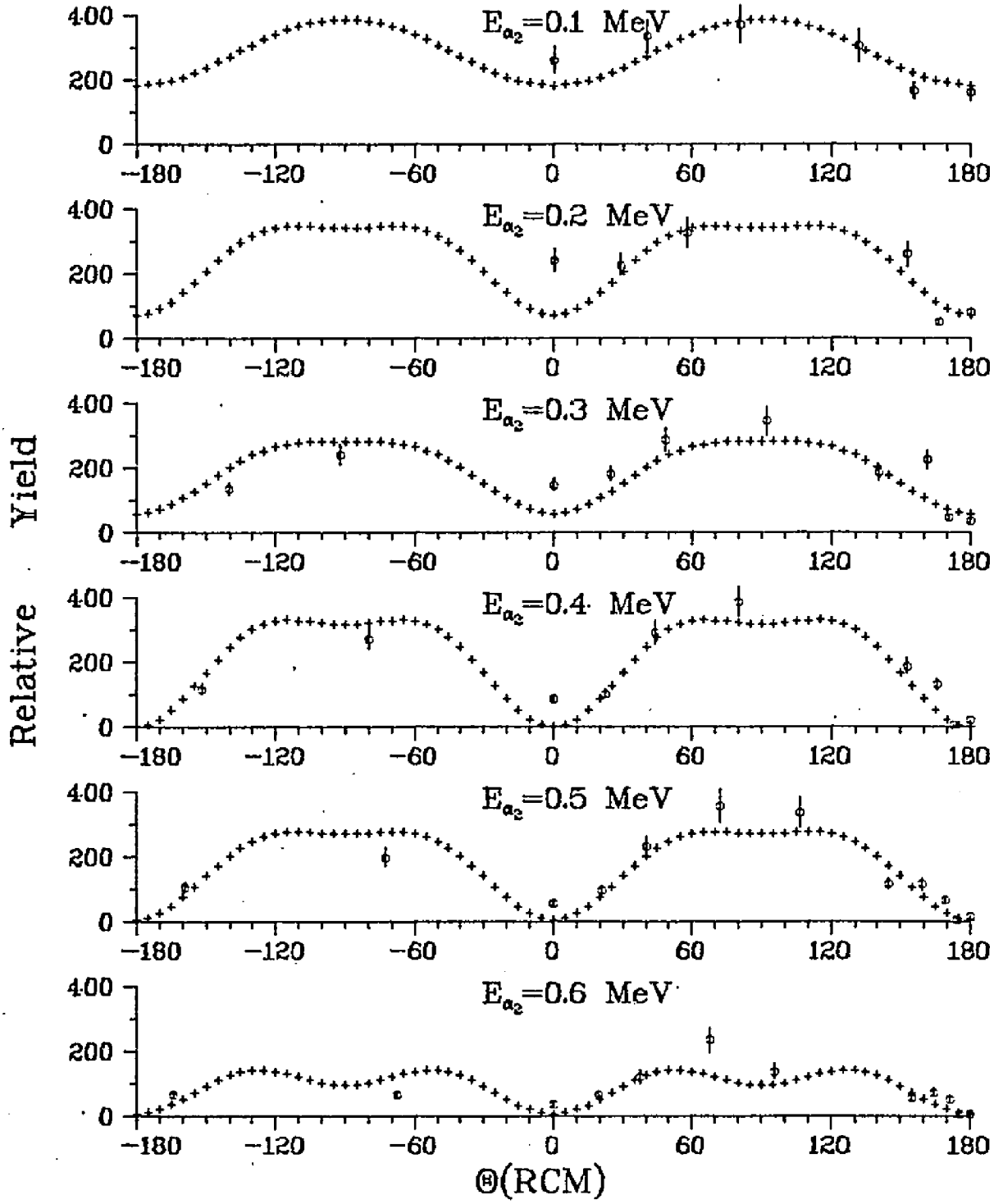

to the measured angular correlation by a least-squares procedure. The coefficients for the angular correlation functions are given in Table 5. It is clear from Fig.53 that, at all α_2 energies, the angular correlation has a fairly pronounced dip at 0^o, correspond to the recoil direction. In the case of a well defined sequential process reaction a periodicity of 180^o is expected in the correlations. The present data do not provide a strong test of the periodicity, but are consistent with this assumption. Likewise, the data support(weakly) the assumption of symmetry in the angular correlation with respect to the ^{6}Li recoil direction.

The observed lack of isotropy in the α-α angular correlation introduces an additional uncertainty in the extraction of decay branching ratios. It is not possible to determine from the present data whether or not the angular correlations for the two allowed decay modes are the same. Measurements providing such a determination, if possible at all, would be extremely time consuming.

Table 6

Absolute Differential Cross Sections for ^{6}Li Ground State

$E_{^3He}$ = 0.9 MeV		$E_{^3He}$ = 1.0 MeV		$E_{^3He}$ = 1.1 MeV	
θ_{cm} (deg)	σ_{cm} (mb/sr)	θ_{cm} (deg)	σ_{cm} (mb/sr)	θ_{cm} (deg)	σ_{cm} (mb/sr)
22.23	0.083(7.9)	22.34	0.167(7.2)	22.45	0.237(5.6)
33.26	0.087(6.8)	33.42	0.160(6.8)	33.58	0.259(5.9)
44.19	0.089(7.6)	44.40	0.164(7.2)	44.61	0.214(6.1)
54.99	0.101(7.9)	55.25	0.162(7.2)	55.49	0.207(5.7)
65.64	0.095(7.4)	65.94	0.186(7.5)	66.21	0.203(6.2)
76.13	0.110(7.9)	76.44	0.182(7.9)	76.74	0.224(6.4)
86.42	0.146(8.0)	86.75	0.199(8.0)	87.06	0.215(6.2)
96.52	0.137(8.9)	96.86	0.264(8.1)	97.18	0.209(7.3)
106.42	0.187(8.2)	106.75	0.248(8.8)	107.07	0.252(7.5)
116.13	0.166(8.1)	116.44	0.205(9.1)	116.74	0.255(7.9)
125.64	0.165(7.6)	125.93	0.281(8.2)	126.21	0.238(7.3)
134.99	0.182(8.1)	135.25	0.221(7.7)	135.49	0.225(6.8)
144.19	0.183(7.8)	144.40	0.246(8.0)	144.60	0.257(7.0)
153.25	0.181(6.9)	153.42	0.208(7.6)	153.58	0.272(6.8)
162.22	0.165(8.3)	162.34	0.232(8.3)	162.45	0.255(6.5)
$E_{^3He}$ = 1.2 MeV		$E_{^3He}$ = 1.3 MeV		$E_{^3He}$ = 1.4 MeV	
θ_{cm} (deg)	σ_{cm} (mb/sr)	θ_{cm} (deg)	σ_{cm} (mb/sr)	θ_{cm} (deg)	σ_{cm} (mb/sr)
22.55	0.312(4.8)	22.65	0.411(3.7)	22.74	0.540(3.4)
33.73	0.272(4.6)	33.87	0.422(3.7)	34.01	0.514(3.5)
44.80	0.275(4.7)	44.98	0.398(4.0)	45.16	0.517(3.6)
55.72	0.261(4.6)	55.94	0.367(4.0)	56.15	0.463(3.6)
66.47	0.242(4.8)	66.72	0.332(3.9)	66.96	0.448(3.5)
77.03	0.208(4.8)	77.30	0.327(3.8)	77.55	0.391(3.6)
87.36	0.199(4.8)	87.65	0.320(3.8)	87.92	0.366(3.8)
97.48	0.190(6.6)	97.97	0.313(4.9)	98.04	0.397(4.4)
107.36	0.228(5.9)	107.65	0.328(4.9)	107.92	0.422(4.5)
117.02	0.251(5.5)	117.30	0.357(4.8)	117.55	0.393(4.2)
126.47	0.257(6.4)	126.72	0.309(5.6)	126.96	0.400(4.5)
135.72	0.264(5.7)	135.94	0.295(5.5)	136.15	0.384(5.0)
144.80	0.262(6.1)	144.98	0.332(5.3)	145.16	0.340(5.1)
153.73	0.231(5.7)	153.87	0.301(5.4)	154.01	0.294(5.2)
162.55	0.261(5.8)	162.65	0.270(5.0)	162.74	0.283(5.6)

The numbers in parentheses are the percentage errors on σ

Table 7

Absolute Differential Cross Sections for ^{6}Li Ground State

$E_{^3He}$ = 1.5 MeV		$E_{^3He}$ = 1.6 MeV		$E_{^3He}$ = 1.7 MeV	
θ_{cm} (deg)	σ_{cm} (mb/sr)	θ_{cm} (deg)	σ_{cm} (mb/sr)	θ_{cm} (deg)	σ_{cm} (mb/sr)
22.83	0.570(3.1)	22.92	0.602(3.4)	23.00	0.820(3.4)
34.14	0.542(3.2)	34.27	0.612(3.4)	34.39	0.842(3.4)
45.33	0.536(3.1)	45.49	0.535(3.4)	45.65	0.793(3.3)
56.35	0.514(3.2)	56.55	0.526(3.4)	56.73	0.704(3.2)
67.19	0.449(3.1)	67.41	0.505(3.5)	67.62	0.679(3.3)
77.80	0.495(3.0)	78.04	0.533(3.5)	78.27	0.754(3.2)
88.18	0.525(3.0)	88.43	0.557(3.4)	88.67	0.771(3.1)
98.31	0.576(3.5)	98.56	0.618(3.8)	98.80	0.870(3.5)
108.18	0.529(3.5)	108.43	0.564(4.1)	108.67	0.826(3.5)
117.80	0.513(4.0)	118.04	0.523(4.2)	118.27	0.705(3.9)
127.19	0.425(4.0)	127.41	0.466(5.0)	127.62	0.648(4.3)
136.35	0.397(4.5)	136.55	0.402(4.5)	136.73	0.567(4.6)
145.33	0.333(4.6)	145.49	0.327(5.0)	145.64	0.484(5.1)
154.14	0.273(5.2)	154.27	0.261(5.2)	154.39	0.392(5.1)
162.83	0.251(5.1)	162.92	0.233(5.9)	163.00	0.305(5.5)

$E_{^3He}$ = 1.8 MeV		$E_{^3He}$ = 1.9 MeV		$E_{^3He}$ = 2.0 MeV	
θ_{cm} (deg)	σ_{cm} (mb/sr)	θ_{cm} (deg)	σ_{cm} (mb/sr)	θ_{cm} (deg)	σ_{cm} (mb/sr)
23.08	1.175(3.0)	23.16	1.347(2.5)	23.23	1.514(3.1)
34.51	1.189(3.1)	34.62	1.474(2.8)	34.73	1.547(3.0)
45.80	1.141(3.1)	45.94	1.622(3.0)	46.08	1.633(3.0)
56.91	1.218(3.1)	57.09	1.467(2.7)	57.25	1.537(2.8)
67.82	1.175(3.0)	68.02	1.428(2.7)	68.21	1.674(2.8)
78.49	1.076(3.0)	78.70	1.394(2.7)	78.91	1.630(2.6)
88.90	1.149(3.0)	89.12	1.444(2.7)	89.34	1.596(2.7)
99.04	1.262(3.3)	99.27	1.510(2.9)	99.49	1.756(3.1)
108.90	1.140(3.5)	109.12	1.432(3.2)	109.34	1.661(3.3)
118.49	1.121(3.8)	118.70	1.276(3.5)	118.91	1.592(3.1)
127.82	1.028(4.0)	128.02	1.211(3.5)	128.21	1.580(3.5)
136.91	0.906(4.4)	137.08	1.054(3.6)	137.25	1.266(3.8)
145.79	0.734(4.4)	145.94	0.991(4.0)	146.08	1.184(4.0)
154.50	0.590(5.1)	154.62	0.854(4.4)	154.73	0.926(4.3)
163.08	0.414(5.4)	163.16	0.701(4.0)	163.23	0.874(4.8)

The numbers in parentheses are the percentage errors on σ

Table 8

Absolute Differential Cross Sections for $^{6}Li(2.18)$ State

$E_{^3He}$ = 0.9 MeV		$E_{^3He}$ = 1.0 MeV		$E_{^3He}$ = 1.1 MeV	
θ_{cm} (deg)	σ_{cm} (mb/sr)	θ_{cm} (deg)	σ_{cm} (mb/sr)	θ_{cm} (deg)	σ_{cm} (mb/sr)
22.42	0.106(8.0)	22.55	0.127(7.9)	22.66	0.117(6.9)
33.55	0.109(6.8)	33.73	0.133(7.3)	33.90	0.136(6.9)
44.56	0.118(7.6)	44.79	0.158(7.5)	45.01	0.156(6.8)
55.44	0.142(7.8)	55.71	0.159(7.5)	55.98	0.145(6.3)
66.15	0.121(7.4)	66.46	0.186(7.7)	66.76	0.145(6.8)
76.67	0.130(7.9)	77.01	0.162(8.1)	77.34	0.159(7.0)
86.99	0.142(8.1)	87.35	0.168(8.3)	87.69	0.149(6.9)
97.10	0.099(9.3)	97.47	0.165(9.6)	97.81	0.125(9.4)
106.99	0.109(8.9)	107.35	0.143(9.6)	107.69	0.113(8.3)
116.67	0.087(9.4)	117.01	0.108(10.5)	117.34	0.104(9.5)
126.15	0.075(9.9)	126.46	0.110(10.7)	126.76	0.063(10.9)
135.43	0.078(9.5)	135.71	0.094(10.6)	135.97	0.078(9.7)
144.56	0.061(8.7)	144.79	0.054(11.0)	145.01	0.065(12.8)
153.54	0.060(8.0)	153.72	0.069(10.7)	153.89	0.051(12.9)
162.42	0.058(10.0)	162.55	0.061(11.6)	162.66	0.069(10.6)

$E_{^3He}$ = 1.2 MeV		$E_{^3He}$ = 1.3 MeV		$E_{^3He}$ = 1.4 MeV	
θ_{cm} (deg)	σ_{cm} (mb/sr)	θ_{cm} (deg)	σ_{cm} (mb/sr)	θ_{cm} (deg)	σ_{cm} (mb/sr)
22.77	0.098(6.5)	22.88	0.111(5.4)	22.98	0.154(4.9)
34.06	0.106(6.1)	34.21	0.150(5.0)	34.36	0.196(4.5)
45.22	0.128(5.8)	45.42	0.167(5.0)	45.61	0.288(4.1)
56.22	0.156(5.4)	56.46	0.212(4.7)	56.69	0.302(4.0)
67.04	0.142(5.7)	67.31	0.202(4.5)	67.56	0.308(3.9)
77.64	0.133(5.7)	77.93	0.205(4.4)	78.21	0.251(4.2)
88.01	0.103(6.0)	88.31	0.190(4.5)	88.61	0.226(4.4)
98.14	0.105(8.8)	98.45	0.137(8.6)	98.74	0.151(7.7)
108.01	0.085(10.3)	108.32	0.132(7.3)	108.61	0.134(6.0)
117.64	0.084(8.8)	117.93	0.129(8.5)	118.21	0.150(12.6)
127.04	0.084(10.4)	127.31	0.075(7.1)	127.56	0.112(9.6)
136.22	0.066(9.9)	136.46	0.078(8.9)	136.69	0.090(9.7)
145.22	0.059(11.2)	145.42	0.069(10.8)	145.61	0.108(9.1)
154.06	0.053(10.6)	154.21	0.059(14.3)	154.36	0.109(8.9)
162.77	0.051(11.4)	162.88	0.088(10.7)	162.98	0.073(10.9)

The numbers in parentheses are the percentage errors on σ

Table 9

Absolute Differential Cross Sections for $^{6}Li(2.18)$ State

$E_{^3He}$ = 1.5 MeV		$E_{^3He}$ = 1.6 MeV		$E_{^3He}$ = 1.7 MeV	
θ_{cm} (deg)	σ_{cm} (mb/sr)	θ_{cm} (deg)	σ_{cm} (mb/sr)	θ_{cm} (deg)	σ_{cm} (mb/sr)
23.08	0.193(4.3)	23.17	0.245(4.4)	23.26	0.373(4.2)
34.50	0.268(3.8)	34.63	0.330(4.0)	34.76	0.551(3.8)
45.79	0.342(3.5)	45.96	0.407(3.7)	46.13	0.679(3.4)
56.90	0.396(3.4)	57.11	0.448(3.6)	57.31	0.648(3.4)
67.81	0.348(3.3)	68.04	0.436(3.7)	68.27	0.621(3.4)
78.48	0.347(3.4)	78.73	0.418(3.8)	78.98	0.580(3.5)
88.89	0.314(3.5)	89.15	0.348(3.9)	89.41	0.503(3.5)
99.03	0.261(4.5)	99.30	0.302(4.7)	99.56	0.448(4.8)
108.89	0.197(5.3)	109.15	0.224(6.8)	109.41	0.318(5.2)
118.48	0.150(7.0)	118.73	0.174(8.0)	118.98	0.270(5.9)
127.81	0.125(6.3)	128.04	0.128(7.9)	128.27	0.268(6.1)
136.90	0.121(7.8)	137.11	0.165(6.8)	137.31	0.240(6.7)
145.79	0.096(8.0)	145.96	0.123(8.0)	146.13	0.272(6.6)
154.50	0.101(8.6)	154.63	0.173(7.4)	154.76	0.267(7.0)
163.07	0.095(8.5)	163.17	0.161(7.8)	163.25	0.246(6.1)
$E_{^3He}$ = 1.8 MeV		$E_{^3He}$ = 1.9 MeV		$E_{^3He}$ = 2.0 MeV	
θ_{cm} (deg)	σ_{cm} (mb/sr)	θ_{cm} (deg)	σ_{cm} (mb/sr)	θ_{cm} (deg)	σ_{cm} (mb/sr)
23.34	0.589(3.6)	23.42	0.603(3.4)	23.50	0.825(3.6)
34.89	0.761(3.4)	35.01	0.978(3.1)	35.12	1.062(3.3)
46.29	0.986(3.2)	46.44	1.259(3.2)	46.59	1.386(3.2)
57.50	1.045(3.2)	57.68	1.239(2.8)	57.86	1.343(2.9)
68.49	0.992(3.1)	68.69	1.109(2.9)	68.90	1.378(2.9)
79.21	0.846(3.2)	79.44	0.969(3.0)	79.66	1.129(2.8)
89.65	0.690(3.4)	89.87	0.840(3.2)	90.15	1.003(3.0)
99.81	0.618(4.7)	100.05	0.752(3.7)	100.29	0.787(4.3)
109.66	0.461(5.2)	109.90	0.533(4.4)	110.13	0.588(5.0)
119.21	0.392(5.3)	119.44	0.485(4.8)	119.66	0.549(5.4)
128.48	0.371(6.9)	128.69	0.428(6.1)	128.90	0.601(5.4)
137.50	0.358(6.2)	137.68	0.465(6.5)	137.86	0.551(5.7)
146.29	0.295(6.1)	146.44	0.477(5.6)	146.59	0.586(6.3)
154.89	0.383(6.5)	155.01	0.456(5.5)	155.12	0.509(5.5)
163.34	0.359(6.7)	163.42	0.448(5.6)	163.50	0.538(6.2)

The numbers in parentheses are the percentage errors on σ

Table 10

Absolute Differential Cross Sections for $^{6}Li(3.56)$ State

$E_{^3He}$ = 0.9 MeV		$E_{^3He}$ = 1.0 MeV		$E_{^3He}$ = 1.1 MeV	
θ_{cm} (deg)	σ_{cm} (mb/sr)	θ_{cm} (deg)	σ_{cm} (mb/sr)	θ_{cm} (deg)	σ_{cm} (mb/sr)
22.58	0.028(12.7)	22.71	0.034(17.2)	22.83	0.060(11.7)
33.77	0.050(8.4)	33.96	0.079(9.8)	34.14	0.112(8.5)
44.85	0.062(9.0)	45.10	0.120(8.9)	45.33	0.177(7.1)
55.79	0.093(8.6)	56.08	0.173(7.8)	56.36	0.199(6.4)
66.54	0.104(7.7)	66.88	0.246(7.7)	67.19	0.253(6.4)
77.10	0.126(8.1)	77.46	0.242(8.0)	77.80	0.333(6.4)
87.44	0.160(8.2)	87.82	0.294(7.9)	88.18	0.336(6.1)
97.56	0.101(9.4)	97.95	0.300(8.0)	98.31	0.255(7.1)
107.45	0.134(9.0)	107.82	0.232(9.0)	108.18	0.296(6.9)
117.10	0.115(9.0)	117.46	0.203(9.5)	117.80	0.258(8.0)
126.54	0.082(8.6)	126.88	0.164(9.5)	127.19	0.206(9.2)
135.78	0.057(9.6)	136.08	0.105(10.9)	136.35	0.134(9.5)
144.85	0.051(10.5)	145.10	0.070(12.7)	145.33	0.105(9.8)
153.77	0.040(9.6)	153.96	0.091(11.3)	154.14	0.064(9.5)
162.58	0.020(14.7)	162.71	0.045(13.3)	162.83	0.032(15.7)

$E_{^3He}$ = 1.2 MeV		$E_{^3He}$ = 1.3 MeV		$E_{^3He}$ = 1.4 MeV	
θ_{cm} (deg)	σ_{cm} (mb/sr)	θ_{cm} (deg)	σ_{cm} (mb/sr)	θ_{cm} (deg)	σ_{cm} (mb/sr)
22.95	0.048(12.5)	23.06	0.060(10.2)	23.17	0.080(8.8)
34.31	0.102(7.2)	34.48	0.136(5.9)	34.63	0.158(5.5)
45.55	0.178(5.7)	45.76	0.207(5.1)	45.96	0.261(4.6)
56.62	0.235(5.1)	56.87	0.313(4.5)	57.10	0.356(4.0)
67.49	0.284(5.1)	67.77	0.362(4.1)	68.04	0.461(3.8)
78.13	0.316(4.8)	78.43	0.477(3.7)	78.73	0.498(3.7)
88.52	0.307(4.7)	88.84	0.476(3.7)	89.14	0.516(3.8)
98.65	0.252(5.4)	98.98	0.416(4.8)	99.29	0.461(4.5)
108.52	0.265(5.7)	108.84	0.421(4.8)	109.15	0.463(4.6)
118.13	0.235(6.4)	118.43	0.371(5.1)	118.72	0.460(5.0)
127.49	0.205(7.0)	127.77	0.287(6.0)	128.04	0.350(5.4)
136.62	0.158(7.3)	136.87	0.202(7.2)	137.10	0.281(5.7)
145.55	0.104(8.9)	145.76	0.134(7.4)	145.96	0.171(8.6)
154.31	0.074(15.1)	154.47	0.090(9.4)	154.63	0.108(8.3)
162.95	0.057(10.8)	163.06	0.057(13.4)	163.16	0.031(12.4)

The numbers in parentheses are the percentage errors on σ

Table 11

Absolute Differential Cross Sections for $^{6}Li(3.56)$ State

$E_{^3He}$ = 1.5 MeV		$E_{^3He}$ = 1.6 MeV		$E_{^3He}$ = 1.7 MeV	
θ_{cm} (deg)	σ_{cm} (mb/sr)	θ_{cm} (deg)	σ_{cm} (mb/sr)	θ_{cm} (deg)	σ_{cm} (mb/sr)
23.27	0.062(10.4)	23.36	0.074(7.6)	23.45	0.059(8.9)
34.78	0.144(5.8)	34.92	0.122(5.5)	35.05	0.144(5.6)
46.15	0.221(4.5)	46.33	0.198(4.3)	46.50	0.248(4.6)
57.33	0.360(3.7)	57.55	0.304(4.0)	57.76	0.333(4.0)
68.29	0.440(3.3)	68.54	0.439(3.8)	68.78	0.474(3.6)
79.00	0.553(3.2)	79.27	0.551(3.5)	79.53	0.679(3.3)
89.43	0.671(3.0)	89.71	0.623(4.3)	89.93	0.752(4.2)
99.59	0.684(3.6)	99.87	0.738(4.5)	100.15	0.867(4.4)
109.44	0.631(4.2)	109.72	0.623(4.9)	109.99	0.726(4.7)
119.00	0.521(4.6)	119.27	0.492(5.9)	119.53	0.575(5.2)
128.29	0.370(6.2)	128.54	0.321(6.1)	128.78	0.317(6.9)
137.33	0.252(6.9)	137.55	0.268(8.4)	137.76	0.302(7.7)
146.14	0.148(9.5)	146.33	0.205(10.2)	146.50	0.159(12.8)
154.78	0.099(20.2)	154.92	0.131(15.8)	155.05	0.071(22.2)
163.26	0.021(10.4)	163.36	0.039(21.2)	163.45	0.082(23.1)

$E_{^3He}$ = 1.8 MeV		$E_{^3He}$ = 1.9 MeV		$E_{^3He}$ = 2.0 MeV	
θ_{cm} (deg)	σ_{cm} (mb/sr)	θ_{cm} (deg)	σ_{cm} (mb/sr)	θ_{cm} (deg)	σ_{cm} (mb/sr)
23.54	0.064(23.1)	23.63	0.108(14.3)	23.71	0.015(11.0)
35.18	0.097(16.2)	35.31	0.119(11.7)	35.43	0.086(17.8)
46.67	0.257(6.6)	46.83	0.223(7.8)	46.99	0.165(11.7)
57.96	0.386(5.1)	58.15	0.332(5.3)	58.34	0.258(7.2)
69.00	0.520(4.1)	69.22	0.445(4.5)	69.43	0.424(5.5)
79.78	0.701(3.7)	80.02	0.638(3.9)	80.25	0.590(4.0)
90.26	0.844(3.5)	90.51	0.834(3.5)	90.47	0.679(3.9)
100.41	0.941(4.1)	100.67	0.914(4.4)	100.91	0.773(5.0)
110.25	0.770(4.6)	110.50	0.782(4.4)	110.74	0.754(5.1)
119.78	0.632(5.1)	120.02	0.680(4.8)	120.25	0.722(5.3)
129.00	0.586(6.0)	129.22	0.475(6.7)	129.43	0.525(6.5)
137.96	0.411(6.6)	138.15	0.309(8.1)	138.34	0.377(14.7)
146.67	0.222(8.5)	146.83	0.245(12.6)	146.99	0.264(10.4)
155.18	0.100(14.1)	155.31	0.095(10.8)	155.43	0.132(22.5)
163.54	0.043(16.1)	163.63	0.095(19.5)	163.71	0.071(25.7)

The numbers in parentheses are the percentage errors on σ

Table 12

Absolute Differential Cross Sections for $^{6}Li(5.37)$ State

$E_{^3He}$ = 0.9 MeV		$E_{^3He}$ = 1.0 MeV		$E_{^3He}$ = 1.1 MeV	
θ_{cm} (deg)	σ_{cm} (mb/sr)	θ_{cm} (deg)	σ_{cm} (mb/sr)	θ_{cm} (deg)	σ_{cm} (mb/sr)
22.84	0.739(7.6)	22.98	1.004(6.8)	23.11	0.999(5.7)
34.15	0.748(6.5)	34.36	0.986(6.4)	34.55	1.045(5.6)
45.34	0.766(7.3)	45.61	1.171(6.7)	45.86	1.096(6.2)
56.37	0.895(7.6)	56.69	1.166(6.7)	56.99	1.033(5.7)
67.20	0.905(7.0)	67.56	1.433(6.9)	67.90	1.125(5.9)
77.82	0.893(7.6)	78.21	1.425(7.4)	78.58	1.215(6.0)
88.20	0.824(7.8)	88.61	1.160(7.7)	88.99	0.965(6.3)
98.32	0.925(8.3)	98.74	1.442(7.1)	99.14	0.979(6.2)
108.20	0.982(7.9)	108.61	1.493(7.8)	109.00	1.020(6.5)
117.82	0.890(7.7)	118.21	1.330(7.7)	118.58	1.107(6.5)
127.20	0.871(7.3)	127.56	1.295(7.3)	127.90	1.107(6.5)
136.37	0.889(7.8)	136.69	1.263(7.2)	136.99	0.968(6.8)
145.34	0.705(7.6)	145.61	1.262(7.6)	145.86	1.062(6.7)
154.15	0.878(6.6)	154.36	1.110(7.7)	154.55	1.144(6.9)
162.84	0.755(7.9)	162.98	1.080(5.3)	163.11	1.011(4.9)

$E_{^3He}$ = 1.2 MeV		$E_{^3He}$ = 1.3 MeV		$E_{^3He}$ = 1.4 MeV	
θ_{cm} (deg)	σ_{cm} (mb/sr)	θ_{cm} (deg)	σ_{cm} (mb/sr)	θ_{cm} (deg)	σ_{cm} (mb/sr)
23.24	0.787(4.6)	23.36	0.891(4.0)	23.47	0.939(3.8)
34.74	0.826(4.6)	34.91	0.868(4.5)	35.08	0.891(2.9)
46.09	0.951(4.6)	46.32	0.764(4.3)	46.53	0.964(4.0)
57.27	0.888(4.8)	57.54	0.866(4.3)	57.79	1.068(3.8)
68.22	0.852(4.7)	68.53	0.792(3.9)	68.82	1.035(3.8)
78.93	0.774(5.4)	79.26	1.047(4.2)	79.57	1.030(3.9)
89.36	0.553(6.0)	89.69	0.826(5.2)	90.09	0.963(4.1)
99.51	0.570(5.4)	99.86	0.729(4.8)	100.20	0.944(5.4)
109.36	0.655(5.6)	109.71	0.859(4.5)	110.04	0.993(4.7)
118.93	0.649(5.7)	119.26	0.812(5.6)	119.57	1.065(4.9)
128.22	0.743(5.8)	128.53	0.853(5.5)	128.82	1.158(4.6)
137.27	0.829(5.9)	137.54	0.903(5.6)	137.79	1.118(5.0)
146.09	0.746(6.3)	146.32	0.868(4.9)	146.53	1.246(5.1)
154.74	0.784(6.1)	154.91	1.061(5.3)	155.08	1.143(4.8)
163.24	0.905(3.9)	163.36	0.963(5.0)	163.47	1.269(4.9)

The numbers in parentheses are the percentage errors on σ

Table 13

Absolute Differential Cross Sections for $^{6}Li(5.37)$ State

$E_{^3He}$ = 1.5 MeV		$E_{^3He}$ = 1.6 MeV		$E_{^3He}$ = 1.7 MeV	
θ_{cm} (deg)	σ_{cm} (mb/sr)	θ_{cm} (deg)	σ_{cm} (mb/sr)	θ_{cm} (deg)	σ_{cm} (mb/sr)
23.58	0.883(3.6)	23.68	0.780(4.2)	23.78	0.877(4.4)
35.24	0.919(3.6)	35.39	0.637(4.5)	35.53	0.952(4.2)
46.74	0.882(3.6)	46.93	0.906(3.9)	47.12	0.932(4.3)
58.04	0.942(3.6)	58.27	0.842(4.0)	58.49	0.927(4.2)
69.09	0.823(3.6)	69.36	0.777(4.3)	69.61	0.976(4.2)
79.87	0.980(3.5)	80.16	1.000(4.1)	80.44	1.027(4.2)
90.36	1.035(3.5)	90.66	0.972(4.0)	90.95	1.015(4.2)
100.52	1.085(4.1)	100.82	0.931(6.0)	101.12	1.124(5.2)
110.35	1.025(4.1)	110.66	1.113(5.1)	110.95	1.154(5.1)
119.87	1.343(4.0)	120.16	1.082(5.1)	120.44	1.015(5.7)
129.09	0.982(4.4)	129.36	0.966(5.6)	129.61	1.392(5.2)
138.04	1.140(4.8)	138.27	1.034(5.3)	138.49	1.249(5.5)
146.74	1.126(4.8)	146.93	0.973(5.8)	147.12	1.505(5.6)
155.23	1.200(4.7)	155.39	1.045(5.7)	155.53	1.590(5.4)
163.58	1.322(4.9)	163.68	1.348(5.3)	163.78	1.520(5.3)
$E_{^3He}$ = 1.8 MeV		$E_{^3He}$ = 1.9 MeV		$E_{^3He}$ = 2.0 MeV	
θ_{cm} (deg)	σ_{cm} (mb/sr)	θ_{cm} (deg)	σ_{cm} (mb/sr)	θ_{cm} (deg)	σ_{cm} (mb/sr)
23.88	0.939(4.4)	23.97	0.957(4.6)	24.06	1.330(4.5)
35.67	1.046(4.4)	35.81	1.098(4.4)	35.93	1.070(4.8)
47.30	1.036(4.4)	47.47	1.046(4.8)	47.64	1.135(4.9)
58.71	1.124(4.5)	58.91	0.952(4.8)	59.11	0.853(5.7)
69.86	1.125(4.3)	70.09	0.860(5.1)	70.32	1.293(4.2)
80.70	0.921(5.0)	80.96	0.759(5.7)	81.20	0.808(5.7)
91.23	0.986(5.0)	91.49	0.950(5.0)	91.75	0.735(6.7)
101.40	1.310(5.1)	101.67	1.230(4.9)	101.93	1.310(5.1)
111.22	1.138(5.4)	111.49	1.168(5.2)	111.75	1.068(6.6)
120.70	1.453(5.7)	120.96	1.325(5.8)	121.20	1.071(5.6)
129.85	1.565(5.2)	130.09	1.463(5.2)	130.31	1.289(5.5)
138.71	1.684(6.4)	138.91	1.265(6.9)	139.11	1.283(6.1)
147.30	1.737(5.9)	147.47	1.775(5.9)	147.64	1.865(6.2)
155.67	1.612(6.2)	155.80	1.530(6.3)	155.93	1.972(6.5)
163.87	1.775(5.4)	163.97	1.535(5.0)	164.05	2.822(5.2)

The numbers in parentheses are the percentage errors on σ

Table 14

Absolute Differential Cross Sections for ^{6}Li Ground State

$E_{^3He}$ = 2.15 MeV		$E_{^3He}$ = 2.50 MeV	
θ_{cm} (deg)	σ_{cm} (mb/sr)	θ_{cm} (deg)	σ_{cm} (mb/sr)
23.34	1.681(2.6)	23.57	1.248(3.2)
34.88	1.637(2.6)	35.22	1.507(3.3)
46.28	1.798(2.6)	46.72	1.985(3.1)
57.50	1.842(2.8)	58.02	2.135(2.9)
68.48	1.926(2.6)	69.07	2.821(3.4)
79.21	2.046(2.5)	79.85	2.821(3.4)
89.64	2.089(2.8)	90.34	3.004(3.0)
99.80	2.338(2.9)	100.49	3.203(4.0)
109.65	2.261(2.9)	110.33	2.876(3.3)
119.21	2.075(2.8)	119.85	2.760(3.7)
128.48	1.983(2.8)	129.07	2.844(3.4)
137.49	1.815(3.2)	138.02	2.387(3.3)
146.28	1.641(3.3)	146.72	2.479(3.6)
154.88	1.457(3.3)	155.22	2.295(3.8)
163.34	1.387(3.7)	163.57	2.267(3.8)

Table 15

Absolute Differential Cross Sections for $^{6}Li(2.18)$ State

$E_{^3He}$ = 2.15 MeV		$E_{^3He}$ = 2.50 MeV	
θ_{cm} (deg)	σ_{cm} (mb/sr)	θ_{cm} (deg)	σ_{cm} (mb/sr)
23.62	0.953(3.1)	23.86	1.404(3.3)
35.29	1.322(2.7)	35.65	1.889(3.3)
46.81	1.622(2.7)	47.27	2.401(3.1)
58.12	1.779(2.8)	58.68	2.237(2.9)
69.19	1.707(2.7)	69.82	2.474(3.2)
79.98	1.539(2.7)	80.66	2.167(3.5)
90.47	1.437(3.0)	91.19	1.988(3.3)
100.63	1.082(3.7)	101.36	1.851(4.5)
110.46	0.937(4.4)	111.18	1.392(4.0)
119.98	0.826(4.0)	120.67	1.244(4.7)
129.19	0.800(5.0)	129.82	1.209(4.9)
138.12	0.730(5.2)	138.68	0.916(4.7)
146.81	0.730(5.0)	147.27	0.981(5.0)
155.29	0.690(4.9)	155.65	0.807(6.2)
163.61	0.642(5.3)	163.86	0.792(5.5)

The numbers in parentheses are the percentage errors on σ

Table 16

Absolute Differential Cross Sections for $^{6}Li(3.56)$ State

$E_{^3He}$ = 2.15 MeV		$E_{^3He}$ = 2.50 MeV	
θ_{cm} (deg)	σ_{cm} (mb/sr)	θ_{cm} (deg)	σ_{cm} (mb/sr)
23.83	0.061(26.6)	24.09	0.091(18.0)
35.61	0.096(15.6)	35.98	0.120(15.2)
47.21	0.131(11.9)	47.70	0.196(10.2)
58.61	0.255(7.8)	59.19	0.194(10.0)
69.74	0.397(5.6)	70.40	0.418(6.8)
80.58	0.567(4.4)	81.29	0.599(5.7)
91.09	0.757(4.2)	91.84	0.867(4.6)
101.26	0.796(4.8)	102.03	1.025(6.0)
111.09	0.921(5.2)	111.84	1.122(4.9)
120.58	0.855(4.9)	121.29	0.862(6.4)
129.74	0.648(6.8)	130.40	0.873(6.5)
138.61	0.454(9.3)	139.19	0.622(7.3)
147.21	0.426(10.9)	147.70	0.706(6.5)
155.60	0.438(9.1)	155.98	0.589(10.2)
163.83	0.411(9.6)	164.09	0.835(9.0)

Table 17

Absolute Differential Cross Sections for $^{6}Li(5.37)$ State

$E_{^3He}$ = 2.15 MeV		$E_{^3He}$ = 2.50 MeV	
θ_{cm} (deg)	σ_{cm} (mb/sr)	θ_{cm} (deg)	σ_{cm} (mb/sr)
24.18	1.947(3.3)	24.45	1.566(4.0)
36.12	1.565(3.6)	36.52	1.020(5.3)
47.88	1.420(4.0)	48.39	1.064(4.9)
59.40	1.228(4.6)	60.01	0.841(5.3)
70.64	1.290(4.1)	71.34	1.469(4.6)
81.56	0.931(5.4)	82.31	1.570(4.8)
92.12	1.243(4.6)	92.92	1.517(4.5)
102.31	1.913(5.0)	103.12	1.509(12.5)
112.12	1.479(5.7)	112.92	0.964(12.7)
121.56	1.148(4.7)	122.31	1.219(11.3)
130.64	1.397(4.4)	131.34	1.227(8.0)
139.40	1.932(5.2)	140.01	1.344(8.5)
147.88	1.855(4.8)	148.39	1.717(8.4)
156.12	3.203(4.2)	156.52	1.857(6.3)
164.18	3.392(4.2)	164.45	2.417(6.2)

The numbers in parentheses are the percentage errors on σ

Table 18 Cross Sections for the ^{6}Li Ground State As a Function of ^{3}He Bombarding Energies

	$\theta_{Lab} = 30^{\circ}$	$\theta_{Lab} = 90^{\circ}$	$\theta_{Lab} = 150^{\circ}$
$E_{^{3}He}$ (MeV)	σ_{Lab} (mb/sr)	σ_{Lab} (mb/sr)	σ_{Lab} (mb/sr)
0.75	0.008(3.2)	0.009(2.8)	0.015(2.5)
0.80	0.029(2.8)	0.029(3.5)	0.050(3.5)
0.85	0.052(2.5)	0.043(4.0)	0.081(2.2)
0.90	0.075(2.5)	0.058(3.2)	0.111(2.4)
0.93	0.097(3.9)	0.076(4.1)	0.144(4.2)
0.97	0.127(2.2)	0.099(2.1)	0.189(2.5)
1.00	0.149(3.3)	0.116(3.4)	0.224(4.2)
1.05	0.188(3.3)	0.157(4.5)	0.247(4.2)
1.10	0.224(2.9)	0.200(4.2)	0.267(4.1)
1.15	0.264(2.4)	0.242(3.5)	0.289(3.6)
1.20	0.304(2.4)	0.283(3.8)	0.311(3.8)
1.25	0.352(2.1)	0.328(2.8)	0.314(3.7)
1.30	0.409(1.9)	0.373(2.9)	0.322(3.3)
1.35	0.478(1.8)	0.412(2.6)	0.321(3.3)
1.37	0.502(2.4)	0.427(2.6)	0.324(4.4)
1.40	0.539(1.8)	0.451(2.8)	0.327(3.5)
1.42	0.545(2.3)	0.454(2.6)	0.321(4.4)
1.45	0.555(1.7)	0.457(2.3)	0.311(3.6)
1.47	0.561(2.0)	0.459(2.4)	0.304(4.2)
1.50	0.570(1.7)	0.464(1.9)	0.293(3.6)
1.52	0.576(2.8)	0.468(2.3)	0.287(4.2)
1.55	0.587(1.9)	0.475(2.3)	0.276(4.3)
1.60	0.608(1.7)	0.490(2.2)	0.262(4.0)
1.65	0.704(1.9)	0.554(2.1)	0.284(4.4)
1.70	0.803(1.7)	0.623(2.0)	0.306(3.7)
1.75	0.964(1.7)	0.735(2.0)	0.365(3.9)
1.80	1.128(1.6)	0.854(1.8)	0.423(3.4)
1.85	1.218(1.5)	0.936(1.8)	0.458(3.4)
1.90	1.309(1.4)	1.018(1.7)	0.489(2.8)
1.95	1.395(1.4)	1.105(1.7)	0.517(2.9)
2.00	1.481(1.5)	1.197(1.7)	0.551(3.1)
2.05	1.551(1.3)	1.260(1.7)	0.641(2.4)
2.07	1.580(1.5)	1.287(1.9)	0.676(2.8)
2.10	1.622(1.2)	1.326(1.4)	0.730(2.1)
2.12	1.638(1.4)	1.334(1.5)	0.759(2.4)
2.15	1.661(1.3)	1.346(1.4)	0.804(2.2)
2.17	1.680(1.3)	1.355(1.5)	0.835(2.2)
2.20	1.706(1.4)	1.367(1.8)	0.882(2.3)
2.22	1.685(1.5)	1.379(1.7)	0.924(2.2)
2.25	1.651(1.5)	1.397(1.7)	0.988(2.2)
2.30	1.593(1.5)	1.431(1.7)	1.091(2.2)
2.35	1.592(1.5)	1.453(1.6)	1.164(2.1)
2.40	1.591(1.5)	1.475(1.5)	1.237(2.0)
2.45	1.573(1.7)	1.526(1.7)	1.264(2.3)
2.50	1.555(1.6)	1.577(1.5)	1.288(2.1)

The numbers in parentheses are the percentage errors on σ

Table 19 Cross Sections for the $^{6}Li(2.18)$ State As a Function of ^{3}He Bombarding Energies

	$\theta_{Lab} = 30^{\circ}$	$\theta_{Lab} = 90^{\circ}$	$\theta_{Lab} = 150^{\circ}$
$E_{^{3}He}$ (MeV)	σ_{Lab} (mb/sr)	σ_{Lab} (mb/sr)	σ_{Lab} (mb/sr)
0.75	0.013(4.3)	0.007(4.8)	0.007(5.1)
0.80	0.045(3.8)	0.022(5.8)	0.021(7.4)
0.85	0.080(3.4)	0.033(6.8)	0.030(5.0)
0.90	0.095(3.5)	0.042(5.5)	0.036(5.9)
0.93	0.108(5.7)	0.059(6.9)	0.045(10.8)
0.97	0.117(3.5)	0.071(3.5)	0.051(6.9)
1.00	0.126(5.3)	0.073(6.2)	0.073(10.2)
1.05	0.122(5.9)	0.104(8.1)	0.066(12.0)
1.10	0.120(5.5)	0.119(7.8)	0.069(12.2)
1.15	0.113(5.0)	0.139(6.6)	0.073(10.7)
1.20	0.121(5.3)	0.156(7.5)	0.070(12.8)
1.25	0.135(4.4)	0.149(6.0)	0.058(14.3)
1.30	0.148(4.2)	0.162(6.3)	0.062(12.9)
1.35	0.185(4.0)	0.174(5.8)	0.073(11.2)
1.37	0.199(4.8)	0.218(5.2)	0.106(10.8)
1.40	0.209(3.8)	0.172(6.6)	0.119(8.5)
1.42	0.225(4.6)	0.202(5.5)	0.122(10.6)
1.45	0.263(3.4)	0.203(5.0)	0.129(8.8)
1.47	0.244(4.2)	0.228(4.8)	0.104(11.4)
1.50	0.287(3.2)	0.210(4.0)	0.106(9.5)
1.52	0.309(3.8)	0.212(5.0)	0.143(8.9)
1.55	0.308(3.6)	0.242(4.4)	0.139(9.3)
1.60	0.334(3.2)	0.238(4.4)	0.169(7.5)
1.65	0.448(3.3)	0.288(4.1)	0.145(9.7)
1.70	0.536(2.9)	0.320(3.9)	0.203(7.0)
1.75	0.640(3.0)	0.359(3.9)	0.239(6.0)
1.80	0.736(2.7)	0.417(3.8)	0.267(6.6)
1.85	0.821(2.6)	0.404(3.9)	0.276(6.8)
1.90	0.886(2.4)	0.506(3.4)	0.254(6.4)
1.95	0.954(2.4)	0.502(3.4)	0.262(6.6)
2.00	1.038(2.5)	0.535(4.3)	0.295(6.8)
2.05	1.125(2.1)	0.578(3.4)	0.339(5.0)
2.07	1.112(2.6)	0.627(3.7)	0.331(6.1)
2.10	1.184(2.0)	0.627(3.0)	0.361(4.6)
2.12	1.267(2.2)	0.648(3.0)	0.332(5.6)
2.15	1.369(2.1)	0.621(3.0)	0.370(5.0)
2.17	1.384(2.1)	0.711(2.9)	0.403(4.7)
2.20	1.440(2.3)	0.681(3.7)	0.404(5.1)
2.22	1.580(2.3)	0.737(3.2)	0.378(5.3)
2.25	1.562(2.3)	0.669(3.6)	0.392(5.4)
2.30	1.620(2.2)	0.764(3.4)	0.418(5.3)
2.35	1.777(2.3)	0.795(3.1)	0.423(5.4)
2.40	1.788(2.2)	0.693(3.2)	0.436(5.0)
2.45	1.934(2.4)	0.813(3.4)	0.443(6.1)
2.50	1.993(2.2)	0.909(2.7)	0.439(5.4)

The numbers in parentheses are the percentage errors on σ

Table 20 Cross Sections for the $^{6}Li(3.56)$ State As a Function of ^{3}He Bombarding Energies

	$\theta_{Lab} = 30^{\circ}$	$\theta_{Lab} = 90^{\circ}$	$\theta_{Lab} = 150^{\circ}$
$E_{^{3}He}$ (MeV)	σ_{Lab} (mb/sr)	σ_{Lab} (mb/sr)	σ_{Lab} (mb/sr)
0.75	0.005(7.4)	0.005(6.5)	0.002(18.8)
0.80	0.019(6.7)	0.019(7.7)	0.008(21.9)
0.85	0.031(6.0)	0.031(8.8)	0.012(16.1)
0.90	0.044(6.0)	0.042(6.8)	0.024(11.8)
0.93	0.050(10.2)	0.076(7.3)	0.027(22.5)
0.97	0.064(5.7)	0.107(3.5)	0.037(14.1)
1.00	0.076(8.4)	0.131(5.7)	0.094(12.7)
1.05	0.093(8.3)	0.204(7.3)	0.057(22.0)
1.10	0.100(7.4)	0.243(6.9)	0.061(22.7)
1.15	0.087(7.7)	0.346(5.4)	0.081(15.3)
1.20	0.118(9.0)	0.374(6.1)	0.096(15.2)
1.25	0.124(6.0)	0.436(4.3)	0.107(14.7)
1.30	0.136(5.3)	0.493(4.5)	0.093(14.8)
1.35	0.137(6.0)	0.511(4.0)	0.124(11.2)
1.37	0.148(6.6)	0.641(3.7)	0.137(14.8)
1.40	0.171(4.9)	0.521(4.5)	0.115(13.2)
1.42	0.152(7.0)	0.588(3.9)	0.135(13.4)
1.45	0.159(5.5)	0.475(3.9)	0.112(13.9)
1.47	0.152(6.3)	0.546(3.8)	0.079(23.5)
1.50	0.157(5.4)	0.548(3.1)	0.102(14.2)
1.52	0.144(6.9)	0.518(3.7)	0.106(16.0)
1.55	0.150(7.1)	0.523(3.6)	0.102(18.0)
1.60	0.126(7.2)	0.582(3.4)	0.125(12.7)
1.65	0.137(8.0)	0.597(3.3)	0.073(24.6)
1.70	0.142(8.6)	0.618(3.4)	0.053(29.4)
1.75	0.144(8.8)	0.612(3.6)	0.070(29.2)
1.80	0.096(16.1)	0.634(3.5)	0.068(29.8)
1.85	0.119(12.4)	0.598(4.7)	0.113(19.5)
1.90	0.109(11.6)	0.614(3.8)	0.052(35.1)
1.95	0.094(16.4)	0.544(4.3)	0.133(16.2)
2.00	0.086(17.7)	0.524(5.1)	0.074(27.2)
2.05	0.105(12.5)	0.505(5.0)	0.135(14.1)
2.07	0.082(21.1)	0.526(5.2)	0.147(16.1)
2.10	0.055(24.5)	0.579(3.9)	0.136(12.3)
2.12	0.078(19.4)	0.498(4.4)	0.204(10.3)
2.15	0.101(15.5)	0.456(4.7)	0.229(9.6)
2.17	0.068(24.3)	0.444(5.0)	0.200(11.3)
2.20	0.053(35.1)	0.426(6.1)	0.165(14.2)
2.22	0.108(17.3)	0.523(4.9)	0.257(9.7)
2.25	0.082(25.0)	0.416(6.2)	0.271(9.4)
2.30	0.068(25.0)	0.420(6.3)	0.379(7.1)
2.35	0.102(18.0)	0.462(5.2)	0.189(15.4)
2.40	0.125(13.0)	0.417(5.9)	0.211(13.8)
2.45	0.154(15.3)	0.484(5.9)	0.130(23.5)
2.50	0.129(15.0)	0.502(4.9)	0.183(17.4)

The numbers in parentheses are the percentage errors on σ

Table 21 Cross Sections for the $^{6}Li(5.37)$ State As a Function of ^{3}He Bombarding Energies

	$\theta_{Lab} = 30^{\circ}$	$\theta_{Lab} = 90^{\circ}$	$\theta_{Lab} = 150^{\circ}$
$E_{^{3}He}$ (MeV)	σ_{Lab} (mb/sr)	σ_{Lab} (mb/sr)	σ_{Lab} (mb/sr)
0.75	0.066(3.7)	0.031(4.3)	0.035(4.2)
0.80	0.251(3.2)	0.132(4.7)	0.197(4.6)
0.85	0.515(2.8)	0.247(5.1)	0.297(3.4)
0.90	0.677(2.9)	0.388(3.9)	0.506(3.2)
0.93	0.790(4.5)	0.530(5.0)	0.745(5.4)
0.97	0.837(2.7)	0.603(2.7)	0.920(3.3)
1.00	0.967(4.0)	0.630(4.4)	1.124(5.6)
1.05	0.989(4.1)	0.901(5.7)	1.240(5.5)
1.10	0.953(3.8)	0.930(5.7)	1.050(5.9)
1.15	0.911(3.3)	0.915(5.1)	1.028(5.5)
1.20	0.974(3.5)	0.842(5.9)	0.982(6.2)
1.25	0.903(3.2)	0.742(5.3)	0.995(6.0)
1.30	0.887(3.1)	0.863(5.1)	1.056(5.3)
1.35	0.948(3.1)	0.912(4.5)	1.078(5.2)
1.37	0.931(4.1)	0.944(4.8)	1.077(7.0)
1.40	0.988(3.1)	0.953(5.2)	1.176(5.3)
1.42	1.050(3.8)	0.955(4.7)	1.232(6.7)
1.45	1.048(2.9)	1.049(3.7)	1.317(5.2)
1.47	1.018(3.5)	0.944(4.4)	1.201(6.2)
1.50	1.023(2.9)	0.868(3.6)	1.189(5.3)
1.52	0.897(3.9)	0.853(4.2)	1.029(6.7)
1.55	0.839(3.6)	0.833(4.5)	1.030(6.6)
1.60	0.670(3.9)	0.733(4.8)	0.968(6.2)
1.65	1.012(3.6)	0.795(4.7)	1.178(6.4)
1.70	0.961(3.5)	0.798(4.7)	1.143(5.7)
1.75	0.977(4.0)	0.852(5.2)	1.171(6.5)
1.80	1.053(3.9)	0.880(4.8)	1.060(6.3)
1.85	1.011(4.0)	0.861(5.1)	0.930(7.2)
1.90	1.035(4.0)	0.823(5.1)	0.803(6.8)
1.95	0.970(4.1)	0.796(5.6)	0.989(6.5)
2.00	1.090(4.4)	0.885(5.2)	1.072(6.5)
2.05	1.333(3.5)	0.963(5.4)	1.201(4.8)
2.07	1.349(4.0)	0.999(5.6)	1.255(5.6)
2.10	1.371(3.2)	0.996(4.5)	1.274(4.4)
2.12	1.603(3.5)	1.112(4.1)	1.571(4.6)
2.15	1.690(3.2)	1.092(4.2)	1.611(4.2)
2.17	1.556(3.5)	1.101(4.6)	1.442(4.6)
2.20	1.481(4.0)	1.072(5.6)	1.340(5.1)
2.22	1.444(4.2)	1.010(6.1)	1.210(5.2)
2.25	1.429(4.2)	0.977(6.7)	1.201(5.5)
2.30	1.354(4.1)	0.969(7.4)	1.063(6.4)
2.35	1.173(5.1)	0.815(8.8)	0.995(6.5)
2.40	1.074(5.2)	0.740(8.1)	0.947(6.5)
2.45	1.094(5.6)	0.774(9.0)	0.927(7.6)
2.50	1.122(4.7)	0.736(7.7)	0.944(6.0)

The numbers in parentheses are the percentage errors on σ

Table 22

Coefficients A_L in the expansion of $\sigma(\theta)=\sum_L A_L P_L(\cos\theta)$ and the total reaction cross section σ_r for ^{6}Li ground state

$E_{^3He}$ (MeV)	A_o (mb/sr)	A_1 (mb/sr)	A_2 (mb/sr)	A_3 (mb/sr)	A_4 (mb/sr)	σ_r (mb)
0.90	0.135	-0.060	-0.007	0.020	-0.002	1.696
1.00	0.206	-0.048	-0.017	0.028	0.009	2.589
1.10	0.231	-0.016	0.026	0.018	0.010	2.903
1.20	0.242	0.015	0.056	0.017	-0.036	3.041
1.30	0.340	0.055	0.028	0.029	-0.022	4.273
1.40	0.417	0.099	0.022	0.055	-0.052	5.240
1.50	0.483	0.102	-0.082	0.116	0.020	6.070
1.60	0.510	0.120	-0.102	0.135	0.028	6.409
1.70	0.713	0.156	-0.141	0.193	0.021	8.960
1.80	1.076	0.225	-0.248	0.207	-0.108	13.521
1.90	1.339	0.271	-0.272	0.092	-0.102	16.826
2.00	1.530	0.190	-0.349	0.207	-0.086	19.227
2.15	1.927	-0.037	-0.484	0.257	-0.023	24.215
2.50	2.498	-0.536	-0.997	-0.074	0.117	31.391

Table 23

Coefficients A_L in the expansion of $\sigma(\theta)=\sum_L A_L P_L(\cos\theta)$ and the total reaction cross section σ_r for ^{6}Li(2.18) state

$E_{^3He}$ (MeV)	A_o (mb/sr)	A_1 (mb/sr)	A_2 (mb/sr)	A_3 (mb/sr)	A_4 (mb/sr)	σ_r (mb)
0.90	0.105	0.033	-0.031	-0.014	0.002	1.319
1.00	0.135	0.044	-0.058	-0.013	0.010	1.696
1.10	0.119	0.047	-0.039	-0.022	0.009	1.495
1.20	0.102	0.039	-0.031	-0.028	-0.018	1.282
1.30	0.144	0.057	-0.069	-0.055	0.005	1.810
1.40	0.189	0.093	-0.071	-0.103	-0.054	2.375
1.50	0.245	0.125	-0.120	-0.117	-0.020	3.079
1.60	0.294	0.145	-0.117	-0.156	-0.004	3.695
1.70	0.446	0.206	-0.131	-0.218	-0.066	5.605
1.80	0.654	0.335	-0.202	-0.343	-0.099	8.218
1.90	0.782	0.371	-0.231	-0.452	-0.191	9.827
2.00	0.907	0.423	-0.226	-0.465	-0.197	11.398
2.15	1.200	0.464	-0.431	-0.531	-0.195	15.080
2.50	1.720	0.656	-0.710	-0.554	-0.169	21.614

Table 24

Coefficients A_L in the expansion of $\sigma(\theta)=\sum_L A_L P_L(\cos\theta)$ and the total reaction cross section σ_r for ^{6}Li(3.56) state

$E_{^3He}$ (MeV)	A_o (mb/sr)	A_1 (mb/sr)	A_2 (mb/sr)	A_3 (mb/sr)	A_4 (mb/sr)	σ_r (mb)
0.90	0.089	0.000	-0.080	0.001	0.005	1.118
1.00	0.180	-0.002	-0.187	-0.015	0.034	2.262
1.10	0.210	0.005	-0.199	0.002	0.003	2.639
1.20	0.209	0.004	-0.190	-0.029	-0.013	2.626
1.30	0.302	-0.009	-0.312	-0.000	0.026	3.795
1.40	0.349	-0.017	-0.340	0.023	-0.029	4.386
1.50	0.397	-0.044	-0.461	0.075	0.071	4.989
1.60	0.389	-0.064	-0.437	0.097	0.087	4.888
1.70	0.443	-0.055	-0.541	0.076	0.156	5.567
1.80	0.500	-0.123	-0.588	0.165	0.098	6.283
1.90	0.476	-0.112	-0.535	0.187	0.158	5.982
2.00	0.434	-0.179	-0.485	0.188	0.039	5.454
2.15	0.497	-0.295	-0.385	0.190	0.115	6.245
2.50	0.589	-0.434	-0.313	0.223	0.138	7.402

Table 25

Coefficients A_L in the expansion of $\sigma(\theta)=\sum_L A_L P_L(\cos\theta)$ and the total reaction cross section σ_r for ^{6}Li(5.37) state

$E_{^3He}$ (MeV)	A_o (mb/sr)	A_1 (mb/sr)	A_2 (mb/sr)	A_3 (mb/sr)	A_4 (mb/sr)	σ_r (mb)
0.90	0.853	-0.033	-0.125	0.006	-0.014	10.719
1.00	1.258	-0.095	-0.260	-0.015	-0.052	15.808
1.10	1.054	0.004	-0.016	-0.066	-0.057	13.245
1.20	0.748	0.070	0.135	-0.179	-0.164	9.400
1.30	0.856	-0.028	0.067	-0.051	0.065	10.757
1.40	1.030	-0.122	0.056	-0.102	-0.055	12.943
1.50	1.016	-0.181	0.042	0.029	0.076	12.767
1.60	0.934	-0.195	-0.033	-0.023	0.109	11.737
1.70	1.092	-0.287	0.145	-0.094	0.041	13.722
1.80	1.214	-0.390	0.229	-0.070	-0.207	15.256
1.90	1.113	-0.324	0.282	0.065	-0.154	13.986
2.00	1.167	-0.312	0.650	-0.248	0.305	14.665
2.15	1.527	-0.285	0.921	-0.179	0.666	19.189
2.50	1.343	-0.196	0.237	-0.112	0.826	16.877

APPENDIX B

Target Thickness and Energy Broadenings

The thickness of the ^{7}Li target, which has to be a maximum to maximize the yield, has to be chosen from the following considerations:

1. The amount of energy lost by the ^{3}He beam in travelling through the ^{7}Li target is comparable to the resolution desired in the excitation function measurement.
2. The amount of energy lost by the α-particles, the protons and the deuterons in travelling through the ^{7}Li target is less than the desired detector resolution.

Target thickness of 50 $\mu g/cm^2$ is thus determined from the above considerations. The energy lost by the ^{3}He beam at 1.5 MeV in 50 $\mu g/cm^2$ of ^{7}Li is 78 keV.

The energy broadenings produced by ^{7}Li thickness of 50 $\mu g/cm^2$ in the energies of various particles are listed below :

Table 26

Particle	Energy (MeV)	Energy Broadenings (keV)
α	4.5-9.1	95-42
d	1.8-8.0	26-8
p	1.0-3.0	12-4.5

Table 27

Stopping Power for the Various Detectors			
Detector Thickness (μm)	Alpha (MeV)	Deuteron (MeV)	Proton (MeV)
300	24.4	8.1	6.1
121	14.0	4.6	3.6
68	9.8	3.2	2.5
22.7	4.8	1.5	1.2

Table 28

Proton Energy Loss in Counter-Telescope Detector						
E_p (MeV)	1.0	2.0	2.5	4.0	5.0	6.0
ΔE (22.7μm)	.86	.59	.51	.36	.31	.27
E (300μm)	.14	1.41	1.99	3.64	4.69	5.73

Table 29

Energy Losses in Various Foils			
Particles	Energy(MeV)	Mylar(keV/μg/cm^2)	Al(keV/μg/cm^2)
$^3He_{scat}$	0.7-1.6	2.11-1.72	1.26-0.97
α	4.5-9.1	0.98-0.56	0.64-0.41
d	1.8-8.0	0.60-0.176	0.372-0.134
p	1.0-3.0	0.274-0.098	0.174-0.074
^6Li	6.0-9.0	1.946-1.447	1.236-0.999

Solid Angles of The Detector

The solid angles of the detectors have to be chosen such that the kinematic broadenings produced in the energies of the alphas, protons, and the deuterons are of the same order of magnitude as the resolution of the detectors. In addition to this requirement, the solid angles have to be as large as possible in order to maximize all the counting rates.

The kinematic broadenings at ^{3}He bombarding energy of 2.0 MeV have been calculated using the computer program for the kinematics. All the relevant quantities and the corresponding solid angles are listed as follows :

Table 30

Kinematic Broadenings at ^{3}He bombarding energy of 2.0 MeV				
Excited State	Particle Detected	Calculated Kinematic Broadening	Max. Kinematic Broadening Desired	Solid Angle Subtended by Detector
2.18	α	50 keV/Deg	150 keV	2.15 msr
	d	48 keV/Deg	150 keV	2.34 msr
4.57	α	46 keV/Deg	150 keV	2.54 msr
	d	36 keV/Deg	150 keV	4.15 msr
5.37	α	43 keV/Deg	150 keV	2.91 msr
	p	31 keV/Deg	150 keV	5.60 msr
2.94	d	37 keV/Deg		
11.4	d	16 keV/Deg		

* apperture size 1/4" X 1/8"

Counting Rates

All the counting rates R will be calculated using the following expression :

$$R_{singles} = (\text{no. of projectiles/sec}) \times (\text{no. of target atoms in the total thickness/area}) \times \left(\frac{d\sigma}{d\Omega}\right) \times d\Omega$$

$$R_{coinc} = (\text{no. of projectiles/sec}) \times (\text{no. of target atoms in the total thickness/area}) \times \left(\frac{d^2\sigma}{d\Omega_1 d\Omega_2}\right) \times d\Omega_1 \times d\Omega_2$$

where 1 and 2 refers to the particles being detected in coincidence. All the detectors are assumed to have 100% efficiency.

$$R_{\text{random coinc}} = 2 \times R_{\text{singles } 1} \times R_{\text{singles } 2} \times \Delta\tau$$

here $\Delta\tau$ is the resolution time of the electronics.

Various counting rates are calculated as follows :

In all the following calculations

1. target thickness = 50 $\mu g/cm^2$
2. beam current = 100 nA
3. time resolution = 10 ns
4. α_1-detector solid angle = 2.4 msr
5. α_2-detector solid angle = 2.6 msr

For elastically scattered ^3He

No cross sections are available in the energy region being studied in the literature. An estimate value using Rutherford scattering cross section gives $(d\sigma/d\Omega)_R$ = 4600 mb/sr at ^3He bombarding energy 1.50 MeV and angle of 30°. Accordingly,

R = 29440 cts/sec

For the study of the sequential process in the $^7Li(^3He,\alpha_1 d)\alpha_2$ and the $^7Li(^3He,\alpha p)^5He$ reactions :

The differential cross section for $\alpha(5.37)$ can be obtained from a preliminary run with a value of 2.8 mb/sr at 1.4 MeV and 30°. For proton an estimation of 1 mb/sr average can be extracted from Ref.42. Accordingly,

$R_{\alpha \text{ singles}}$ = 17.9 cts/sec

$R_{p \text{ singles}}$ = 7 cts/sec

$R_{\text{random coinc}}$ = 0.0000014 cts/sec

$R_{\alpha-\alpha \text{ coin}}$ = 0.019 cts/sec

$R_{\alpha-p \text{ coin}}$ = 0.004 cts/sec

APPENDIX C

Summary of Equations Used in Data Analysis

I. Phase Space Distributions for $^6Li^* \rightarrow \alpha + p + n$

(1) In the $^6Li^*$ rest frame, the phase space distribution for α particles is given by:

$$\frac{d^2W_{cm}}{dE_\alpha' d\Omega_\alpha'} = C_\alpha [E_\alpha'(Q/3 - E_\alpha')]^{1/2}$$

where E_α' is the energy of the α-particle in the $^6Li^*$ rest frame(CM) and Q is the Q-value for the decay. If this distribution is normalized to unity for the decay probability, then

$$1 = \int\int \frac{d^2W_{cm}}{dE_\alpha' d\Omega_\alpha'} dE_\alpha' d\Omega_\alpha' = 4\pi C_\alpha \int_0^{Q/3} [E_\alpha'(Q/3 - E_\alpha')]^{1/2} dE_\alpha'$$

Evaluation of the above integral above yields the result:

$$C_\alpha = \frac{18}{\pi^2 Q^2}$$

(2) The transformation from CM to LAB reference frame is obtained by means of the Jacobian(see p.32 of text):

$$\frac{dE_\alpha' d\Omega_\alpha'}{dE_\alpha d\Omega_\alpha} = \frac{\sin\theta'}{\sin\theta} = \frac{E_o + E_\alpha - E_\alpha'}{2(E_o E_\alpha')^{1/2}\cos\theta}$$

where $E_o = (m_\alpha/m_R)E_R$ and E_R is the LAB energy of the $^6Li^*$

recoil.

Using the relation:

$$E_{\alpha}' = E_{\alpha} - 2(E_o E_{\alpha})^{1/2}\cos\theta + E_o$$

one obtains the following expression for the phase space distribution in the LAB reference frame:

$$\frac{d^2W_{LAB}}{dE_{\alpha}d\Omega_{\alpha}} = C_{\alpha}[E_{\alpha}(Q/3-E_o-E_{\alpha}+2(E_oE_{\alpha})^{1/2}z)]^{1/2}$$

where $z=\cos\theta$ and θ is the LAB angle of the α-particle relative to the $^6Li^*$ recoil directiion; E_{α} is the LAB energy of the α-particle.

(3) For fixed z, the integrated yield of the above phase space distribution is given by:

$$\int_{E_{\alpha min}}^{E_{\alpha max}} \frac{d^2W_{LAB}}{dE_{\alpha}d\Omega_{\alpha}}dE_{\alpha} = \frac{\pi C_{\alpha}}{4}[Q/3-E_o(1-z^2)][Q/3-E_o(1-5z^2)]$$

where $(E_{\alpha min}^{max})^{1/2} = z(E_o)^{1/2} \pm [Q/3-(1-z^2)E_o]^{1/2}$

(4) In the $^6Li^*$ rest frame, the phase space distribution for protons is given by:

$$\frac{d^2W_{cm}}{dE_p'd\Omega_p'} = C_p[E_p'(5Q/6-E_p')]^{1/2}$$

where, for normalization to unity,

$$C_p = \frac{72}{25\pi^2 Q^2}$$

(5) In the LAB reference frame,

$$\frac{d^2W_{LAB}}{dE_p d\Omega_p} = C_p[E_p(5Q/6 - E_o - E_p + 2(E_o E_p)^{1/2} z)]^{1/2}$$

where $E_o = (m_p/m_R)E_R$.

II. Distribution for sequential Decay

(following Morinigo, Ref.45)

$$^6Li^* \longrightarrow {}^5He + p$$
$$\qquad\qquad\quad \llcorner\!\!\longrightarrow \alpha + n$$

(1) $$\frac{d^2W_{LAB}}{dg d\Omega_\alpha} = C\frac{g^2}{(g^2+u^2-2ugz)^{1/2}}$$

where g is the LAB velocity of the α-particle, u is the LAB velocity of the $^6Li^*$ recoil, and $z=\cos\theta$ with θ measured relative to the $^6Li^*$ recoil direction.

In terms of LAB energies,

$$\frac{d^2W_{LAB}}{dE_\alpha d\Omega_\alpha} = \frac{C}{m_\alpha}\left[\frac{E_\alpha}{E_\alpha + E_o - 2(E_o E_\alpha)^{1/2} z}\right]^{1/2}$$

(2) If the above distribution is normalized to unity, then

$$1 = 2\pi C\iiint \frac{g^2 dg dz}{(g^2+u^2-2ugz)^{1/2}} = 2\pi C I$$

Therefore, $C = \frac{1}{2\pi I}$ where the integral I is given by the fol-

lowing expression:

$$I = (w+v)^2\left[\frac{k}{2}(b-a)+\frac{\alpha^2-1}{2\alpha}\ln\left(\frac{\alpha+1}{a\alpha}\right)\right]-2wv-(w-v)^2\,\frac{\beta^2-1}{2\beta}\ln\left(\frac{\beta+1}{b\beta}\right)$$

$$+u^2\left[\frac{1}{2\beta^2}-\frac{1}{2\alpha^2}-\frac{b}{\beta^2}\ln\left(\frac{\alpha}{\beta}\right)+\frac{\beta^2-1}{2\beta^3}\ln\left(\frac{b\beta}{\beta-1}\right)-\frac{\alpha^2-1}{2\alpha^3}\ln\left(\frac{a\alpha}{\alpha-1}\right)\right]$$

where $\alpha = \frac{u}{w+v}$, $\beta = \frac{u}{w-v}$ $(w>v)$

$a = (1-1/\alpha^2)^{1/2}$, $b = (1-1/\beta^2)^{1/2}$, $k = [1-(\alpha/\beta)^2]^{1/2}$

and u is the LAB velocity of $^6Li^*$, v is the velocity of ^5He in the $^6Li^*$ rest frame, w is the velocity of α in the ^5He rest frame(see Fig.5 of text).

REFERENCES

1. J. B. Marion and F. C. Young, Nuclear Reaction Analysis, Graphs and Tables, North Holland Pub. Co., (1968)
2. Proceeding of The Conference on Correlations of Particles emitted in Nuclear Reactions. Rev. of Mod. Phys. 37 (1965) 327
3. J. B. Marion and D. M. Van Patter, "Nuclear Research with Low Energy Accelerators", Academic Press, New York (1967)
4. F. Ajzenberg-Selove and T. Lauritsen. Nucl. Phys. A227(74)1
5. A. Galonsky, R. A. Douglas, W. Haebert, M. T. McEllistrem and H. T. Richards, Phys Rev. 98 (1955) 586
6. R. J. Kane, J. M. Lambert and P. A. Treado, Nucl. Phys. A179 (1972) 725
7. V. Valkovic, C. Joseph, S. T. Emerson and G. C. Phillips, Nucl. Phys. A106 (1968) 138
8. K. H. Bray, J. M. Cameron, H. W. Fearing, D. R. Gill and H. S. Sherif, Phys. Rev. C8 (1973) 881
9. P. T. Debevec, G. T. Garvey and B. E. Hingerty, Phys. Lett. 34B (1971) 497
10. K. P. Artemov, V. Z. Gol'dberg, I. P. Petrov, V. P. Rudakov I. N. Serikov, and V. A. Timofeev, Sov. J. Nucl. Phys., Vol. 17, No. 2 (1973) 115
11. P. Paul, S. L. Blatt, and D. Kohler, Phys. Rev. 137 (1965) B499
12. A. R. Knudson and E. A. Wolicki, Proc. Conf. on Direct Interactions of Nuclear Reaction Mechanism, Pauda, 1962

(Gordon and Breach Science Publishers, 1963) p.981

13. J. L. Duggan, P. D. Miller and R. F. Gabbard, Nucl. Phys. 46 (1963) 336
14. G. U. Din and J. L. Weil, Bulle of Amer. Phys. Soc. 8 (1963) 115
15. P. Paul, S. L. Blatt and D. Kohler, Bullet. of Amer. Phys. Soc. 9 (1964) 391; Phys. Rev. 137(1965) B493
16. D. A. Bromley and E. Almqvist, Reports on Progress in Phys., Vol. 23 (1960) 544
17. C. L. Cocke and J. C. Adloff, Nucl Phys. A172 (1971) 417
18. K. P. Artemov, V. Z. Goldberg, I. P. Petrov, V. P. Rudakov, and I. N. Serikov, Soviet J. of Nucl. Phys. 14 (1972) 615
19. Vignon, Cavaignac and Longequeue, J. Physique 30 (1969) 913
20. M. A. Reimann, P. W. Martin and E. W. Vogt, Phys. Rev. Lett. 18 (1967) 246
21. D. T. Thompson and G. E. Tripard, Phys. Rev. C6 (1972) 452
22. D. L. Livesey and C. J. Piluso, Can. J. of Phys. 52 (1974) 1167
23. J. C. P. Heggie and P. W. Martin, Phys. Lett. 43B (1973) 289
24. O. P. Gupta, Ph. D. Thesis, Brooklyn College, 1977
25. G. C. Phillips, Rev. of Mod. Phys. 37 (1965) 409
26. N. Austern, Direct Nuclear Reaction Theories, John Wiley & Sons, Inc. 1970

27. L. Wolfenstein, Phys. Rev. 82 (1951) 690

28. W. Hauser and H. Feshbach, Phys. Rev. 87 (1952) 366

29. R. G. Sachs, "Nuclear Theory", Addison-Wesley, Cambridge, (1953) 317

30. D. A. Bromley, J. A. Kuehner and E. Almqvist, Bullet. of Amer. Phys. Soc. Ser. II 3 (1958) 199

31. Bromley, Kuehner and Almqvist, Nucl. Phys. 13 (1959) 1

32. A. Bohr, Nucl. Phys. 10 (1959) 486

33. L. C. Biedenharn. "Angular Correlation in Nuclear Spectroscopy" in Pure and Applied Physics 9B, Edited by F. Ajenberg-Selove, Academic Press, 1960

34. H. Frauenfelder, in Alpha-, Beta- and Gamma-Ray Spectroscopy, edited by K. Siegbahn, North-Holland Publishing Co., Amsterdam 1955

35. J. G. Cramer and W. W. Eidson, Nucl. Phys. 55 (1964) 593

36. G. R. Satchler, Nucl. Phys. 55 (1964) 1

37. L. C. Biedenharn and M. E. Rose, Rev. of Mod. Phys. 25 (1953) 729

38. A. J. Fergusson in "Angular Correlation Methods in Gamma Ray Spectroscopy".

39. P. D. Forsyth and R. R. Perry, Nucl. Phys. 67 (1965) 417

40. L. C. Biedenharn, J. M. Blatt and M. E. Rose. Revs. of Mod. Phys. 24 (1952) 249

41. K. Alder, Helv. Phys. Acta 25 (1952) 253

42. R. L. Dixon and R. D. Edge, Nucl. Phys. A156 (1970) 33

43. P. Swan, Rev. of Mod. Phys. 37 (1965) 336

44. D. F. Geesaman, R. L. McGrath, P. M. S. Lesser, P. P. Urone and B. VerWest, Phys. Rev. C15 (1977) 1835

45. F. B. Morinigo, Nucl. Phys. A127 (1969) 116

46. G. Scheklinski, U. Strohbusch and B. Goel, Nucl. Phys. A153 (1970) 97

47. A. R. Zander, K. W. Kemper and N. R. Fletcher, Nucl. Phys. A173 (1971) 273